TARGETED DRUG DELIVERY WITHIN THE EYE

A Thesis
Presented to
The Academic Faculty

by

Yoo Chun Kim

In Partial Fulfillment
of the Requirements for the Degree
Doctor of Philosophy in the
School of Chemical and Biomolecular Engineering

Georgia Institute of Technology
December, 2013

TARGETED DRUG DELIVERY WITHIN THE EYE

Approved by:

Dr. Mark R. Prausnitz, Advisor
School of Chemical and Biomolecular Engineering
Georgia Institute of Technology

Dr. Julie A. Champion
School of Chemical and Biomolecular Engineering
Georgia Institute of Technology

Dr. Dennis W. Hess
School of Chemical and Biomolecular Engineering
Georgia Institute of Technology

Dr. Henry F. Edelhauser
School of Ophthalmology
Emory University

Dr. John M. Nickerson
School of Ophthalmology
Emory University

Date Approved: Nov. 12, 2013

To my dearest sister
For her sacrifices, love, and support

ACKNOWLEDGEMENTS

I would like to thank my advisor Dr. Mark Prausnitz for all the sound advice, and guidance to complete my study. Dr. Prausnitz gave me trust, encouragement and strength to grow as an independent researcher and also as an individual. It really has been a privilege to work and learn under his guidance of Dr. Prausnitz. I would like to thank Dr. Henry Edelhauser for all his insightful advice and necessary help. Dr. Edelhauser has played instrumental role in completing my study. I would also like to thank, my thesis committee members, Dr. John Nickerson, Dr. Dannis Hess, and Dr. Julie Champion, for their scientific advice and effort to help review this work to make it better.

I would like to thank those past and present members of our lab who have helped me in my research and for being such great colleagues and friends: Dr. Jeoung Woo Lee, Dr. Seong-O Choi, Dr. Yeu Chun Kim, Dr. Samantha Andrews, Dr. Leonard Chu, Dr. Joyti Gupta, Dr. James Norman, Dr. Han Jung Park, Dr. Xin Dong Guo, Dr. Haripriya Kalluri, Sebastian Henry, Winston Pewin, Jaya Arya, Bryce Chiang, Chris Edens, Jessica Joyce, Matt Mistilis, Seonhee Park, Pradnya Samant, Aritra Sengupta, Andrew Tadros, Dr. Devin McAllister, Brian Bondy, Dr. Robyn Schlicher, and Dr. Saffar Mansoor.

I would like to especially thank Dr. Samir Patel and Dr. Vladimir Zarnitsyn for their sound advice and help technically to my research. Dr. Patel has served as a great role model for me in the lab. I would thank our administrative coordinator, Donna Bondy, for all her help throughout my time at Georgia Institute of Technology. She provided all the necessary materials for me to continue my research. I would like to also thank Dr.

Bernard McCarey and Dr. Damian Berzovsky at Emory University for their help in my corneal neovascularization study.

Most of all, I would like to thank my dearest family. My father, Pal-Byoung Kim, and my mother, Yang-do Bae, provided love, support, and strength throughout my life. I would like to give my sincere gratitude to my older sister, Yoo-Jin Kim, for her sacrifice, unconditional love and support throughout my life. She sacrificed everything for our family and taught me how to live a more meaningful life and love families. I would like to thank my wife, Kaori Tokuhisa, for being with me in every step of the way to share every bit of sadness and happiness together. I would like to also thank my two boys Omochi and Lambie for the love, laughter, and joy that they bring to my life.

TABLE OF CONTENTS

Page

ACKNOWLEDGEMENTS iv

LIST OF TABLES xi

LIST OF FIGURES xiii

LIST OF SYMBOLS AND ABBREVIATIONS xix

SUMMARY xxi

CHAPTERS

1 INTRODUCTION 1

2 BACKGROUND 3

2.1. Anatomy of the Eye 3

2.2. Eye Diseases 8

2.2.1. Introduction 8

2.2.2. Corneal Neovascularization 8

2.2.3. Glaucoma 11

2.2.4. Age-related Macular Degeneration 13

2.2.5. Diabetic Retinopathy 14

2.3. Ocular Drug Delivery Methods 16

2.3.1. Systemic 16

2.3.2. Oral Delivery 16

2.3.3. Extraocular approaches 17

2.3.4. Intraocular delivery 20

2.3.5. Density-driven drug delivery 23

2.4. Microneedles in Drug Delivery 26

2.4.1. Introduction 26

2.4.2. Types of microneedles 27

3 INTRASTROMAL DELIVERY OF BEVACIZUMAB USING MICRONEEDLES TO TREAT CORNEAL NEOVASCULARIZATION 33

3.1. INTRODUCTION 33

3.2. MATERIALS AND METHODS 35

3.2.1. Fluorescent Labeling of Bevacizumab 35

3.2.2. Enzyme-Linked Immunosorbent Assay (ELISA) of Bevacizumab 36

3.2.3. Microneedle Fabrication And Coating 36

3.2.4. Ex Vivo Injection procedure and microneedle coating. 37

3.2.5. Induction of Corneal Neovascularization 38

3.2.6. Measurement of Neovascularization 39

3.2.7. Experimental Treatment Groups 39

3.3. RESULTS AND DISCUSSION 43

3.3.1. Characterization of Microneedles Coated With Bevacizumab 43

3.3.2. Intrastromal Delivery of Bevacizumab Ex Vivo 44

3.3.3. Intrastromal Delivery of Bevacizumab In Vivo 46

3.3.4. Efficacy Of Intrastromal Delivery of Bevacizumab Using Microneedles Compared To Topical Delivery 47

3.3.5. Efficacy Of Intrastromal Delivery of Bevacizumab Using Microneedles Compared To Subconjunctival Delivery 51

3.3.6. Effect Of Bevacizumab Dose on Efficacy Of Intrastromal Delivery Using Microneedles 55

3.3.7. Safety Of Intrastromal Delivery Of Bevacizumab 58

3.4. DISCUSSION 60

3.5. CONCLUSION 63

4 FORMULATIONS TO TARGET DRUG DELIVERY WITHIN THE SUPRACHOROIDAL SPACE OF THE EYE 65

4.1. INTRODUCTION 65

4.2. MATERIALS AND METHODS 68

4.2.1. Microneedle Fabrication 68

4.2.2. Formulations 68

4.2.3. Viscosity Measurements 69

4.2.4. Ex Vivo Injection Procedure 69

4.2.5. In Vivo Injection Procedure 70

4.2.6. In Vivo Imaging Procedure 71

4.2.7. Tissue Processing And Measurement Of Fluorescence Intensity 71

4.2.8. Statistical Analysis 72

4.3. RESULTS AND DISCUSSION 73

4.3.1. Distribution of Nanoparticles and Microparticles in the Suprachoroidal Space 73
4.3.2. Polymer characterization 77
4.3.3. Formulations to enhance spreading of particles inside the suprachoroidal space 82
4.3.4. Formulations to immobilize particles inside the suprachoroidal space 88
4.4. DISCUSSION 92
4.5. CONCLUSION 94

5 TARGETED DELIVERY OF ANTI-GLAUCOMA DRUGS TO THE SUPRACILIARY SPACE USING MICRONEEDLES 96

5.1. INTRODUCTION 96
5.2. MATERIALS AND METHODS 99
5.2.1. Microneedle Fabrication and Formulation 99
5.2.2. Anesthesia and Euthanasia 99
5.2.3. Pharmacodynamics studies 100
5.2.4. Safety Studies 101
5.2.5. Intraocular Pressure Measurement 101
5.2.6. Calculation of Area Under the Curve And Equivalent Dosage 101
5.2.7. Statistical Analysis 102
5.3. RESULTS 103
5.3.1. Effect Of Anesthesia On Transient IOP Change 103
5.3.2. Anti-Glaucoma Drugs in the Normotensive Rabbit Model 105

5.3.3. Microneedles For Targeted Delivery To the Supraciliary Space 109

5.3.4. Pharmacodynamics of Sulprostone After Supraciliary Delivery 114

5.3.5. Pharmacodynamics Of Brimonidine After Supraciliary Delivery 117

5.3.6. Safety of Microneedle Injection into the Supraciliary Space 120

5.4. DISCUSSION 123

5.5. CONCLUSION 126

6 PARTICLE-STABILIZED EMULSION DROPLETS FOR GRAVITY-MEDIATED TARGETING IN THE POSTERIOR SEGMENT OF THE EYE 127

6.1. INTRODUCTION 127

6.2. MATERIALS AND METHODS 130

6.2.1. Microneedle fabrication 130

6.2.2. Ex vivo injection procedure 131

6.2.3. In vivo microneedle injection 132

6.2.4. Particle stabilized emulsion droplet Formulation 132

6.2.5. Tissue processing and measurement of florescent intensity 133

6.2.6. Particle Stabilized Emulsion droplet Fall Time Measurement 134

6.2.7. Particle Stabilized Emulsion droplet Fall Time Modeling 135

6.2.8. Ultrasound measurement 135

6.2.9. Statistical Analysis 136

6.3. RESULTS 136

6.3.1. Fabrication and characterization of particle-stabilized high-density emulsion droplets (PEDs) 136

6.3.2. Use of gravity to target PEDs within the rabbit eye ex vivo 141

6.3.3. 2.2. Use of gravity to target PEDs within the rabbit eye in vivo 144

6.3.4. Retention of PEDs at the site of targeted delivery 146

6.3.5. Effect of PED size on gravity-mediated targeting 148

6.3.6. Kinetics of suprachoroidal space expansion and collapse 150

6.4. DISCUSSION 153

6.5. CONCLUSION 156

7 CONCLUSIONS 157

8 RECOMMENDATIONS 161

APPENDIX A 166

A.1. Mathematical Modeling And In Vivo Imaging Of Bevacizumab (Chapter 3) 166

A.1.1. Intracorneal Bevacizumab Diffusion Modeling 167

REFERENCES 169

LIST OF TABLES

Page

Table 3.2.7-1: Treatment groups 40

LIST OF FIGURES

Page

Figure 2.2.1.1 Anatomy of the human eye (copied from www.nei.hih.gov)..... 4

Figure 2.2.1.2 Anatomy of the cornea. (Copied from www.nei.hih.gov)..... 5

Figure 2.2.1.3. An image of the eye showing suprachoroidal space (indicated by blue line). The image was copied from www.NIH.gov..... 7

Figure 2.2.3.1. Showing flow of aqueous humor in the eye (copied from www.nei.nih.gov)..... 11

Figure 2.3.3.1. Various different location of periocular injection. Copied from Raghava et al [51]. 19

Figure 2.4.2.1. Microscopic image of a single solid miconeedle used for intracorneal drug delivery. Copied from Jiang et al [94]. 29

Figure 2.4.2.2. A carboxymethylcellulose/trehalose dissolving microneedle patch encapsulating human growth hormone. Adapted from Lee et al 2011 [103]. 30

Figure 2.4.2.3. (A) Low and (B) high magnification image of hollow microneedle for SCS injection. Scale bar: 5 mm (A) and 500 μm (B). Copied from Patel et al [66]. 31

Figure 3.3.1.1. Image of microneedle used in this study. Scale bar indicates 2mm. 44

Figure 3.3.2.1. Coated amount on the microneedles and amount delivered in ex vivo for Texas Red labeled IgG coated microneedles at for different insertion time of 20, 60, 120, and 180 seconds. 45

Figure 3.3.3.1. (a) Measured coating amount (μg), calculated amount delivered (μg), measured amount left on the needle (μg), and measured amount in tear fluid after the injection (μg)..... 47

Figure 3.3.4.1. Corneal neovascularization after suture-induced injury. Photographs of rabbit cornea in vivo 18 days after applying a suture (a) with no treatment (UT) and (b) with a single treatment of bevacizumab using solid microneedles (MN-4bolus)..... 48

Figure 3.3.4.2. (a) Neovascularization area vs. time (days) and (b) comparison between vascularization area at day 10 and 18 for 4 treatment groups; untreated (UT), topical delivery (TOP), microneedle placebo (MN-placebo), and four-microneedles group (MN-4bolus). * - indicates significant difference (two-way ANOVA) relative untreated group; ❖- indicates significant difference (two-way ANOVA) relative to topical eye drop group. 50

Figure 3.3.5.1. (a) Neovascularization area vs. time (days) and (b) comparison between vascularization area at day 10 and 18 for 4 treatment groups; untreated, low dose subconjunctival, high dose subconjunctival, and 4 microneedles group. * - indicates statistical difference (two-way ANOVA) compared to the untreated group. 53

Figure 3.3.6.1. (a) Neovascularization area vs. time (days) and (b) comparison between vascularization area at day 10 and 18for 4 treatment groups; untreated, 1 microneedle group, 1 microneedles for 3 times, 4 microneedles group, and hollow microneedles group. * - indicates statistical difference (two-way ANOVA) compared to the untreated group. 57

Figure 3.3.7.1. High magnification images of the cornea at the site of insertion of non-coated microneedles. Arrow points to site of microneedle insertion. Scale bar indicates 1 mm. 59

Figure 4.2.8.1. Bright field image of flat mounted eye (a), florescent image of the red fluorescent particles (b), and fluorescent image of near-infrared particles (c). 73

Figure 4.2.8.2. Suprachoroidal space injection of nanoparticles and microparticles. (a) Suprachoroidal surface coverage area as function of time and particle sizes. (b) Mass of particles in suprachoroidal space as a function of time and particle sizes. * - Statistical difference (one-way ANOVA) between day 14 and 112. ❖- Statistical difference (two-way ANOVA) between day 14 and 112. 76

Figure 4.3.2.1. Molecular structure of (a) carboxymethyl cellulose (CMC), (b) hyaluronic acid (HA), (c) methyl cellulose (MC), and (d) poly vinyl alcohol (PVA). 78

Figure 4.3.2.2. Rheological behavior of hyaluronic acid and Discovisc® showing the viscosity as a function of shear rate (s^{-1})..... 80

Figure 4.3.2.3. Rheological behavior of CMC, MC, and HA showing the viscosity as a function of shear rate (s^{-1}). (b) Rheological behavior of different molecular weight of CMC (log-log plot). 82

Figure 4.3.3.1. (a) Suprachoroidal surface coverage area for different HA based polymeric compounds between 0 and 14 days. (b) Eyes injected with 4X concentration of DiscoVisc® formulation after 14 days. Merged bright field florescent image showing the

spreading of particles inside the suprachoroidal space. (c) Change in signal intensity at the site of injection over the period of 14 days after the injection for different polymeric formulations. 85

Figure 4.3.3.2. Distribution of particles inside the suprachoroidal space in different locations within the ocular globe. (a) Distribution of particles (wt%) in anterior and posterior SCS (b) Distribution of particles (wt%) in superior and inferior SCS from the injection site. 87

Figure 4.3.4.1. (a) Suprachoroidal space coverage area as a function of polymeric excipient formulation and time. (b) Rheological behavior of different weight percent of 700kDa carboxymethylcellulose. * - indicated no data are available. 91

Figure 5.3.1.1. Effect of general anesthetics on IOP in the rabbit eye. (a) Ketamine/xylazine (25/2.5 mg/kg) was administered by subcutaneous injection. (b) Isoflurane (up to 3%) was administered by inhalation for 15 min. IOP was measured in both eyes periodically for up to 9 h. Data points represent the average ± SEM (n = 4-6). 104

Figure 5.3.2.1. Effect of topical sulprostone administration on IOP in the rabbit eye. A single drop containing 2.5 µg sulprostone was administered to one eye. IOP was then followed for 9 h in both the treated eye and the untreated/contralateral eye. Data points represent the average ± SEM (n = 4). 107

Figure 5.3.2.2. Effect of topical brimonidine administration on IOP in the rabbit eye. A single drop containing (a) 75 µg or (b) 225 µg brimonidine was administered to one eye. IOP was then followed for 9 h in both the treated eye and the untreated/contralateral eye. Data points represent the average ± SEM (n = 3). 108

Figure 5.3.3.1. Hollow microneedle (at arrow) measuring 720 µm in length shown next to a liquid drop of approximately 50 µl volume from a conventional eye dropper..... 110

Figure 5.3.3.2. Supraciliary targeting of injections using a high-viscosity formulation injected using a microneedle. (a) Injection of 10 µl of red-fluorescent particles (1 µm diameter, 0.5% w/v) into the rabbit eye ex vivo spread only a few millimeters from the site of injection. The whole eye was imaged by a digital camera 60 min after injection. (b) Injection of 50 µl of red-fluorescent particles (1 µm diameter, 0.5% w/v) into the rabbit eye ex vivo was localized to the supraciliary space, directly above and adjacent to the ciliary body. The eye was frozen immediately after injection, prepared as frozen sections and imaged by brightfield microscopy. (c) Injection of 30 µl of red-fluorescent microparticles (10 µm diameter, 0.5% w/v) into a human cadaver eye was localized to the supraciliary space. The eye was fixed in formalin immediately after injection, prepared as frozen sections and imaged by overlaying a brightfield microscopy image to show ocular anatomy

with a fluorescent microscopy image of the same histological section showing fluorescent particles. 111

Figure 5.3.3.3. Effect of supraciliary injection on IOP in the rabbit eye. A single injection of 10 µl of a 2% w/v solution of CMC was administered to one eye. IOP was then followed for 9 h in both the treated eye and the untreated/contralateral eye. Data points represent the average ± SEM (n = 3). 113

Figure 5.3.4.1. Effect of supraciliary injection of sulprostone on IOP in the rabbit eye. A single injection of (a) 0.05 µg, (b) 0.005 µg and (c) 0.0005 µg sulprostone was administered to one eye. IOP was then followed for 9 h in both the treated eye and the untreated/contralateral eye. Data points represent the average ± SEM (n = 3-4)..... 115

Figure 5.3.4.2. Comparison of IOP drop caused by supraciliary delivery versus topical delivery of sulprostone. (a) Data from Figs. 5.3.2.1. and 5.3.4.1. are graphed together to show the dose-response relationship after supraciliary delivery and to facilitate comparison with topical delivery in the treated eyes. (b) Pharmacodynamic area under the curve (AUC_{PD}) after supraciliary delivery in treated and contralateral eyes, and in comparison with topical delivery. Data are from Figs. 5.3.2.1. and 5.3.4.1. AUC_{PD} was calculated using Eq. 1. 116

Figure 5.3.5.1. Effect of supraciliary injection of brimonidine on IOP in the rabbit eye. A single injection of (a) 15 µg, (b) 0.15 µg, (c) 0.0015 µg and (d) 0.00015 µg brimonidine was administered to one eye. IOP was then followed for 9 h in both the treated eye and the untreated/contralateral eye. Data points represent the average ± SEM (n = 3)..... 118

Figure 5.3.5.2. Comparison of IOP drop caused by supraciliary delivery versus topical delivery of brimonidine. (a) Data from Figs. 5.3.2.2.a and 5.3.5.1. are graphed together to show the dose-response relationship after supraciliary delivery and to facilitate comparison with topical delivery in the treated eyes. (b) Pharmacodynamic area under the curve (AUC_{PD}) after supraciliary delivery in treated and contralateral eyes, and in comparison with topical delivery. Data are from Figs. 5.3.2.2. a and 5.3.5.1. AUC_{PD} was calculated using Eq. 1. 120

Figure 5.3.6.1. Representative images of a rabbit eye (a) before (b) 1 hour after and (c) on day after supraciliary injection of the placebo formulation (2% CMC). All images are of the same rabbit eye. The lower row of images shows magnified views of the injection site of the eyes shown in the upper row of images. 122

Figure 5.3.6.2. IOP increase due to injection of 50 µl of HBSS into the intravitreal space (IVT) and 10 µl and 50 µl of 2% carboxymethylcellulose placebo formulation (CMC) into the supraciliary space (SCS). 123

Figure 5.3.6.1. Schematic showing the structure of PEDs (a). Schematics showing injection of PEDs into suprachoroidal space of the eye. Prior to injection procedure, suprachoroidal space is collapsed and does not exist (b). Following the injection, suprachoroidal space expand (c) and give space or PEDs to migrate towards back of the eye (d). After several minutes suprachoroidal space will clear aqueous phase to hold the PEDs in place (d). 128

Figure 6.2.1.1. Hollow microneedle (a) and a hollow microneedle mounted on a leur adapter attached to a syringe (b) 131

Figure 6.2.5.1. (a). Picture of posterior segment of the eye showing the radial cuts and how ocular tissues were divided into 4 radial quadrants. Picture of an ocular globe showing the 3 mm cuts from the anterior to posterior segment (b). 134

Figure 6.3.1.1. (a) Diameter of the emulsion droplet as a function of nanoparticle concentration in aqueous phase. (b) Size distribution of emulsion droplet as a function of nanoparticle concentration in aqueous phase. 138

Figure 6.3.1.2. Confocal microscope image of 14 μm (a), 25 μm (b), and 35 μm (c) PEDs. The scale bar indicates 40 μm. Florescent image of 35 μm PEDs immediately after violently shaking the vial and 30 seconds after (d)..... 139

Figure 6.3.1.3. Measured time it take for the emulsion droplets to fall 1 cm in 1% PVA solution. 141

Figure 6.3.2.1. Image showing how the ocular tissue was dissected (a). Injection of 35 μm of PEDs into a rabbit eyes showing localization to the anterior segment (b) and posterior segment (c) by changing orientation of the eye. The eyes were enucleated and frozen immediately and imaged by overlaying a brightfield microscopy image to show ocular anatomy with a fluorescent microscopy image of the same eye showing fluorescent nanoparticles. (e) Distribution of percentage of particles towards posterior segment for two different orientations (cornea down and up). (e) Radial distribution of percentage of particles away from the injection site. The arrow indicates the injection site. * - Indicates statistical significance between two different orientations. 143

Figure 6.3.3.1. (c) Distribution of percentage of PEDs towards posterior segment. (d) Radial distribution of percentage of PEDs away from the injection site. The arrow indicates the injection site. 145

Figure 6.3.3.2. (a) Injection of 32 μm of polystyrene microparticles into a rabbit eyes showing distribution of microparticles. The eyes were enucleated and frozen immediately and imaged by overlaying a brightfield microscopy image to show ocular anatomy with a fluorescent microscopy image of the same eye showing fluorescent nanoparticles. (b) Injection of 35 μm of PEDs into a rabbit eyes showing localization to the posterior

segment. The eyes were enucleated and frozen immediately and imaged by overlaying a brightfield microscopy image to show ocular anatomy with a fluorescent microscopy image of the same eye showing fluorescent nanoparticles. (c) Distribution of percentage of microparticles towards posterior segment. (d) Radial distribution of percentage of PEDs away from the injection site. The arrow indicates the injection site. *- Indicates statistical significance between 32 μm micronparticles and PEDs..... 146

Figure 6.3.4.1. Injection of 35 μm PEDs into a rabbit eyes in vivo showing localization to the posterior segment after 0 day (a) and 5 days (b). The eyes were enucleated and frozen immediately and imaged by overlaying a brightfield microscopy image to show ocular anatomy with a fluorescent microscopy image of the same eye showing fluorescent nanoparticles. (n = 3-4) (c) Distribution of percentage of PEDs towards posterior segment. (d) Radial distribution of percentage of PEDs away from the injection site. The arrow indicates the injection site. *- Indicates statistical significance between day 0 and 5…. 148

Figure 6.3.5.1. Injection of 14 (a), 25 (b), and 35 μm (c) of PEDs into a rabbit eyes showing distribution. The eyes were enucleated and frozen immediately and imaged by overlaying a brightfield microscopy image to show ocular anatomy with a fluorescent microscopy image of the same eye showing fluorescent nanoparticles. (d) Distribution of percentage of PEDs towards posterior segment. (e) Radial distribution of percentage of PEDs away from the injection site. The arrow indicates the injection site. *- Indicates statistical significance between 14 and 25 μm PEDs. 150

Figure 6.3.6.1. Intraocular pressure change after injecting 200 μl of BSS into suprachoroidal space (a). Ultrasound images of the rabbit eye showing kinetics of the suprachoroidal space expansion and subsequent collapse after injecting 200 μl of BSS into suprachoroidal space (b-f). The ultrasound probe was positioned 45 degrees away from the injection site radially in the superior side of the eye. The scale bar indicates 1mm. 152

LIST OF SYMBOLS AND ABBREVIATIONS

AMD	Age-related Macular Degeneration
ANOVA	Analysis of Variance
BSS	Balanced Salt Solution
HBSS	Hanks Balanced Salt Solution
PBS	Phosphate Buffered Saline
CMC	Carboxymethyl Cellulose
PVA	Poly vinyl Alcohol
HA	Hyaluronic Acid
MC	Methyl Cellulose
IACUC	Institutional Animal Care and Use Committee
IOP	Intraocular Pressure
IVT	Intravitreal
kDa	kilo Daltons
PLGA	Poly(lactic-co-glycolic acid)
VEGF	Vascular Endothelial Growth Factor
bFGF	Basic Fibroblast Growth Factor
PDGF	Platelet Derived Growth Factor
PED	Particle Stabilized Emulsion Droplet
AUC	Area Under the Curve
ELISA	Enzyme Linked Immunosorbent Assay
IgG	Immunoglobulin G
TMB	Tetramethylbenzidine
ARVO	Association for Research in Vision and Ophthalmology

LASIK	Laser-Assisted In Situ Keratomileusis
AMD	Age-Related Macular Degeneration
DM	Diabetic Retinopathy
CNV	Choroidal Neovascularization
FDA	Federal Food and Drug Administration
IND	Investigational New Drug Application
GLP	Good Laboratory Practices

SUMMARY

Delivering drugs to the eye can be challenging due to complex anatomy and unique physiology of the eye. In order to treat ophthalmic diseases effectively, we must consider both effectiveness of the drug and the delivery method. This is because regardless of pharmacological therapies, complex ocular anatomy might prevent penetration of the drug to the targeted location, which will reduce the efficiency of the pharmacotherapies.

This work introduces novel approaches to enhance targeting of pharmacotherapies to cornea, ciliary body, choroid, and posterior segment of the eye using microneedles as a drug delivery platform. The highly targeted drug delivery method using microneedles provides many advantages: (i) bioavailability approaches 100% by delivering drugs directly to the targeted tissue, (ii) side effects are reduced due to lower dosage requirement by delivering more drugs to the targeted site, (iii) patient compliance can be improved by administering longer controlled-release formulations which is not possible without highly targeted delivery, (iv) all these can be done in a minimally invasive way using microneedles. Research presented here involves utilizing microneedles as a device and novel pharmaceutical formulations to enhance targeting ability of drugs.

First part of the work determines the ability to deliver protein therapeutics into the cornea using coated microneedles to suppress corneal neovascularization in an injury-induced rabbit model. The results show that we were able to coat and deliver a protein therapeutic (bevacizumab) locally into the intracorneal space of the cornea in a minimally invasive way and demonstrated that this approach could be effective to suppress

neovascularization after suture-induced injury using a much lower dose compared to other conventionally used methods. The data show that highly targeted delivery of the protein therapeutic gave a better biological response with 11,000 times less dosage compared to topical administration.

The second part of the research aims to develop novel formulations to target ciliary body and choroid via suprachoroidal space injection. In this study, we develop novel polymeric excipient formulations that immobilize injected polymeric particles to target ciliary body or to enhance mobility of polymeric particles to target entire layer of the choroid. The results show that a strongly non-Newtonian fluid can be used to immobilize the particles at the injection site up to 2 months. The results also show that high molecular weight formulation with weakly non-Newtonian fluid can be used to increase the spreading of particles away from the injection site and are able to reach 100% coverage of the choroidal surface with a single injection.

The third part of the research aims to determine the biological response of targeting anti-glaucoma therapeutics to the ciliary body in rabbit model. The targeting of ciliary body was achieved via injection into the supraciliary space, the anterior part of the suprachoroidal space. This represents the first study to target anti-glaucoma therapies to the ciliary body and compares them to the topical delivery. The results show we can achieve 500 – 1000-fold dose sparing of two major classes of anti-glaucoma drugs by targeted delivery via supraciliary space injection.

The fourth and last part of the research aims to develop novel emulsion droplets to target different locations within the eye using gravity-mediated delivery technique via suprachoroidal space injection. This work demonstrates nanoparticles can be used to

stabilize the emulsion droplets and to enhance targeting ability within the eye. The results show that particle-stabilized emulsion droplets of a high-density emulsion can create movement inside the suprachoroidal space in the direction of gravity. Consequently, by simply changing the orientation of the eye, we can deliver nanoparticles preferentially towards the front or the back of the eye.

Overall this work demonstrates that microneedles have the capability to deliver pharmacotherapies to cornea, ciliary body, choroid, and posterior of the eye in a highly targeted manner and provide significant dose sparing in the rabbit model. Delivery can be done in a minimally invasive way to deliver polymeric particles in a highly targeted manner that is much better than currently used methods. This work represents the first study to specifically target specific locations in the eye by using novel formulations and delivery methods. The highly targeted delivery method can reduce the side effects due to low dosage requirement by delivering more drugs to the targeting site. This low dosage requirement will allow us to improve patient compliance by formulating longer controlled-release formulations for targeted administration in a simple, reliable, and in a minimally invasive way.

1 INTRODUCTION

Ocular diseases affect many people worldwide. It is estimated about 80 million people worldwide are visually impaired or disabled, and the number of patients increases approximately 7 million people per year. In United States alone, about 3.4 million people over the age of 40 are blind or visually impaired [1, 2]. Many ocular diseases can lead to blindness and are preventable if managed correctly. However, current ophthalmic drug delivery is constrained by the complex anatomy of the eye, which prevents easy penetration of drugs.

Most often used methods to deliver drugs to both anterior and posterior of the eyes in clinic are topical, intravitreal, and periocular administrations. Topical delivery is the mainstay to deliver drugs to the anterior segment but only acts transiently. Ocular barriers such as tear fluid, corneal epithelium, and conjunctiva only allow small amount of applied drugs into the eye. Low penetration of the drug forces patients to follow stringent dosage regimens, which reduces patient compliance [3, 4].

There are limited options for delivering drugs to their targets in the posterior segment of the eye. The periocular administration delivers drugs on the outer surface of the eye for it to diffuse into the eye. Periocular method offers minimal tissue damage but suffers from low targeting efficiency. The intravitreal injection involves administering the drug formulation directly into the center of the eye for it to diffuse outward towards choroid and retina. The intravitreal route is an invasive way to deliver drugs and often carries risk of ocular infections.

Conventional methods are not targeted to the pharmacological site of action effectively. Hence, there is great need for novel delivery strategies for eyes. The effective drug delivery system should be (i) minimally invasive, (ii) safe, and (iii) selctively targeted. Minimal invasiveness reduces any damage to the ocular tissue, possible infections and pain associated with delivery, which increases patient compliance. Highly targeted drug delivery method allows significant amount of dose sparing by having high amount of drug at the targeting site and also reduces possible side effects. Due to low penetration of the many ophthalmic drugs, it is often impossible to deliver long-term controlled release formulation. Significant dose sparing will allow us to formulate controlled release formulation, which would not be possible without highly targeted delivery method.

Using previously developed microneedles based ophthalmic drug delivery method as a tool, the research presented here demonstrates the capabilities to deliver macromolecules in vivo and develop novel formulations to enhance targeting ability within the eye. More specifically, we aim to develop highly targeted approaches to deliver drugs to cornea, ciliary body, choroid, and back of the eye. Overall objectives of this research are to (i) demonstrate the effectiveness of coated microneedles to deliver protein therapeutics into cornea in the injury-induced neovascularization animal model, (ii) develop formulations to target polymeric particles to ciliary body and choroid using polymeric excipient formulations, (iii) demonstrate the effectiveness of ciliary body targeting in glaucoma animal model, and (iv) develop an effective formulation to target polymeric particles to back of the eye using high-density particle-stabilized emulsion droplets.

2 BACKGROUND

2.1. Anatomy of the Eye

The human eye is spherical in shape but slightly flattened in the anteroposterior direction with diameter of 23-24 mm [5]. The inner portion of the eye, between lens and retina, is filled with gelatinous fluid called vitreous humor. The outer layer of the eye, which surrounds the vitreous, is comprised of three layers. The outermost layer is the sclera, the middle is the choroid and the inner layer is the retina. The anterior portion of the eye consists of cornea, ciliary body, iris, aqueous humor and lens. The aqueous humor is the fluid inside the anterior chamber that is produced by the ciliary body. The aqueous humor travels around the iris and it drains into trabecular meshwork.

The thin, transparent mucous membrane that lines the inner surface of eyelids is the conjunctiva. The conjunctiva starts at the limbus and continues to the inner surface of the eyelid that covers anterior portion of the eye. The conjunctiva also helps lubricate eyes by producing mucous. The conjunctiva is transparent, but it contains many small blood vessels. Conjunctivitis, commonly known as red eye, is characterized by inflammation of these small vessels. Since the conjunctiva is exposed to external environment; it protects the sclera and other inner components of the eye from harmful substances.

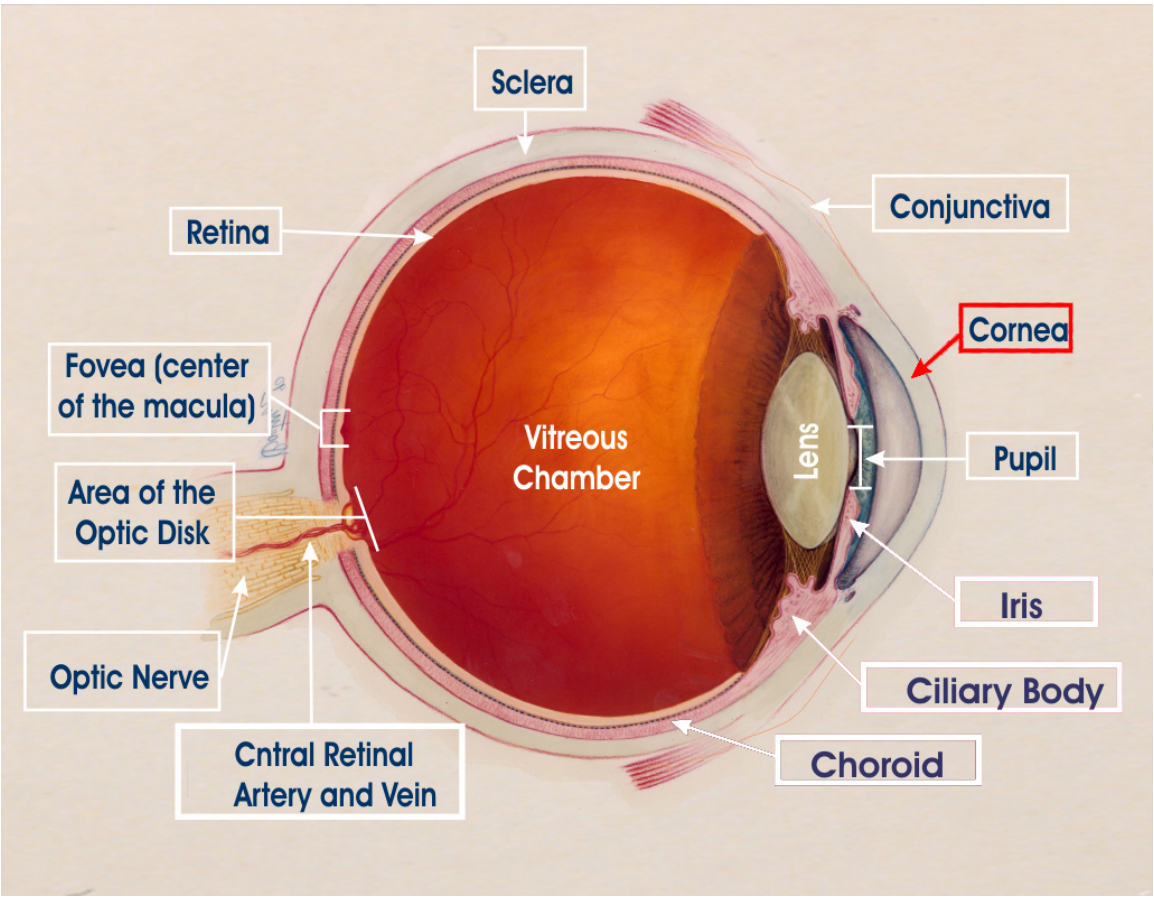

Figure 2.2.1.1 Anatomy of the human eye (copied from www.nei.hih.gov)

The clear transparent portion of the eye is the cornea. The cornea is a thin, concave tissue layer bathed on the posterior surface by the aqueous humor and abuts air on the anterior side across a thin tear film. The thickness of human cornea, at central region, is about 0.52 mm to 0.67 mm [5]. The corneal structure can be largely divided into three distinctive layers, which are epithelium, stroma and endothelium, respectively from anterior to posterior.

The corneal endothelium consists of regularly arranged polygonal cells that do not regenerate themselves. Thus, the human corneal endothelial cell density decreases with age and the cells stretch to compensate for dead cells. The endothelium is responsible for

regulating fluids and transporting solutes between the aqueous humor and the cornea. The corneal endothelium plays a very important role in maintaining corneal transparency. The endothelium actively pumps fluid out the cornea to the aqueous humor. This maintenance of fluid volume inside the cornea is required for its transparency [6].

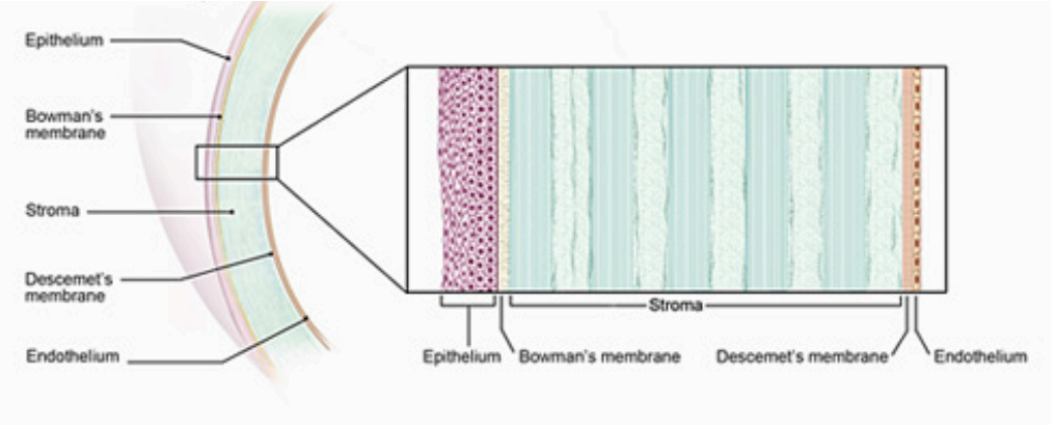

Figure 2.2.1.2 Anatomy of the cornea. (Copied from www.nei.hih.gov)

The corneal stroma is comprised of over 90 percent of the thickness of cornea. The stroma is predominately comprised of extracellular matrix that is made of lamellar structure of collagen fibers that run parallel to surface of the cornea. This alignment of collagen fibers is important for the cornea to stay transparent. The stroma is composed of 200 – 250 lamellae of collagen fibers and they stretch from one side of limbus to the other [6]. Fibroblasts are the cells that can form collagen fibers, and keratocytes. Fibroblasts contribute to corneal healing and they are present throughout the stroma [7].

The corneal epithelium is the outermost layer of the cornea that is stratified, non-keratinized, squamous epithelium. The epithelium has five to seven cells with three forms of cells: two layers of flattened epithelial cells, two or three layers of polygonal

cells, and a single internal layer of basal cells [7]. The squamous cells at the surface of cornea are constantly shed off from abrasion caused by eyelids. The basal cells of the cornea undergo mitosis and the daughter cells move toward the surface of the cornea and begin to differentiate. This movement of the cell takes about 7 days [6]. The corneal epithelium is one of the fastest healing tissues in the human body.

The sclera, the white portion of the eye, is a continuation of the corneal stroma. The sclera is composed of about 70 percent water that is primarily supported by collagen fibers. Collagen fibers provide the structural integrity and shape of the sclera and the eye. Although the sclera is composed of the same material as corneal stroma, the sclera is nearly opaque because of the irregular arrangements of the collagen fibers [6].

The choroid is a vascular layer that lies between the retina and the sclera that provides oxygen and other nutrients only to the outer layers of the retina. Along with ciliary body and iris, the choroid forms uveal track. The retinal and uveal circulations are two different types of blood circulation in the eye. Uveal circulation supplies nutrients to the uvea, and outer and middle layer of the retina. On the other hand, retinal circulation supplies nutrients to the inner layer of retina [6].

The retina is the light sensitive tissue layer that is located at the most inner layer of the eye. When light strikes the retina it starts cascade of events that sends signals to the various parts of the brain through the optic nerve. The retina is comprised of complex layers of neurons that are interconnected by synapses. There are only two kinds of neurons that are directly sensitive to the light; they are the photoreceptors. The three types of photoreceptors are the rods, cones, and intrinsically photosensitive retinal

ganglion cells, which are located at the inner layer of the retina. The retina is the only part of the central nervous system that is visible [6].

The Suprachoroidal space is a potential space in the eye that lies in between sclera and choroid. Suprachoroidal space is part of the uveoscleral outflow system that provides path for aqueous humor drainage [8]. The suprachroidal space becomes evident when an injection of fluid is made. During the injection, the suprachoroidal space rapidly expands to incorporate large amounts of fluid. Fluid injected in this area is drained from the eye rapidly. Supraciliary space is the anterior portion of the suprachoroidal space that lies just above the ciliary body of the eye.

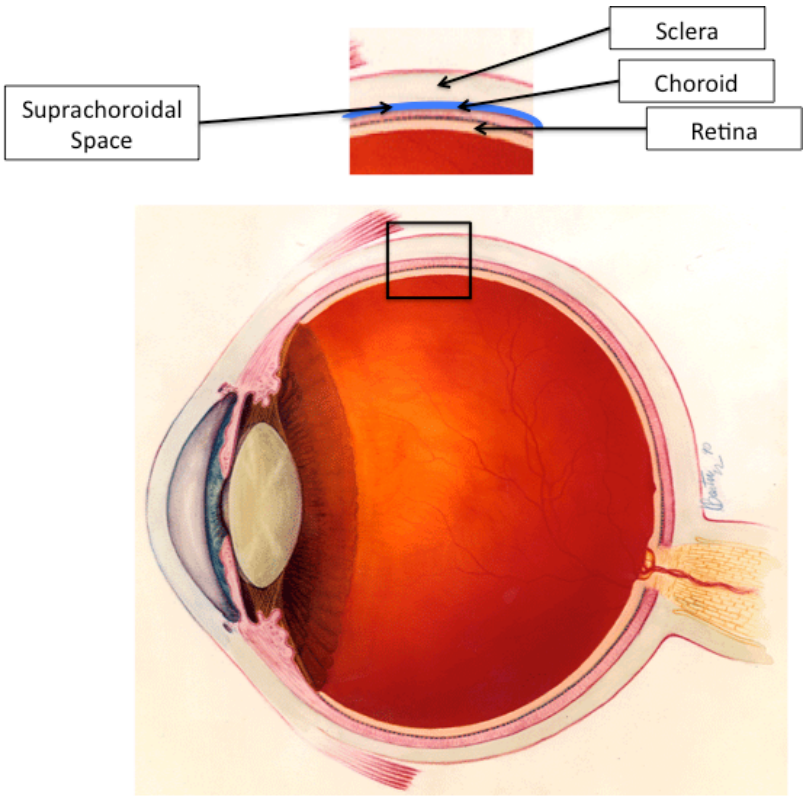

Figure 2.2.1.3. An image of the eye showing suprachoroidal space (indicated by blue line). The image was copied from www.NIH.gov

2.2. Eye Diseases

2.2.1. Introduction

Ocular diseases affect many people worldwide. It is estimated about 80 million people worldwide are visually impaired or disabled, and the number of patients increases approximately 7 million people per year. In United States alone, about 3.4 million people over the age of 40 are blind or visually impaired [1, 2]. Many ocular diseases can lead to blindness and are preventable if managed correctly. However, current ophthalmic drug delivery is constrained by the complex anatomy of eye, which prevents easy penetration of drugs. Moreover, low penetration of drugs requires patients to closely follow strenuous dosage regimens, which reduces patient compliance [3, 4]. Below is summary of diseases that are relevant to the research presented in this paper.

2.2.2. Corneal Neovascularization

Corneal neovascularization is excess growth of blood vessels in the cornea, which originates from the vasculature in the conjunctiva at the corneal edge. The main causes of corneal neovascularization include oxygen deprivation and excessive damage to ocular tissue. This is the natural response of our body to provide necessary nutrients and oxygen to the damaged corneal tissue. Human cornea is avascular tissue because it needs to be transparent to allow passage of light for proper vision. Since the cornea is avascular, it needs to obtain oxygen from the air and anything that blocks this process will cause corneal neovascularization. As a result, the most common cause of corneal

neovacularization is contact lens wear. The prevalence of corneal neovascularization among contact lens wearers is as high as 30 percent more than non-contact lens wearers. Corneal neovascularization can block a patient's vision and may cause pain, excessive tearing, light sensitivity and redness [9].

Neovascularization is a very complex process that requires many different extracellular factors and processes. Neovascularization process starts from the release of pro-angiogenic factors, such as vascular endothelial cell growth factor (VEGF), basic fibroblast growth factor (bFGF) and platelet derived growth factor (PDGF), by damaged cells in cornea. After this, several cascades of processes, such as extracellular matrix degradation and arteriogenesis, are triggered to form mature blood vessels. However, the exact mechanism, all the responsible biological factors, and receptors still remain to be elucidated [10, 11]. There have been many attempts to prevent neovascularization by inhibiting biological factors throughout the cascade of processes [12]. The most successful method was to prevent neovascularization by inhibiting pro-angiogenic factors [13].

Currently, Genentech is marketing bevacizumab (trade name of Avastin®), which inhibits vascular endothelial growth factor (VEGF). Bevacizumab is a humanized monoclonal antibody that binds to VEGF that has molecular weight of 125 kDa. United States Food and Drug Administration (FDA) first approved Bevacizumab in 2004 for use in metastatic colon cancer [14]. Since then, bevacizumab gained substantial interest in ophthalmology. As of August 2010, over 500 articles have been published related to use of anti-VEGF drug in the eye. Since bevacizumab is a monoclonal antibody that binds to

VEGF to stop the vessel growth at the initial stage of the long process, this drug is known to be very effective in preventing ocular neovascularization [11, 12].

More recently (2011), FDA approved a new anti-VEGF therapy, VEGF-Trap, which binds to more angiogenic factors: VEGF-A, VEGF-B, and placental growth factor (PIGF). It was designed to bind to all isoforms of VEGF, as opposed to pegaptanib which binds to only $VEGF_{165}$. Afibercept is a recombinant fusion protein consisting of a portion of human VEGF receptor 1 and 2 extracellular domains fused to the Fc portion of human IgG1 formulated for intravitreal administration. It is known to have stronger binding affinity to VEGF compared to ranibizumab or bevacizumab [15]. Clinical trial for the VEGF-Trap showed that injection every 2 months produced similar efficacy and safety outcomes as monthly ranibizumab [16].

Corneal transport is the most common tissue transplant, with 40,000 corneal transplants per year in the United States and 65,000 worldwide [17, 18]. Absent complications, corneal transplants are extremely successful and can be permanent cures for blindness [17]. However in 22% of transplants, there is a foreign body reaction to the sutures used to secure the transplant, which leads to blood vessel in-growth from the conjunctiva across the limbus and into the normally avascular cornea [19]. Despite conventional therapy with topical steroids or experimental therapy with topical or subconjunctiaval anti-VEGF antibody (ranibizumab, bevacizumab), this corneal neovascularization leads to transplant failure that requires removal of the transplant 15% of the time [19]. This is believed to be because steroids are not effective enough and the antibody, as a large protein, cannot be easily delivered to the site of action in the cornea.

2.2.3. Glaucoma

Glaucoma is the second leading cause of blindness worldwide and is also the first leading cause among African Americans. Glaucoma is a non-curable disease. It is estimated that 4 million Americans have glaucoma but only about half of them know that they have it. There are 80,000 people who are already blind in America due to this disease [1, 20]. After the onset of glaucoma, a patient must rely on medication for rest of their life.

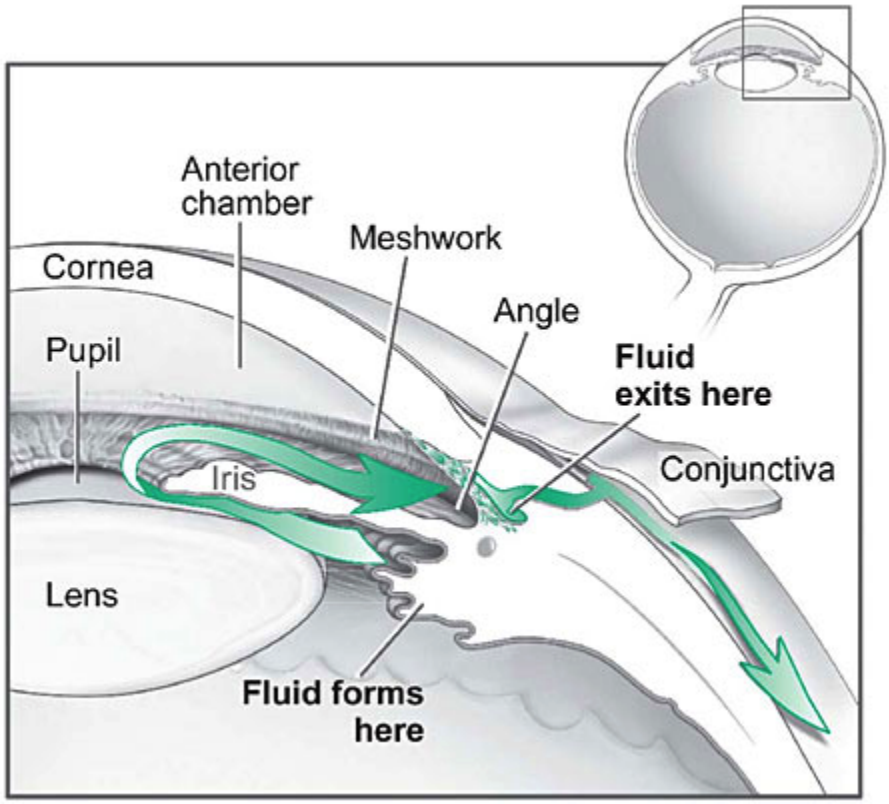

Figure 2.2.3.1. Showing flow of aqueous humor in the eye (copied from www.nei.nih.gov).

Glaucoma causes optic nerve damage due to an increase in intraocular pressure. An increase in intraocular pressure can lead to permanent visual field loss. The visual field loss tends to occur very slowly from the peripheral side of the vision. Thus, many of the patients do not realize their gradual vision loss. However, if the condition is detected at an early stage, it is possible to arrest or slow down the progression of disease with medication. The rise in intraocular pressure occurs when there is increase in aqueous production or a decrease in the outflow of the aqueous humor. The aqueous humor is a fluid in the anterior portion of eyes that bathes the ocular lens. This fluid flow provides nutrients for avascular ocular tissue, such as the cornea and the lens. If there is an imbalance of production or drainage of the aqueous humor, intraocular pressure can be elevated. This elevated pressure, which is believed to push the optic nerve at the back of the eye against the rigid structure of sclera, causing the death of retinal cells. The two main types of glaucoma drugs target either aqueous production (ciliary body) or outflow (trabecular meshwork). Most glaucoma medication requires patients to follow a strict regimen that is often 3-4 times a day. If medication cannot control the flow of aqueous flow, surgical procedure is necessary to control intraocular pressure [3].

Patient compliance with glaucoma medication is a major problem in preventing blindness. It is estimated that 50 percent of patients failed to refill their prescription the first time and 25 percent of them failed to refill their prescription the second time. This low patient compliance comes from gradual peripheral vision loss and stringent dosage regimens. It is estimated that out of 4 million Americans who have glaucoma, only half of people know that they have it. Even if the patient is aware of this disease, low absorption of ophthalmic drugs into the eye requires patients to apply the drug multiple

times a day. This low patient compliance and bioavailability of glaucoma drugs creates need for a better delivery method [3].

2.2.4. Age-related Macular Degeneration

Age-related macular degeneration (AMD) is a disease that affects older generation and results in a vision loss due to damage in central part of the retina called the macula. AMD is the third leading cause of blindness. It is estimated that more than 1.8 million individuals in United States are afflicted by wet AMD and that number is expected to grow to almost 3 million by 2020 [21, 22].

The dry (non-exudative) form of AMD is characterized by accumulation of cellular debris between choroid and retina called drusen, which causes progressive death of retinal cells. Unfortunately, there is no pharmacological therapy available for the dry form of AMD so far [23]. The wet form (exudative) is more severe case of AMD and is caused by choroidal neovascularization (CNV); abnormal blood vessels grow in choroid. Although the AMD is characterized by death of the retinal cells, the underlying problem lies in choroid.

CNV can be further categorized as “classic” or “occult” based on fluorescein angiography. In “occult”, new vessels are generally found in choroid, whereas in “classic” CNV vessels break through the RPE and enter the sub-retinal space [24, 25]. Despite the pathophysiological differences in “classic” and “occult” CNV, there are no distinctions in treatments made between classic and occult choroidal neovascularization.

Pharmacological therapies involve use of drugs, such as anti-angiogenesis drugs, and steroids [26-28]. Only within the past decade, many revolutionary therapeutic agents became available to effectively manage chorioretinal diseases [29, 30]. Macugen® was the first anti-VEGF drug that was approved for intravitreal injection for treatment for AMD. Macugen® acts by binding specifically to the $VEGF_{165}$, a protein that plays critical role in angiogenesis. Clinical trial showed significant effectiveness in preventing further vision loss [27]. Largely successful ranibizumab or Lucentis®, an anti-VEGF drug, which was approved in 2006, followed Macugen®. Ranibizumab is a monoclonal antibody fragment derived from the bevacizumab, a whole IgG molecule. Bevecizumab (Avastin®) had been approved earlier than ranibizumab, but there was a concern with its capability to diffuse into the retina due to its large size. Therefore, this triggered the development of a ranibizumab in order to resolve this issue [28].

The main method to deliver anti-VEGF molecules is an intravitreal injection. It is thought to be intravitreal delivery of anti-VEGF is more effective with the patient with classic CNV compared to occult CNV [31-33]. This is because compromised RPE and retinal layer allows better penetration in classic CNV, whereas, intact RPE and retinal layer prevents easy penetration of the molecules to the choroid in occult CNV. However, there are no clinically used methods to deliver therapeutics to the targeting tissue layer to obtain best treatment efficacy.

2.2.5. Diabetic Retinopathy

Diabetic retinopathy caused by complication of diabetes damages to the retina. Fluctuations of the sugar levels cause microvascular complication in the blood vessels in

the retina. The prevalence of diabetic retinopathy increases with duration of diabetes, and nearly all persons with type I diabetes and more than 70-90% of those with type II have some retinopathy after 20 years [34, 35]. Diabetic retinopathy can be classified into two stages namely non-proliferative and proliferative. Non-proliferative diabetic retinopathy is characterized by retinal hemorrhages or leakages of the vessels. Proliferative diabetic retinopathy occurs with further retinal ischemia and is characterized by growth of new blood vessels on the surface of the retina or the optic disc.

Treatments for the advanced stage of diabetic retinopathy involve the use of laser therapy or a surgical procedure called vitrectomy. For early stage diabetic retinopathy, available pharmacological treatments are use of anti-angiogenics, steroids, and neuroprotectants. However, conventional delivery methods suffer from poor targeting ability to the site of action. Therefore, more effective and improved delivery methods of the medications could prevent patients from moving into more advanced stages.

For instance, intravitreal injection is pharmacological treatment that requires once a month injection into the vitreous body of the eye for six months or more if necessary. It requires follow up and maintenance to control the outcome of the disease. A highly targeted method of delivery would allow high level of drug concentration at the targeting site that could give significant dose sparing [26, 36, 37]. This would allow flexibility in dosing regimen that could deliver long term controlled release formulation.

2.3. Ocular Drug Delivery Methods

2.3.1. Systemic

Drug delivery into the eye poses significant challenges due to complex anatomy and unique physiology of the eye. Systemic (parenteral) administration could be used to target molecules to the places to overcome inefficiencies of the topical delivery. However, this non-targeted method requires high dosage to deliver therapeutic drug concentration. Following systemic administration, the blood-aqueous barrier and blood-retinal barrier are the major barriers for the systemic administration [38]. Both layers express tight junctions that prevent the drugs from penetrating into the eye [39].

A drug administered could reach the anterior segment of the eye via blood vessels in ciliary body. Drug can then diffuse from the iris into the aqueous humor. Access to the posterior segment via systemic administration is severely limited by blood-retinal barrier [38] as mentioned earlier. Lipophilic compounds have more ability to move across the blood-retinal barriers compared to hydrophilic compounds via passive cellular diffusion [40]. However, hydrophilic compounds have very slim chance of penetrating into the blood-retinal barrier [40].

2.3.2. Oral Delivery

Oral delivery was studied as a possible noninvasive method to deliver drugs systemically however, it has been shown that limited penetration into the targeting tissue and systemic side effects are associated with oral delivery [41]. Furthermore, very limited compounds were investigated as oral medications for ocular diseases. These compounds

only include analgesics, antibiotics, and antiviral agents [42-44]. The major prerequisites for the oral delivery is the high dosage to increase the bioavailability, which will inevitably increase side effects.

2.3.3. Extraocular approaches

2.3.3.1 Topical delivery

Topical eye drops are a classical and predominant method to deliver drugs to the anterior portion of the eye. Topical application is used often because of its noninvasive nature, ease of self-administration, and accessibility to the surface of eyes. However, it is limited by very low drug bioavailability due to rapid clearance by tear drainage, absorption into vasculature, and poor absorption into the corneal epithelium. It is estimated that 75 percent of the applied dose is lost almost instantly through nasolacrimal drainage with topical eye drops. This high turnover rate of tears lowers absorption of drugs through ocular tissue. For a small molecular weight drug, the bioavailability for the anterior segment of the eye is about 5 percent or less of topically applied drugs. And for large molecular weight drugs, the bioavailability for the anterior segment of the eye is far less than 1 percent of topically applied drugs [45-47].

The foremost barrier that prevents topically applied drug from penetrating into inner components of the eye is the tear fluid. Tear film has two very efficient ways to protect our eyes from foreign substances. Tear fluid is composed of dual layers, top film is an aqueous layer and the bottom film is a mucin layer. The first barrier property of tears is rapid drainage of tear fluid. Baseline and reflex blinking of the eye causes rapid drainage of tear fluid, which quickly removes any noxious agents [6]. The second barrier

property of tear film is adhesion of foreign particles to the mucin layer. The mucin layer of tear film adheres to foreign particles and prevents them from reaching the surface of cornea. These two properties of tear film prevent noxious substances from penetrating into the cornea. However, this can also act as a disadvantage because it also prevents the penetration of topically applied drugs [48].

Tear film is not the only barrier that prevents topically applied drugs to penetrate the inner components of the eye. Other barriers are the cornea and the conjunctiva. Any amount of drug that is able to remain in tear film must diffuse across the cornea or conjunctiva to reach its target. The cornea is, however, a trilaminar structure that blocks the penetration of drugs. The three layers are the epithelium, stroma, and endothelium. The epithelium, a hydrophobic layer, has very tight junctions around the cells that effectively blocks the penetration of both large and hydrophilic compounds. The stroma, a hydrophilic layer, prevents penetration of hydrophobic compounds. Furthermore, even if an applied drug gets absorbed into conjunctiva, the drug gets removed by the conjunctival capillaries. The combination of these two barriers results in very low bioavailability for topically applied drugs. It is generally considered that less than five percent of the topically applied small molecular weight drugs penetrate into the ocular tissue. Current research in topical drug delivery is aimed at prolonging the residence time of the drug in the cul-de-sac to increase the penetration [49, 50].

2.3.3.2 Periocular Administration

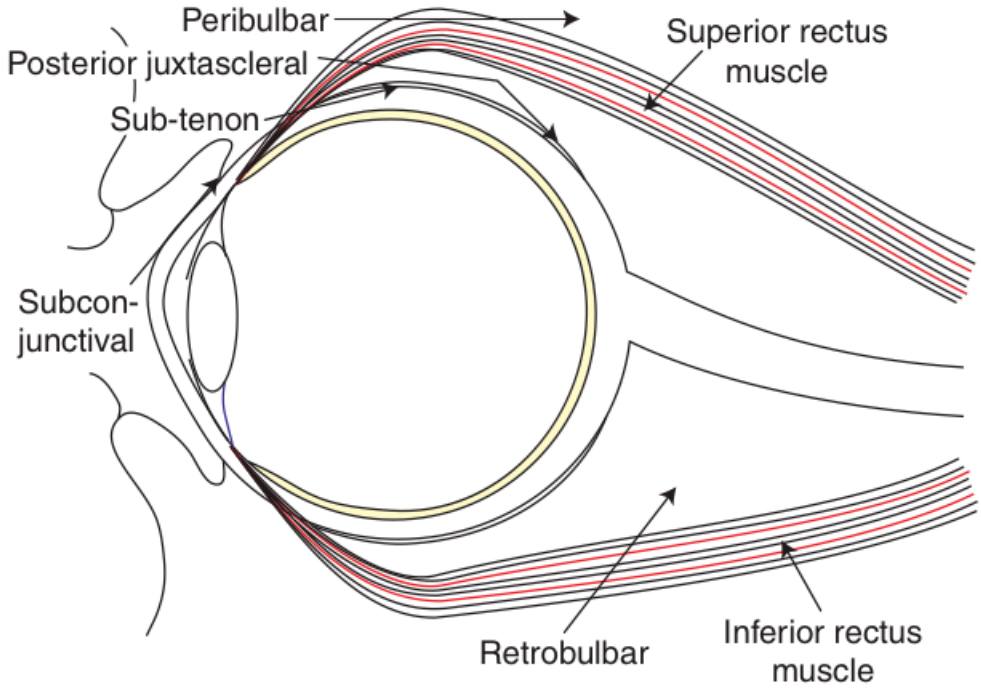

Figure 2.3.3.1. Various different location of periocular injection. Copied from Raghava et al [51].

Periocular injection refers to injection around the peripheral tissue of eyes. Different types of periocular injections include the subconjunctival, sub-tenon, peribulbar, retrobulbar, posterior juxtascleral, inferior rectus muscle and superior rectus. Periocular injection is used when large quantities, i.e., hundreds of microliters, of drugs need to be delivered. Most of the topically applied drugs will not reach posterior segment of the eye. If the drug needs to be delivered to the back of the eye, periocular injection can be used. Periocular injection provides a great efficacy advantage over traditional topical eye drops for delivering drugs to posterior segment of the eye, but has other limitations.

The periocular injections, such as subconjuctival injection, could be used for delivering drugs to the anterior portion of the eye. Subconjuctival drug delivery has limitations for delivering drugs to the anterior portion of the eye, such as glaucoma and corneal neovascularization. The main drawback of subconjunctival injection is rapid clearance of injected drugs into systemic circulation. The subconjunctival space is full of capillary blood vessels that clear injected drug quickly. In addition to this, injected drugs must diffuse across the sclera and the choroid to reach the inner part of the eye. Since a large portion of drugs injected into subconjuctival space gets absorbed into systemic circulation, it may bring side effects due to its non-localized delivery method [51].

2.3.4. Intraocular delivery

2.3.4.1 Intravitreal Administration

Currently, drugs are delivered to treat diseases of the choroid and retina by intravitreal administration. This is commonly done by injecting a liquid formulation into the vitreous, which is not the pharmacological target. Intravitreal injection was first reported in 1911 by Ohm [52] as a method to introduce air into the vitreous for a treatment for retinal detachment. In mid-1940s pharmaceutical administration, penicillin, was first introduced for treatment for endophthalmitis. However, the treatment was often delayed until the infections became worse, which made the treatment unsuccessful. This prevented the adaptation of the treatment until 1970s. New antimicrobial agents, combined with the poor success of alternatively available treatment of endophthalmitis led to renewed interest in intravitreal injection [53] and followed by successful treatment of endophthalmitis in human patients [54]. In 1980s, there was increase in adaptation of

the intravitreal injection for other pharmacological therapies. Finally in 1998, FDA approved an intravitreal injection of antisense compound used to treat retinitis [55]. The gradually increasing confidence in the safety of intreavitreal injection led to widespread us of injection techniques. In early 2000s, vascular endothelial growth factor inhibitors ranibizumab [56], and pegaptanib sodium [57] for the treatment of neovascular age-related macular degeneration was approved by FDA. The injection procedure only requires the local anesthesia and is performed with 27 or 30 gauge needle approximately 3 mm away from the limbus. And the injection volume ranges from 20-100 µl [58].

Intravitreal injection is an invasive procedure that requires a large needle to penetrate across the whole layer of the eye, therefore, some associated complications are inevitable. Possible complications include endophthalmitis, retinal detachments, iritis, uveitis, intraocular hemorrhage, cataract, and hypotony, which could be caused by either injection procedure or injected drug. The prevalence of endophthalmitis is estimated to be 0.3% per injection and 0.9% per eye [58]. If these complications arise, it could lead to permanent vision loss [58]. Although repeated injections potentially increase the rate of complications, it is not uncommon to have intravitreal injection at monthly basis. Therefore, novel delivery method that can deliver long term controlled release formulation could significantly improve complications caused by repeated injections.

2.3.4.2 Intravitreal Implants

Increased risk related with intravitreal administration prompted an effort to reduce possible complications of repeated intravitreal injections. There are numerous products in

markets that are capable of releasing drug into the vitreous for up to 3 years for non-biodegradable implants and up to 6 months for biodegradable implants.

Many of implants are placed directly in the vitreous or attached to the globe for the drug formulation to release into the vitreous [59]. While all of the non-biodegradable implants require removal of the implants once the implant fully releases the drug [60], biodegradable polymeric drug delivery system poses promise for the treatment of ocular diseases.

2.3.4.3 Suprachoroidal delivery

In previous research, researchers had used invasive surgical methods and catheters [61-65], in order to access the suprachoroidal space. However, these methods required surgical incision of the sclera and insertion of the long cannula towards the posterior site before formulation was injected into the suprachoroidal space [63].

Microneedles' microscopic size makes it possible to deliver materials into suprachoroidal space without complex surgical procedures. Microneedle allows precise placement of the needle tip right at the suprachoroidal space. In addition, microneedles have been shown to inject fluid into suprachoroidal space in rabbit, pig, and human eyes in a minimally invasive way [66] compared to existing methods. Since suprachoroidal space is right above the choroidal blood bed, delivered drugs in this region tends to be cleared out fast [65]. Therefore, controlled release formulation becomes a desired method to deliver drugs efficiently when the drugs are injected into suprachoroidal space.

Progress in this field, however, has been limited by the poorly targeted ability of suprachoroidal injection. Injected polymeric particles cover a portion of the

suprachoroidial space but not well targeted towards either anteriorly to ciliary body or posteriorly to the whole layer of the choroid. For example, a high pressure point at the back of the eye makes it hard for injected particles to penetrate towards the back of the human eyes [67]. Meanwhile, an anteriorly injected formulation quickly spreads away from the injection site when ciliary body is targeted [66-69].

2.3.5. Density-driven drug delivery

2.3.5.1 Introduction

The idea of creating density differences to enhance drug delivery has been used before in creating floating particles to enhance gastric retention of drugs and pulmonary delivery [70-72]. Both approaches are similar in a sense that the key parameter that was considered was a density difference between particles and the carrier fluid to enhance delivery of drugs to the targeted site.

2.3.5.2 Pulmonary drug delivery

Delivering drugs to the lung by inhalation is very attractive due to highly permeable epithelium of the human lungs and can be easily accessible by inhaled dose [73]. Human lungs have very efficient ways to clear foreign materials. In the upper airways, mucosal layer will rapidly clear away the particles. In the deep lung, alveolar macrophages clear away soon after the deposition of the particles [74].

Conventional pulmonary controlled release particles have 10 to 20% bioavailability and are prone to rapid clearance by alveolar macrophages [71]. Normally

aerosol particles are in a range of 1- 3 μm diameter in an effort to increase the penetration into deep lungs [71]. However, the aerosol particles are still rapidly cleared away from the lung tissue by macrophages due to its small size. In order to address the issue, Edwards et al. [75] developed low-density porous, which enables significantly higher penetration rate into deep lung with large particle size (~7μm) by slowing down the clearance rate.

2.3.5.3 Gastrointestinal drug delivery

Periodic gastric empting creates the problem to orally ingested delivery of drugs to stomach. In an effort to prolong delivery of drugs to stomach, various floating dosage forms to the gastrointestinal tract were developed as early as 1978 by Sheth and Tossounian [76]. As the shell of the capsule dissolves, a gel with density less than gastric fluid is formed and this allows the capsule to float to increase the retention of tablets inside the stomach. After this, various oral delivery systems have been developed using many different techniques such as polymeric matrices [77], microcapsules [78], microparticles [79], and bioadhesives [80].

There are two main types of floating dosage forms: effervescent and non-effervescent floating dosage forms. Effervescent dosage forms are formulated using various effervescent compounds such as sodium bicarbonate, tartaric acid, and citric acid. The contact with acidic gastric contents will liberate CO_2, which become entrapped in swollen hydrocolloids providing buoyancy to the dosage forms. Studies showed that the gastric residence time was prolonged considerably (24 hours) compared to uncoated beads (1 to 3 hours) [81].

Non-effervescent floating dosage forms use a gel forming or swellable cellulose type of hydrocolloids, polysaccharides, and matrix-forming polymers like polycarbonate, polyacrylate, polymethacrylate, and polystyrene [72]. Upon contact with gastric fluids, it attains the density of < 1. The polymer matrix also serves as a reservoir and allows sustained release of drug through the gel.

2.3.5.4 Particle stabilized emulsion (Pickering emulsion)

The idea of stabilizing emulsion droplets using solid particles is named after S.U. Pickering, who described this phenomenon in 1907 [82]. Pickering recognized the role of solid particles in stabilizing emulsions. He also noticed that solid particles were wetted more by water than by oil and that acted as emulsifying agents for oil-in-water emulsion. Since then, many investigators have studied the stability of particle-stabilized emulsion droplets [83-85]. Due to this distinct characteristic, particle stabilized emulsion droplet had been studied in drug delivery applications [86]. Also, since particle stabilized emulsion droplets could be stabilized using particles such as silica, clays, titanium dioxide, latex and many others [87-90], this type of droplet is used in many industries, such as food industry, cosmetic industry, pharmaceutical industry, petroleum industry, and agricultural industry [83].

2.4. Microneedles in Drug Delivery

2.4.1. Introduction

Although idea of microneedles was first proposed in 1971, it was not popularized until 1990's due to lack of required technology for microneedle production [91]. The initial application of microneedles was in the area of transdermal drug delivery. Also, the first published study of microneedles in transdermal drug delivery in 1998 triggered the emergence of many different types of microneedles [92, 93].

The concept behind microneedle usage is to create a pathway for drugs to penetrate across surface of the skin. Only a micron-sized needle is able to increase drug transport because the main barrier of the skin, stratum corneum, is about 10 to 20 micron in thickness. Due to this micron-sized needle, damage to the tissue and pain can be minimized, compared to conventional needles.

The first in vivo test of microneedles in ocular drug delivery showed coated and hollow microneedles could be used to deliver drugs safely into the eyes. The major advantage of using microneedles compared to traditional topical eye drops is that microneedles avoid two of the major barriers of ophthalmic drug delivery, which are tear fluid and the corneal epithelium. Furthermore, micron sized tips allow highly localized delivery of drugs compared to traditional topical eye drops [94, 95].

Microneedles can provide an advantage over traditional methods by targeted drug delivery in a minimally invasive manner. Because the drug is directly delivered to the targeted site, dosage requirement can be minimized. Minimal dosage can provide lower side effects and cost for patients. In addition, targeted delivery shows higher efficacy of applied drugs compared to traditional methods. In contrast, most conventional ophthalmic

drugs cannot provide a controlled release device without invasive surgery because of the high dosage requirement. Therefore, microneedles can provide distinct advantages over conventional methods due to lower dosage requirements, ability of utilizing polymeric devices to achieve controlled release of drugs in longer period of time.

2.4.2. Types of microneedles

The types of microneedles include: solid, dissolvable, and hollow microneedles. The solid microneedles can be coated with drugs and then inserted into the targeted site. Dissolvable microneedles were developed and used to achieve controlled release of drugs into inserted tissue [93, 96]. Hollow microneedles, which contain a hollow bore, offer the possibility of transporting drugs through the interior of the needle by diffusion or pressure-driven flow. Since the first practical introduction of microneedles in 1998, the application has been mostly limited to transdermal drug delivery and limited amount of work has been done in other fields including ocular drug delivery.

2.4.2.1 Solid microneedles

Solid microneedles were designed to create micron-scale holes in the skin and the hole allows molecules to be transported more easily into the tissue. Solid microneedles can be fabricated using materials such as silicon and metal. Solid microneedles arrays were first made using silicon wafer and developed for intracellular delivery in vitro [97] and these needles were inserted into cells to enhance molecular uptake and gene transfection. Three years later after this in vitro study, another study to increase

transdermal drug delivery was conducted by Henry et al. [98]. In this study, the authors showed that the penetration of microneedles through the upper most layer of the skin (stratum corneum) created the direct pathways for molecules to diffuse into the skin. Furthermore, the follow-up study by McAllister et al [99] showed permeability of calcein, fluorescently-tagged bovine serum albumin (BSA), and nanospheres could be increased up to 10,000 fold using silicon microneedles. However this strategy requires two steps. First step is creation of microscopic pores and second step is application of the drug afterword, which makes the treatment to be more complicated.

This strategy can be applied to the eye as well. Solid microneedles can be used to create microscopic pores across the cornea and sclera. Topical eye drops could then be applied to the conjunctival sack to enhance penetration of the drug into the ocular tissue. However, rapid clearance rate of topical delivery makes this method less attractive. In order to reduce this two-step process to one simple procedure, new approach was developed. This method involves coating drug formulation on the surface of the solid microneedles. After the insertion of the coated microneedle into the tissue, the formulation will rapidly dissolve off to deposit drugs directly into the targeting tissue. Inserted microneedles can then be removed right away leaving the coated drug in the tissue.

Jiang et al published the first usage of coated microneedles in ocular drug delivery in 2007 [94]. Jiang and others demonstrated that coated microneedle could be used to deliver drugs into the eye via intracorneal route. Sodium fluorescein was coated and delivered into rabbit cornea using metal microneedles. Then the concentration of fluorescein was measured in cornea, aqueous humor and lens over time. The sodium

fluorescein concentration after 3 hours was approximately 60 times higher than a topical application of an equivalent dose. Similar study was also done using pilocarpine by Jiang et al. They showed similar constriction of the pupil with approximately 100 fold less does, compared to topical application. These experiments showed that a drug could be administered into cornea using microneedles and allow much larger amounts to be penetrated to the anterior segment of the eye compared to topical delivery.

Figure 2.4.2.1. Microscopic image of a single solid miconeedle used for intracorneal drug delivery. Copied from Jiang et al [94].

2.4.2.2 Dissolvable microneedles

Alternative to inserting a microneedle, depositing the drug, and removing the microneedles, the drug-loaded microneedles itself could be left in the tissue. These

microneedles are usually made of biodegradable polymers that encapsulate a drug and as the polymer dissolves it releases the drug over time. The benefits of using dissolvable microneedles are that they do not produce sharp wastes, and offer sustained release of a loaded drug. Dissolvable microneedles have been fabricated using various materials such as poly lactic-co-glycolic acids (PLGA) [100], and carboxymethylcellulose (CMC) [101]. However, applications of the dissolvable microneedles were limited to transdermal drug delivery. Even though various compounds such as small molecules [102], proteins [103], and vaccines [104] were shown to deliver into the skin, dissolvable microneedles have not been tested in the eye so far.

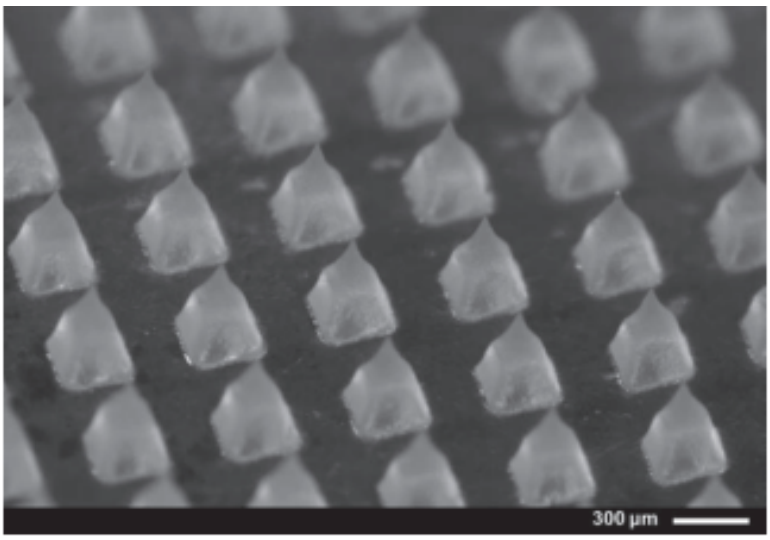

Figure 2.4.2.2. A carboxymethylcellulose/trehalose dissolving microneedle patch encapsulating human growth hormone. Adapted from Lee et al 2011 [103].

2.4.2.3 Hollow microneedles

A limitation of coated microneedles is limited surface area that allows only small amount of drug to be delivered. In order to overcome this limitation, hollow microneedles

were developed. The fabrication of the hollow microneedles can be challenging because of the internal bore needs to be made within the structure of the needle. Many different materials, such as silicon, nickel, gold, and glass have been used to create hollow microneedles [105-107]. Glass microneedles were fabricated using micropipette-pulling techniques and were shown to deliver insulin into human skin in vivo [108]. Jiang et al. published first usage in hollow microneedles in ocular drug delivery. Jiang also studied usage of a hollow microneedle via intrascleral route of delivery. Jiang demonstrated tens of microliters of fluid could be injected into sclera. The major problem with this approach is that only a small amount of drug can be delivered using hollow microneedles [94, 95].

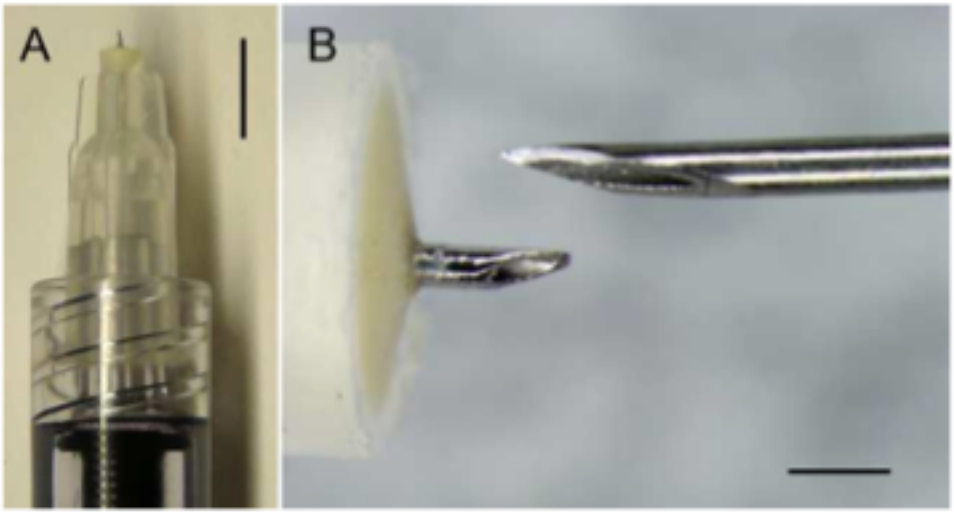

Figure 2.4.2.3. (A) Low and (B) high magnification image of hollow microneedle for SCS injection. Scale bar: 5 mm (A) and 500 μm (B). Copied from Patel et al [66].

This problem was solved by a novel approach of injecting fluid into the suprachoroidal space using a hollow microneedle. The suprachoroidal space is a virtual space between the choroid and sclera that can expand to incorporate injected fluid. It is called a virtual space because the space does not exist but can be separated. The

attachment between the choroid and sclera is thought to be at the edge of two locations, which is the anterior and posterior portion of the eye. This allows injected fluid to flow freely between the posterior portion of the eye. If the drug was injected into the side of the eye, the physiological feature of suprachoroidal space allows fluid to flow to the posterior portion of the eye [69].

Patel et al. demonstrated the suprachoroidal space could be used to inject 50-100 microliters of fluid [67]. Another major advantage of using a suprachoroidal injection is that it can be used to put drugs directly to the back of the eye. Patel et al. showed materials can be injected into the suprachoroidal space of rabbit, pig, and human eyes [67]. Patel also demonstrated that when various materials such as fluorescein and fluorescently tagged dextrans, bevacizumab, and polymeric particles were injected into rabbit eyes, their presence at the back of the eye was measured [66]. This technology was recently used to inject bevacizumab in a group of four patients and it was shown that the procedure was well tolerated with just a topical anesthesia [109]. Suprachoroidal space injection gives easy access to many unique locations inside the eye, such as ciliary body or macula, that are pharmacological targeting sites for many diseases such as age-related macular degeneration and glaucoma [23, 110, 111]. However, one of the problems for the suprachoroidal delivery is uncontrolled flow of fluid inside the suprachoroidal space allows only limited targeting ability. Therefore the injected fluid covers part of the eye but is not well targeted to ciliary body or back of the eye.

3 INTRASTROMAL DELIVERY OF BEVACIZUMAB USING MICRONEEDLES TO TREAT CORNEAL NEOVASCULARIZATION

3.1. INTRODUCTION

Corneal neovascularization is invasion of vessels into the clear cornea. Corneal neovascularization can cause visual impairment due to blockage of visual field by ingrowth of vessels. It is estimated that corneal neovascularization develops in 1.4 million patients per year and 12 % of these patients experience vision loss [112]. Corneal neovascularization could be caused by infectious pathogens, inflammatory responses, physical traumas, or degenerative diseases [113]. Conventional therapy for corneal neovascularization relies on steroids such as hydrocortisone, dexamethasone, prednisone, triamcinolone acetonide [113]. However, steroids carry concerns for serious side effects such as cataract and glaucoma and the increased in injection [114].

Recently, anti-vascular endothelial growth factor (VEGF) treatments showed very promising results against treating corneal neovascularization [115]. Currently, topical and subconjunctival injection of bevacizumab is used in clinic to treat corneal neovascularization as an off-labeled use [116-118]. However, topical administration is extremely inefficient due to the effective barrier properties of corneal epithelium, and systemic delivery is often accompanied by side effects [6, 113, 119-121]. Subconjunctival administration is a better delivery method. However, there are still the possibility of causing side effects due to high dosage requirements and may not be suitable for long-term use. Possible side effects with prolonged use includes, causing thinning or erosive changes to the conjunctiva, sclera, and epithelium [113, 122, 123].

Recently, intrastromal delivery of bevacizumab using a hypodermic needle have shown promising results [124]. Microneedle could make the intrastromal delivery simple and reliable procedure.

Microneedles are individual needles or arrays of micrometer-sized needles that are manufactured by adapting the tools of the microelectronics industry [104, 125, 126]. Solid microneedles were originally used for drug delivery to the skin, either by creating micron-scale holes in the skin to increase permeability [92] or by coating drug onto microneedles for rapid or controlled release by dissolution within the skin [127, 128]. A number of different drugs and vaccines have been delivered to animals and human subjects in this way [129-132].

More recently, microneedles have been studies for applications in the eye [69]. In a first study, solid microneedles coated with pilocarpine were applied to the cornea and shown to dramatically increase bioavailability of the drug in the anterior segment as evidenced by pupil dilation in rabbits [94]. Additional studies have addressed posterior segment delivery using solid and hollow microneedles for drug delivery into a scleral depot [95, 133] as well as drug delivery into the suprachoroidal space [66, 134].

In this study, we tested the hypothesis that microneedles coated with bevacizumab can deliver drug into the corneal stroma in a highly targeted and minimally invasive manner and thereby allow dramatic dose sparing compared to subconjunctival and topical delivery in an injury-induced neovascularization model. We designed the microneedles to be small enough to penetrate to a depth of hundreds of micrometers into the corneal stroma without crossing the corneal endothelium. This study assesses the efficacy of intrastromal delivery using microneedles in an injury-induced neovascularization model

and compares microneedle-based therapy to conventional topical and subconjunctival delivery of bevacizumab. We expect microneedle-based delivery to enable significant dose sparing by targeting bevacizumab precisely at the site of neovascularization in the corneal stroma to suppress blood vessel growth. This study presents the design, fabrication and characterization of microneedles coated with bevacizumab in both the ex vivo and in vivo rabbit eye to examine the efficacy and safety of this drug delivery method compared to topical and subconjunctival delivery.

3.2. MATERIALS AND METHODS

3.2.1. Fluorescent Labeling of Bevacizumab

Bevacizumab (Avastin, Genentech, South San Francisco, CA) was labeled using a SAIVI Alexa Fluor 750 Antibody/Protein labeling kit protocol (Invitrogen-Molecular Probes, Eugene, OR). Briefly, Alexa Fluor NHS esters were incubated with the protein in a basic medium (pH 9.3). Labeled protein (bevacizumab) was isolated and purified by gel filtration. The final dye-to-protein ratio (number of Alexa Fluor molecules coupled to each protein molecule) was determined to be between 2.5 and 3.5 according to a protocol from Invitrogen. Finally, this solution of labeled protein (8 mg/ml) was mixed with untagged bevacizumab (i.e, Avastin, 25 mg/ml) at a volumetric ratio of 1:1 and was stored in the dark at -4°C.

3.2.2. Enzyme-Linked Immunosorbent Assay (ELISA) of Bevacizumab

A serial dilution of bevacizumab (6.25–50 ng⁄ml) was used to generate a standard curve. Bevacizumab-coated microneedles were dissolved in phosphate-buffered saline (PBS) and diluted as needed to bring the concentration in the ELISA assay range. Diluted solutions were put in triplicates into wells in a Maxisorp ELISA plate (Nunc, Roskilde, Denmark). Plates with vascular endothelial growth factor ($VEGF_{165}$, R&D Systems, Minneapolis, MN) were coated overnight at 4°C in sodium carbonate buffer at pH 9.6. Plates were washed three times with PBS-T (PBS with 0.05% Tween-20) and blocked with 300 µl per well of 1% bovine serum albumin (BSA) in PBS for 2 h at room temperature. After three washes with 300 µl PBS-T each, 100 µl of bevacizumab-containing samples were added in triplicate for 2 h at room temperature. They were then washed three times with PBS-T as above and 100 µl horseradish peroxidase-labeled goat-anti-human IgG (R&D Systems) in 0.1% BSA per well and then incubated for 2 h at room temperature. Washing was performed as described and 100 µL of TMB (3,3', 5,5"-tetramethylbenzidine) substrate reagent solution (R&D Systems) was transferred into each well. Reaction was terminated after 20 min by adding 50 µl of 0.5 M HCl to each well. Absorbance was measured spectrophotometrically at a wavelength of 450 nm (iMark Microplate Reader, Bio-Rad, Hercules, CA).

3.2.3. Microneedle Fabrication And Coating

To make coating formulations, above solution was further diluted with stock solution of bevacizumab (i.e., Avastin, 25 mg/mL) at a volumetric ratio of 1:1. The mixed solution was repeatedly centrifuged using Nanosep centrifuge filters (Port

Washington, NY) with a 3 kDa molecular weight cutoff until the retentate reached a concentration of 100 mg/mL of bevacizumab. This solution was then immediately mixed with 5% carboxymethylcellulose at a volumetric ratio of 1:3 to make the final coating formulation [135]

Solid microneedles were fabricated by cutting needle structures from stainless steel sheets (SS304, 75 μm thick; McMaster Carr, Atlanta, GA) using an infrared laser (Resonetics Maestro, Nashua, NH) and then electropolished to yield microneedles of defined geometry that are 400 μm in length, 150 μm in width, 75 μm in thickness, and 55° in tip angle, as described previously [127]. Prior to coating, microneedles were treated with plasma cleaner to enhance coating of the formulation on the needle. Microneedles were coated by dipping 10 to 40 times into an aqueous coating solution at room temperature.

Hollow microneedles were fabricated from borosilicate micropipette tubes (Sutter Instrument, Novato, CA), as described previously [95]. A custom, pen-like device with a threaded cap was fabricated to position the microneedle and allow precise adjustment of its length, as described previously [67]. This device was attached to a gas-tight, 10-μl glass syringe (Thermo Scientific, Waltham, MA).

3.2.4. Ex Vivo Injection procedure and microneedle coating.

As a model drug, IgG antibody (20 mg/mL) was purchased from (Novus Biological, Littleton, CO) and mixed with carboxymethyl cellulose (2 wt%) at a volumetric ratio of 1:1 to make the final coating formulation [135]. Whole rabbit eyes were

purchased (Pel-Freez Biologicals, Rogers, AR) with the optic nerve attached. Eyes were shipped on ice and stored wet at 4°C for up to 2 days prior to use. Before use, eyes were allowed to come to room temperature, and any fat and conjunctiva were removed to expose the sclera. A catheter was inserted through the optic nerve into the vitreous and connected to a bottle of HBSS raised to a height that generated an internal eye pressure of 10 mm Hg, which mimics the lowered intraocular pressure in the rabbit eye under general anesthesia. The microneedle was then inserted perpendicular to the corneal surface for 20, 60, 120, and 180 s, and then removed.

3.2.5. Induction of Corneal Neovascularization

All animal studies adhered to the ARVO statement for the Use of Animals in Ophthalmic and Vision Research and were approved by the Georgia Institute of Technology Institutional Animal Care and Use Committee (IACUC). To simulate corneal neovascularization associated with minor traumatic injury, male and female New Zealand rabbits (2.2–2.5 kg) were anesthetized with ketamine (17 mg/kg), xylazine (8.5 mg/kg) and acepromazine (0.5 mg/kg) subcutaneously. Following topical administration of 0.5% proparacaine hydrochloride to minimize discomfort, a single 7.0-gauge silk suture (Ethicon TG140, Blue Ash, OH) was placed at midstromal depth 1 mm away from the limbus of the rabbit cornea. This silk suture was left in the rabbit cornea for the duration of the experiment to induce neovascularization [136, 137]. For each animal, a suture was placed in one eye and the companion eye was left untreated.

3.2.6. Measurement of Neovascularization

During the experiment, the rabbit eye was imaged using a digital camera (Cannon Rebel T1i, Melvile, NY) with macroscopic lens (Cannon MP-E 65mm) at 3X magnification every two days after placement of the suture. The area of neovascularization was quantified by determining the area using Adobe Photoshop (Adobe, Jan Jose, CA).

3.2.7. Experimental Treatment Groups

Prior to all treatment procedures except for topical delivery, rabbits were anesthetized with ketamine (6 mg/kg), xylazine (4 mg/kg) and acepromazine (0.25 mg/kg) subcutaneously. Reduced dose of anesthesia to reduce possible stress to an animal. A single drop of topical proparacaine ophthalmic solution was given as anesthesia. The duration of each study was 18 days and, after the suture insertion, we waited 4 days for neovascularization to develop. All the treatments were done at day 4 except for the untreated group that received no treatment. The treatment groups are listed in Table 3.2.7-1.

Table 3.2.7-1. Treatment groups for injury induced corneal neovascularization study

UT	Untreated group
TOP	Topical delivery group
SC	Subconjunctival groups
SC-high	High dose subconjunctival group
SC-low	Low dose subconjunctival group
MN	Microneedle delivery groups
MN-1bolus	1 microneedle bolus delivery group
MN-4bolus	4 microneedle bolus delivery group
MN-1x3	1 microneedle, 3 doses delivery group
MN-placebo	1 microneedle placebo group
MN-hollow	Hollow microneedle bolus delivery group

3.2.7.1 Untreated Group (UT)

Other than applying sutures to the eye, these animals received no further treatments.

3.2.7.2 Topical Delivery Group (TOP)

Topical delivery of bevacizumab was given into the upper conjunctival sack without anesthesia three times per day (at approximately noon, 3:00 pm and 6:00 pm) on day 4 through day 18. Each drop contained 1250 μg of bevacizumab in 50 μl, for a daily dose of 3750 μg of bevacizumab and a total dose of 52500 μg of bevacizumab over the course of 14 days of treatment.

3.2.7.3 Subconjunctival Delivery Groups (SC)

Bevacizumab was injected subconjunctivally with a 30-gauge hypodermic needle at the upper bulbar conjunctiva four days after suture placement. The high-dose group (SC-high) received 2500 μg of bevacuzumab (in 100 μL, i.e., Avastin). The low-dose group (SC-low) received 4.4 μg of bevacuzumab (Avastin was diluted with HBSS to 100 μL).

3.2.7.4 Microneedle Delivery Groups (MN)

Microneedles each coated with 1.1 μg of bevacizumab were inserted at the site of a silk suture and left in place for 1 min to allow dissolution of the coating. For the one-microneedle bolus delivery group (MN-1bolus), a single microneedle (i.e., 1.1 μg of bevacizumab) was given as a bolus dose four days after suture placement. For the four-microneedle bolus delivery group (MN-4bolus), four microneedles (i.e., 4.4 μg of bevacizumab) were given as a bolus dose four days after suture placement. For the one microneedle – three doses delivery group (MN-1x3), a single microneedle (i.e., 1.1 μg of bevacizumab) was given as at 4, 6 and 8 days after suture placement (i.e., for a total dose of 3.3 μg of bevacizumab). For the microneedle placebo group (MN-placebo), four microneedles coated with formulation containing no bevacizumab was given as a bolus dose four days after suture placement. Finally, for the hollow microneedle bolus delivery group (MN-hollow), a hollow microneedle was used to inject 2 μl of 25 mg/mL bevacizumab (i.e., Avastin, dose of 50 μg bevacizumab) intrastromally at the site of a silk suture as a bolus dose four days after suture placement. Eyelid was left closed for 5 min

and all the tear fluid was wiped off to collect all the residual bevacizumab that was not able to penetrate into the stroma using small piece of a kimwipe. The used kimwipes and microneedles were collected and dissolved into HBSS to collected residual bevacizumab.

3.2.7.5 Fluorescently Labeled Bevacizumab Imaging Study

Prior to imaging procedure, rabbits were anesthetized by subcutaneous injection of ketamine/xylazine/acepromazine at a concentration of 6/4/0.25 mg/kg. Eyes were kept open using lid speculum for the whole duration of the imaging procedures. The fluorescent signal intensity in the rabbits was imaged on a Caliper Xenogen Lumina In Vivo Imaging System (IVIS) at 0, 2, and 4 days post insertion. Animals were imaged at 745 nm excitation, 780 nm emission and 1 second exposure time. Fluorescence intensity was measured as background-subtracted average efficiency within a fixed region of interest (ROI) centered on the insertion site.

3.2.7.6 Safety Study

To identify possible microanatomical changes after intrastromal delivery using microneedles, we conducted a histological safety study using four study groups: (i) The untreated group received no suture and no other treatments. (ii) The suture-only group received a suture at day 0, but no other treatments. Animals were sacrificed on days 1, 10 and 18 for histological analysis. (iii). The suture with non-coated microneedles group received a suture on day 0 and four non-coated microneedles inserted at the site of the suture on day 4. Animals were sacrificed on days 1, 6 and 14 for histological analysis. (iv) The suture with coated microneedles group received a suture on day 0 and four microneedles each coated with 1.1 μg of bevacizumab inserted at the site of the suture on

day 4. Animals were sacrificed on days 10 and 18 for histological analysis. Suture placement and microneedle application were carried out as described above. High magnification images were taken every day in all study groups to assess possible gross corneal damage. Corneal tissues were fixed in 10% formalin and embedded in paraffin. Hematoxylin-eosin (HE) or periodic acid-Schiff (PAS) staining was performed.

3.2.7.7 Statistical Analysis

Replicate pharmacodynamics experiments were done for each treatment group above, multiple (3 – 6) images from which the mean and standard error of means were calculated. Experimental data were analyzed using two-way analysis of variance (ANOVA) to examine the difference between treatments. In all cases, a value of $p < 0.05$ was considered statistically significant.

3.3. RESULTS AND DISCUSSION

3.3.1. Characterization of Microneedles Coated With Bevacizumab

We first designed solid microneedles to penetrate into, but not across, the cornea and in that way deposit drug coated onto the microneedles within the corneal stroma at the site of microneedle penetration. These microneedles were made by laser-cutting the needle structures from stainless-steel sheets. Guided by the average rabbit corneal thickness of 400 μm [138] and possible tissue deformation during the needle insertion, the microneedles used for rabbit corneal insertion were 400 μm in length, 150 μm in width, 75 μm in thickness, and 55° in tip angle (Fig. 3.3.1.1.).

These microneedles were coated with a dry film of bevacizumab designed to rapidly dissolve off the microneedle after insertion into the cornea. Coatings were applied by dipping 10 – 40 times into a solution of bevacizumab using an automated coating machine.

Figure 3.3.1.1. Image of microneedle used in this study. Scale bar indicates 2mm.

3.3.2. Intrastromal Delivery of Bevacizumab Ex Vivo

To determine whether microneedles were strong and sharp enough to penetrate and deliver coated bevacizumab into the cornea, Texas Red-labeled IgG was used as a model compound, coated onto microneedles and inserted into rabbit cadaveric cornea for 20, 60, 120, and 180 s, and then removed. Bioavailability of IgG delivered using coated

microneedles was determined as a function of insertion time and coating amount (Fig. 3.3.2.1.). Bioavailability increased with longer insertion time, probably because of incomplete coating dissolution at shorter insertion times. Bioavailability increased with smaller amounts of IgG coated probably because thinner coating films dissolved more quickly.

We also sought to confirm that coated IgG molecules were delivered into the corneal stroma by taking brightfield, fluorescent, and H&E-stained images of the cornea before and after IgG delivery using microneedles.

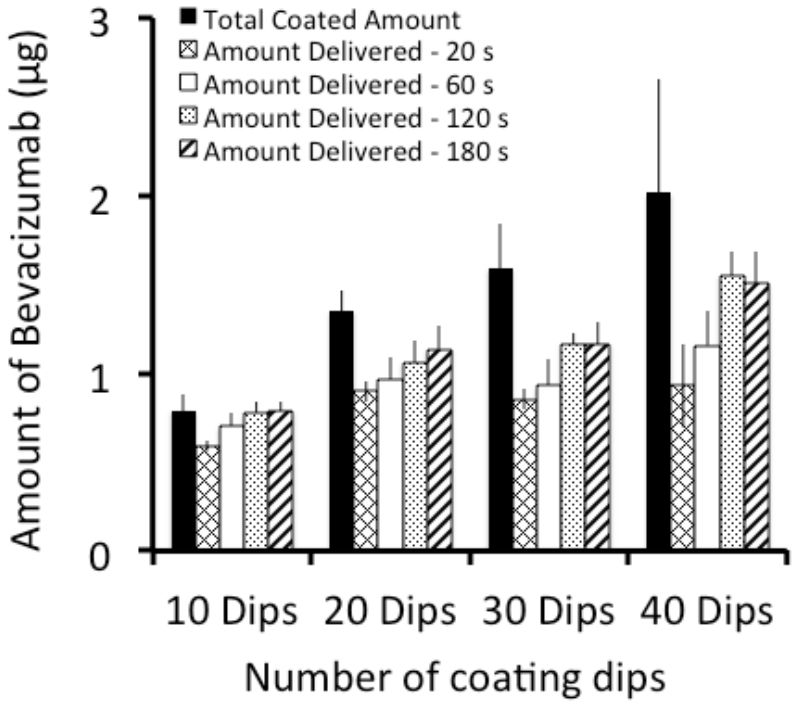

Figure 3.3.2.1. Coated amount on the microneedles and amount delivered in ex vivo for Texas Red labeled IgG coated microneedles at for different insertion time of 20, 60, 120, and 180 seconds.

3.3.3. Intrastromal Delivery of Bevacizumab In Vivo

We wanted to quantify in vivo bioavailability of bevacizumab delivered from coated microneedles by tagging the bevacizumab with florescent dye. Although we characterized the delivery of IgG molecules using microneedles ex vivo, for the in vivo study we expect to have lower bioavailability due to washout by tear fluid. Alexa Fluor 750 dyes were tagged to bevacizumab to quantify using ELISA. Two of the 10, 20, 30 or 40 dips coated microneedles were inserted into the cornea of an anesthetized rabbit. Amount was quantified using ELISA. Labeled-bevacizumab-coated microneedles were inserted into but not across the cornea for 60 s and then removed. We decided to use insertion time of 60 s because drying of the corneal surface might cause pain in patients and we wanted to mimic possible clinical scenarios as much as possible for our experiments.

Coating amount of bevacizumab on the microneedle increased linearly from 1.15 μg to 7.6 μg (Fig. 3.3.3.1a). On the other hand, the delivery amount does not increase linearly with coating amount (Fig. 3.3.3.1a). As mentioned previously, large coating volume makes it difficult for the entire coating to penetrate and dissolve into mid layer of a cornea. Measured in vivo bioavailability is lower compared to ex vivo bioavailability, which was expected due to low hydration of the cornea in vivo compared to ex vivo and washout from the tear fluid that is only present in vivo. Endothelial cells cornea is constantly pumping water out from the cornea and this allows in vivo cornea to be less hydrated. The calculated delivery amounts of microneedles were similar to our previous in vivo study using fluorescein in rabbit [94]. Due to large loss of bioavailability for 30

and 40 dips-coated microneedles, we decided to use 20 dips-coated microneedles, which can deliver 1.14 ± 0.11 μg of bevacizumab, for all of our pharmacodynamics test.

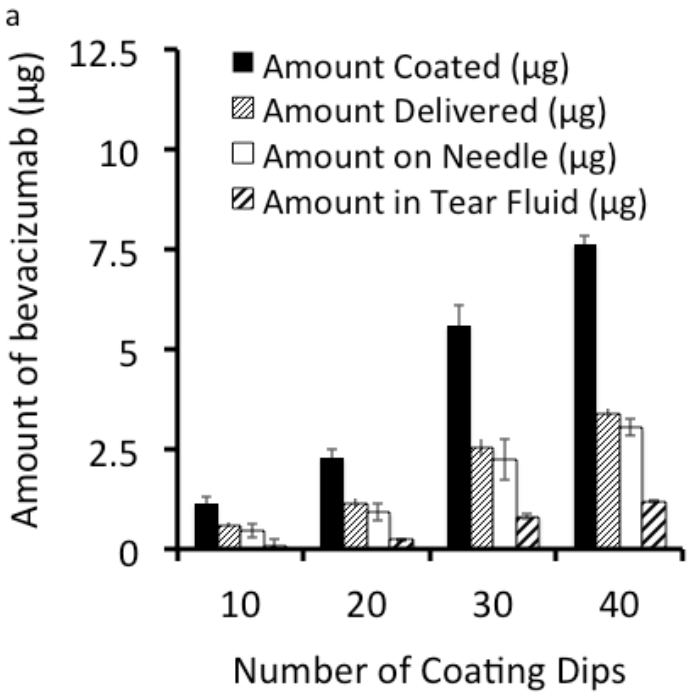

Figure 3.3.3.1. (a) Measured coating amount (μg), calculated amount delivered (μg), measured amount left on the needle (μg), and measured amount in tear fluid after the injection (μg).

3.3.4. Efficacy Of Intrastromal Delivery of Bevacizumab Using Microneedles Compared To Topical Delivery

To further assess the capability of microneedles as a drug delivery platform, we created injury-induced neovascularization in a rabbit model and delivered bevacizumab using both microneedles and topical eye drops. Topical eye drops of bevacizumab have been used before to treat corneal neovascularization, but with limited efficacy and adverse events for prolonged use [122, 123, 139]. We hypothesized that the highly

targeted delivery of bevacizumab within the corneal stroma provides a significant amount of dose sparing and better efficacy to suppress injury-induced neovascularization in a rabbit compared to topical delivery. A suture was inserted into the mid space of the cornea. After waiting for 4 days for the neovascularization to develop, all the treatments were started at day 4. All of the microneedles were coated one day prior to the animal experiments. To compare the pharmacodynamics between topical and microneedle delivery, we measured changes in vascularization area in the eyes using image analysis.

Figure 3.3.4.1. Corneal neovascularization after suture-induced injury. Photographs of rabbit cornea in vivo 18 days after applying a suture (a) with no treatment (UT) and (b) with a single treatment of bevacizumab using solid microneedles (MN-4bolus).

As negative controls, a group of rabbits were left untreated (UT) and another group of rabbits were treated with four placebo microneedles (MN-placebo). Untreated and placebo microneedles group showed similar kinetics with no statistical difference ($p = 0.11$) where the neovascularization area increased until day 10 and decreased slightly until day 18 (Figs. 3.3.4.1.a and 3.3.4.2.a). The peak neovascularization area for the

untreated group was 0.60 ± 0.06 mm^2 on day 10 and by day 18 area was 0.49 ± 0.05 mm^2 (Fig. 3.3.4.2.b).

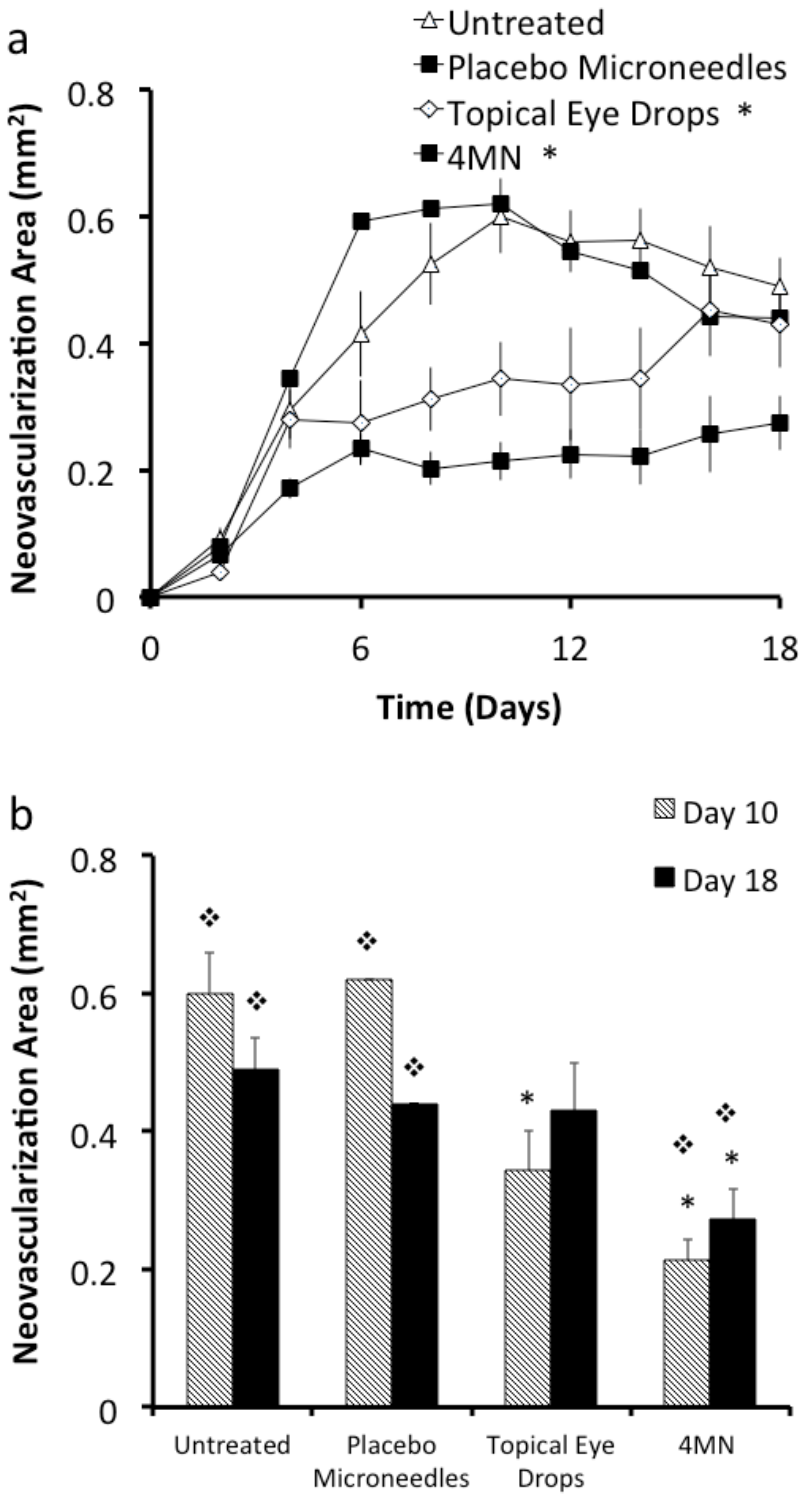

Figure 3.3.4.2. (a) Neovascularization area vs. time (days) and (b) comparison between vascularization area at day 10 and 18 for 4 treatment groups; untreated (UT), topical delivery (TOP), microneedle placebo (MN-placebo), and four-microneedles group (MN-4bolus). * - indicates significant difference (two-way ANOVA) relative untreated group; ❖- indicates significant difference (two-way ANOVA) relative to topical eye drop group.

For the topical delivery group (TOP), 3 topical eye drops were given every day from day 4 until the end of the experiment (day 18), which is a 52,500 μg of bevacizumab over period of 14 days or 3750 μg/day. Topical eye drops reduced neovascularization compared to the untreated eyes by 44% (day 10) and 6% (day 18) (Fig. 3.3.4.2.). The topical eye drops group showed an immediate inhibition of the blood vessel growth after starting the treatment at day 4. However, subsequently neovascularization area increased steadily until the end of the experiment. At day 18, topical eye drops group showed no significant difference between the untreated eyes (one-way ANOVA, $p = 0.36$). Two-way ANOVA analysis showed that change in vasculature area for topical group over time was significantly different from the untreated group ($p < 0.0001$).

For the microneedles group (MN-4bolus), eyes were treated with 4.4 μg of bevacizumab using 4 microneedles. Microneedles reduced vasculature area compared to the untreated eyes by 65% (day 10) and 44% (day 18) (Figs. 3.3.4.1. b and 3.3.4.2. b). Two-way ANOVA analysis showed a significant difference between the microneedles group and untreated group ($p < 0.0001$). Total topical bevacizumab dose that was given during the whole experiment was 52,500 μg. Although microneedles group resulted significantly better response, the dose sparing that we were able to achieve using

microneedles was 11931 times compared to topical delivery. The fact that the delivery of just 4.4 μg of intrastromal delivery using microneedles outperformed the 52,500 μg of topical application shows the ineffectiveness of the topical delivery. Assuming that delivery by microneedles achieved 100% bioavailability, the ratio between the two delivery amounts gives us an estimated bioavailability of less than 0.01% for topical delivery. Topical administration is a very valuable route for delivering small molecules into the cornea because it is non-invasive and results in minimal adverse events compared with systemic administration. However, topical delivery is not an effective method to deliver high molecular weight protein therapeutics into cornea due to its low bioavailability.

3.3.5. Efficacy Of Intrastromal Delivery of Bevacizumab Using Microneedles Compared To Subconjunctival Delivery

Next we sought to compare the pharmacodynamics effect between subconjunctival and microneedles delivery methods. There are reports in the literature that showed inhibition of blood vessel growth via subconjunctival delivery of bevacizumab [140-143]. We hypothesized highly targeted delivery of bevacizumab within the corneal stroma provides significant amount of dose sparing to suppress injury-induced neovascularization in a rabbit compared to subconjunctival delivery.

Compared to the untreated group (UT), we measured change in vascularization area in the eyes that were treated with high-dose (SC-high) and low-dose (SC-low) subconjunctival injection of bevacizumab. Based on the reported effective dose in literature [140-142], 2500 μg (i.e., 100 μL at 25 μg/μL) was given as a bolus on day 4 for the high-dose subconjunctival injection. For the low-dose subconjunctival injection, we

decided to match the microneedles dose that was able to inhibit neovascularization (Fig. 3.3.5.1.). For this group, 4.4 µg of bevacizumab was given as a bolus on day 4.

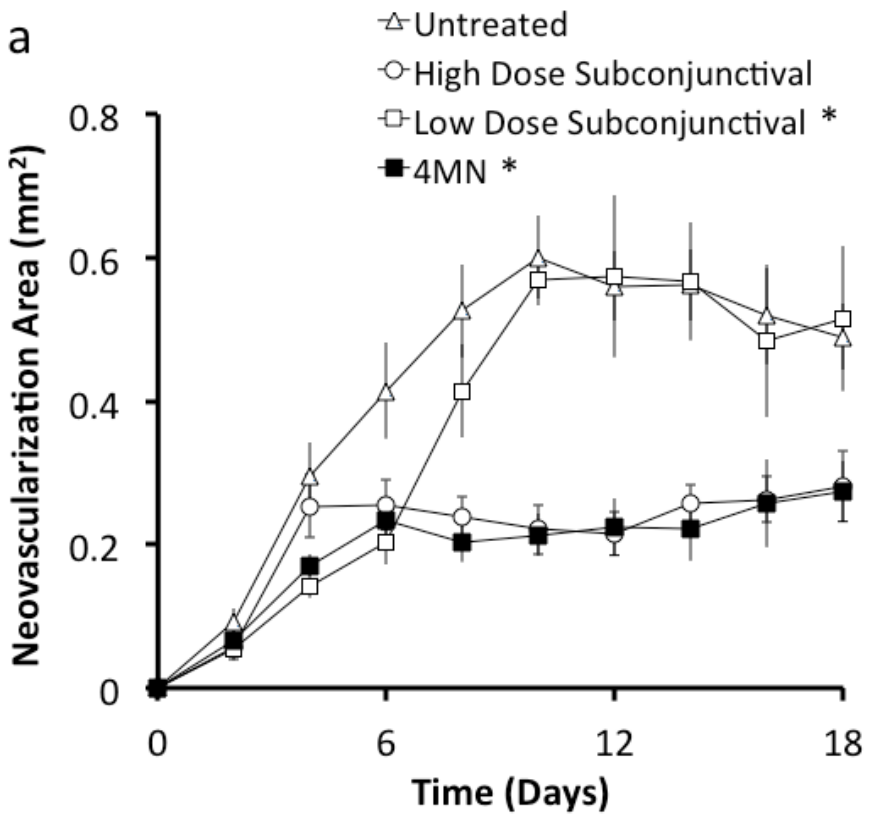

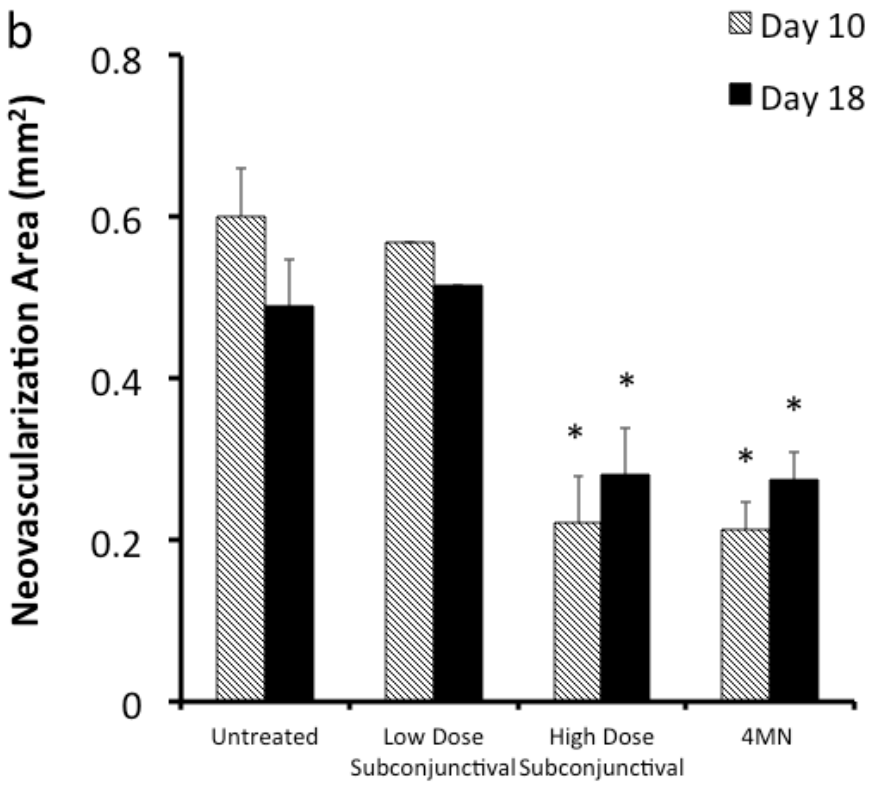

Figure 3.3.5.1. (a) Neovascularization area vs. time (days) and (b) comparison between vascularization area at day 10 and 18 for 4 treatment groups; untreated, low dose subconjunctival, high dose subconjunctival, and 4 microneedles group. * - indicates statistical difference (two-way ANOVA) compared to the untreated group.

Eyes treated with a low dose of 4.4 µg of bevacizumab using subconjunctival injection (SC-low) reduced neovascularization compared to the untreated eyes (UT) by 5% (day 10) and –5% (day 18). However, two-way ANOVA analysis showed that change in vasculature area for the low-dose subconjunctival group over time was not significantly different from the untreated group ($p = 0.05$).

For the high-dose subconjunctival injection (SC-high), eyes treated with 2500 µg of bevacizumab reduced neovascularization compared to the untreated eye by 62% (day

10) and 29% (day 18). A two-way ANOVA analysis showed that change in vasculature area for the high-dose subconjunctival group over time was significantly different from the untreated group (UT, $p < 0.0001$) and was not significantly different compared to the microneedles group (MN-4bolus, two-way ANOVA, $p = 0.45$).

Although the pharmacodynamic responses for both microneedles group and high dose subconjunctival injection were similar, the dose sparing that we were able to achieve using microneedles was 568 times compared high-dose subconjunctival injection. The intrastromal delivery of just 4.4 μg gave a similar response to 2500 μg given by subconjunctival injection. Assuming that delivery by microneedles achieved 100% bioavailability, the ratio between the two delivery amounts gives us an estimated bioavailability of 0.18% for high-dose subconjunctival delivery.

Subconjunctival injection is a valuable route for delivering therapeutics for corneal neovascularization. Subconjunctival injection delivers molecules into the site of neovascularization by using already generated vessels in the cornea, which acts as a conduit to deliver molecules to the site of action. This is because invasion of the blood vessel occurs from the subconjunctival space. However, subconjunctival delivery still requires a 568 times the dose of highly targeted intrastromal delivery. Considering possibility of high frequency of adverse events for prolonged topical administration of bevacizumab [113, 117, 122, 123], we expect intrastromal delivery could be an excellent alternative treatment to subconjunctival injection due to such a low dosage requirement.

3.3.6. Effect Of Bevacizumab Dose on Efficacy Of Intrastromal Delivery Using Microneedles

In the experiments so far, a single bevacizumab dose of 4.4 μg was given by microneedles. We therefore investigated other doses to better optimize the dosing regimen. We first investigated a lower dose of 1.1 μg given as a bolus on day 4 using a single microneedle (MN-1bolus). This treatment reduced neovascularization compared to the untreated eye by 34% (day 10) and 10% (day 18), which was significantly better reduction in neovascularization compared to the untreated group (UT, two-way ANOVA, $p = 0.001$) and was significant worse reduction in neovascularization compared to higher-dose microneedle group (MN-4bolus, two-way ANOVA, $p < 0.0009$). This shows that an intrastromal bolus of 1.1 μg bevacizumab is effective, but a bolus of 4.4 μg bevacizumab is more effective.

We next investigated administration of bevacizumab as multiple sequential doses, in which eyes were treated with one microneedle administering 1.1 μg bevacizumab on days 4, 6 and 8 (i.e., for a total of 3.3 μg bevacizumab). This protocol reduced neovascularization area compared to the untreated eye by 50% (day 10) and 41% (day 18), which was significantly better reduction in neovascularization compared to the untreated group (UT, two-way ANOVA, $p < 0.0009$) and was significantly different compared to the bolus high-dose microneedle group (MN-4bolus, two-way ANOVA, $p = 0.019$). The three-dose protocol appeared to have a delayed effect on inhibiting neovascularization, where the first dose had only a partial effect, but after the third dose inhibition of neovascularization was equivalent to that achieve with the high dose bolus.

This shows that multiple small doses can be as effective as a single high-dose bolus, but administration of a single bolus dose should be simpler in possible future clinical practice.

We finally investigated bolus intrastromal administration of an even higher dose of 50 μg of bevacizumab. This high dose would have required the use of 46-coated microneedles, which is impractical. We therefore used a Injection with a hollow microneedle (MN-hollow) reduced neovascularization compared to the untreated eye by 74% (day 10) and 45% (day 18), which was significantly better reduction in neovascularization compared to the untreated group (UT, two-way ANOVA, $p < 0.0009$) and was not significantly different compared to the bolus high-dose microneedle group (MN-4bolus, two-way ANOVA, $p = 0.154$). This shows that giving a bolus dose more than 4.4 μg of bevacizumab does not provide additional improvement. This may be because the 4.4 μg dose was able to inhibit further neovascularization and, based on the mechanism of bevacizumab action. Thus, the maximum effect of bevacizumab was achieved at an intrastromal dose of 4.4 μg.

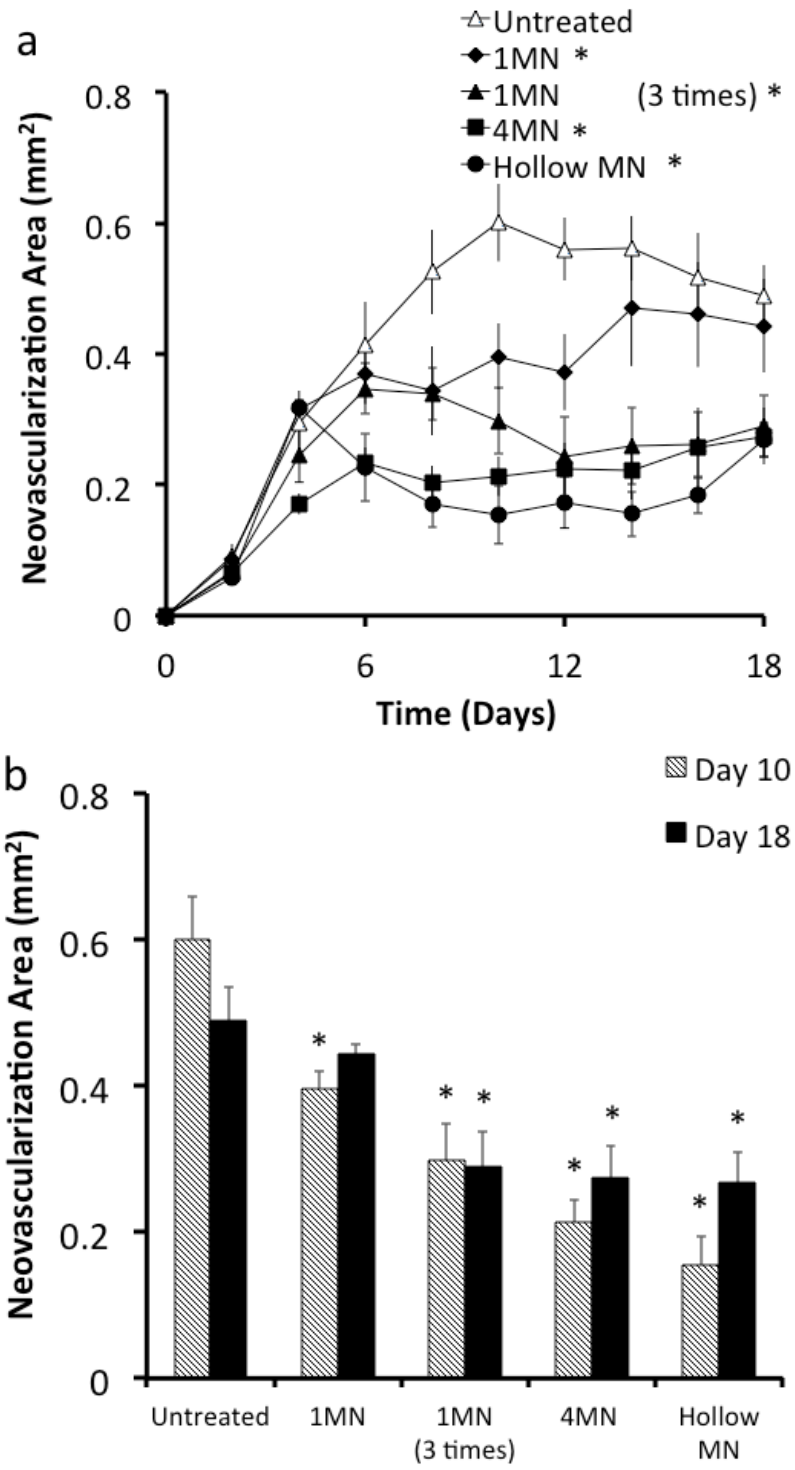

Figure 3.3.6.1. (a) Neovascularization area vs. time (days) and (b) comparison between vascularization area at day 10 and 18for 4 treatment groups; untreated, 1 microneedle group, 1 microneedles for 3 times, 4 microneedles group, and hollow microneedles

group. * - indicates statistical difference (two-way ANOVA) compared to the untreated group.

3.3.7. Safety Of Intrastromal Delivery Of Bevacizumab

We analyzed the corneas of four study groups to assess the safety of microneedles insertion by both magnified inspection of the corneal surface *in vivo* and histological examination of tissue sections obtained at various times after microneedle treatment. Fig. 3.3.7.2. a – 3.3.7.2. d shows a representative set of images of the corneal surface of a rabbit *in vivo* after insertion of a non-coated microneedle. Immediately after insertion and removal of the microneedle, a small puncture in the corneal epithelium is evident with a size on the order of ~100 μm (Fig. 3.3.7.1. a). By the next day, it was not possible to locate the insertion site even due to apparent repair of the epithelium (Fig. 3.3.7.1. b). Similarly, at later times the corneal surface continued to look fully intact and normal (Figs. 3.3.7.2. c – 3.3.7.2. d). We examined the injection site on a daily basis throughout the 18-day experiment, but we never saw any evidence of corneal opacity. We also examined eyes treated with bevacizumab-coated microneedles and again saw only a microscopic puncture in the corneal epithelium that disappeared within one day and was not associated with any complications (data not shown).

In addition to examining the corneal surface, we sacrificed animals at different time points to look for changes in corneal microanatomical structure. Histological analysis was carried out by an investigator board certified in both ophthalmology and anatomic pathology. Comparison between untreated eyes and eyes treated by insertion of non-coated microneedles exhibited no significant changes in microanatomical structure of the cornea; no evidence of the corneal puncture could be found (Fig. 3.3.7.2. e –

3.3.7.2. f). There was also no presence of macrophages or significant vascularization observed. We also compared histological sections from eyes that only had a suture applied to eyes that had been suture and then treated four days later with 1.1 µg bevacizumab using a microneedle. In the sutured eyes, there were large numbers of inflammatory cells present (Fig. 3.3.7.2. g) but there were no significant differences seen between sutured eye with and without no bevacizumab treatment using microneedles (Fig. 3.3.7.2. h).

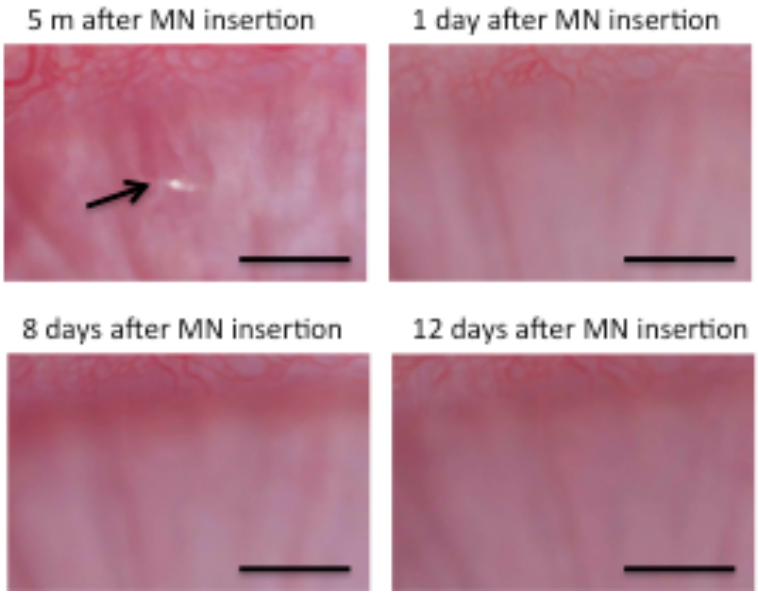

Figure 3.3.7.1. High magnification images of the cornea at the site of insertion of non-coated microneedles. Arrow points to site of microneedle insertion. Scale bar indicates 1 mm.

Altogether, these data indicate that insertion of microneedles into the corneal is minimally invasive and thereby has few or no adverse effects on the eye. Overall, no adverse effects were seen in any experiments in this study. Although this analysis

suggests that microneedle insertion into the eye may be well tolerated, additional studies are needed to assess safety more fully.

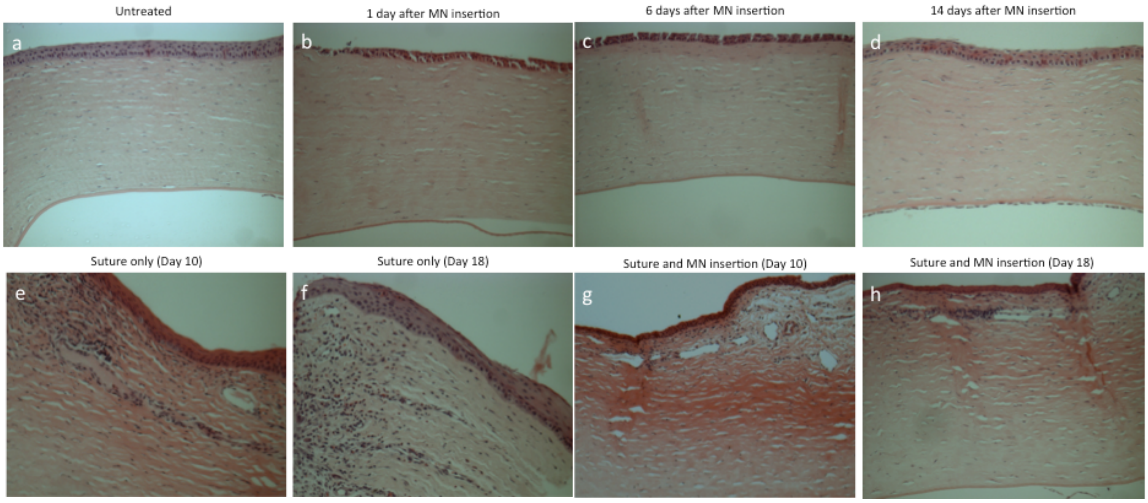

Figure 3.3.7.2. Histology images showing microanatomical structure of cornea for 4 treatment groups; (a) untreated, (b-d) microneedle placebo, (e-f) suture only, (g-h) and suture and MN insertion.

3.4. DISCUSSION

In this study, we sought to study capability of coated microneedle to deliver protein therapeutics to treat corneal neovascularization and compare them to subconjunctival and topical delivery. A series of experiment were conducted to measure the vascularization area in rabbit model using various different delivery methods. In vivo studies showed that bevacizumab can be rapidly delivered into the rabbit cornea for sustained delivery for many hours from a depot formed in the cornea with approximately 50% bioavailability. Injury induced corneal neovascularization model showed 52500 µg of topical delivery of bevacizumab decreased neovascularization area of 6% (day 18)

compared to untreated group. Topical delivery showed no statistical difference between untreated group at day 18. Whereas, 4.4 μg microneedle delivery was able to decrease in neovascularization area of 44% (day 18) compared to untreated group. This shows topical eye drops are very ineffective way to deliver protein therapeutics. We can expect that very small amount of drug will diffuse across the corneal epithelium, which has tight junctions around the epithelial cell that blocks penetration of the small molecules [6]. We expect damage caused by using large 7-gauge silk suture should enhance the topical penetration. However, the large hole created by the suture was not enough to create enough penetration to suppress neovascularization for 14 days.

Subconjunctival injection of 2500 μg of bevacizumab reduced neovascularization compared to the untreated eye by 29% (day 18). High dose subconjunctival injection gave same response compared to the 4.4 μg bevacizumab coated microneedle delivery group. Two-way ANOVA showed no statistical difference between the microneedle and high dose subconjunctival delivery group with p-value of 0.484. Microneedle group were able to achieve same response compared to high dose of subconjunctival injection with 568 times less dosage. Highly targeted delivery of an anti-VEGF therapeutic within the corneal stroma provides an effective means to suppress injury-induced neovascularization in the rabbit compared to subconjunctival and topical delivery. We expect dosage will be significantly lower in human because bevacizumab-binding kinetics is 7-8 times less in rabbits than human [144], thereby enabling long residence time of bevacizumab in the cornea.

Safety study was done to examine the effect of intrastromal delivery using microneedles on corneal opacity and micro-anatomical structure. We expect that small

incision using microneedles do not change corneal opacity because of a minimal damage it causes. Much more invasive surgery such as laser-assisted in situ keratomileusis (LASIK) is preformed in about 1 million patients each year in United States [145] alone without causing corneal opacity. We also expect very minimal concern with possible infection due to the damages in corneal epithelium since corneal epithelium is one of the fastest healing tissues in our body [6]. During the duration of the safety and pharmacodynamics study more than 8000 high magnification images were taken around the insertion site and at all times, there was never an evidence in change in corneal transparency. Multiple highly magnified images were taken to examination of microneedle-treated eyes revealed no adverse effects.

Recently there have been an increasing number of reports showing the efficacy of off label use of bevacizumab in treating corneal neovascularization [116-118]. However penetration of the high molecular weight (149kDa) drug into intact corneal epithelium is an issue. High dosage requirement for topical administration can results unwanted side effects with prolonged use includes, causing thinning or erosive changes to the conjunctiva, sclera, and epithelium [113, 122, 123]. Subconjunctival delivery gives better modality of delivery. However, there are still the possibility of causing side effects due to high dosage requirements and may not be suitable for long-term use. In clinics we expect microneedles treatment to be used as a supplementary treatment to immediately suppress the blood vessel ingrowth to cornea in addition to traditional topical or subconjunctival treatment. In clinics, we expect clinicians to make thoughtful decisions if patients can tolerate high dose of bevacizumab and its side effects. If not, we believe microneedles based delivery method is a great alternative treatment due to its significant amount of

dose sparing. The solid needles using for intrastromal delivery to administer a smaller payload (but given the tiny required dose of bevacizumab, it should be sufficient for this and other applications), but deposit the drug exactly at the site of microneedle insertion. This targeted deliver will enable us to achieve significant amount of dose sparing and formulation the system for longer-term bevacizumab delivery using the microneedles and microparticles.

The microneedle delivery methods developed for bevacizumab delivery to treat corneal neovascularization set the stage for delivery of other agents into the corneal stroma, for example to treat corneal infections, or to deliver agents into other ocular target tissues, such as conjunctiva, sclera [146].

3.5. CONCLUSION

This study provides the first demonstration of intrastromal administration using coated microneedles to deliver of protein therapeutic. We compared the pharmacodynamics of bevacizumab in treating corneal neovascularization in injury induced animal model. We showed microneedle enable targeted administration into the midstromal space and that anti-VEGF drugs administered this way show four and two-order-of-magnitude reduction in dose compared to topical and subconjunctival delivery, respectively. We showed microneedles does not affect corneal transparency and microanatomical structure. We concluded that highly targeted administration of bevacizumab into mid-stromal space allows significant dose sparing compared to both topical and subconjunctival delivery and may be applicable to minimally invasive

treatment of diseases of the anterior segments of the eye and may be applicable to minimally invasive treatment of diseases of the anterior segments of the eye.

4 FORMULATIONS TO TARGET DRUG DELIVERY WITHIN THE SUPRACHOROIDAL SPACE OF THE EYE

4.1. INTRODUCTION

Current ophthalmic drug delivery is constrained by the many natural barriers of eye, which prevent a drug from effectively penetrating into targeting tissues [47]. Many ocular diseases can lead to blindness and are preventable if managed correctly. However, pharmacotherapies for many vision-threatening diseases are not delivered to the targeting part of the eye to best obtain treatment efficacy. Currently, free drug formulations are administered by topical or intravitreal injection. And sustained release formulations are delivered as an implant that are placed in vitreous. However, targeting sites for vision threatening disease such as glaucoma, uveitis, and age related macular degeneration are located in the uvea [147, 148]. In the case of many anti-glaucoma drugs, that site of therapeutic action is not on the corneal surface but at the ciliary body [110, 111]. And the targeting sites for many of the posterior diseases are not at the center but along the periphery of the eye in the layer of choroid [147, 148]. Furthermore the non-targeted nature of currently used delivery methods allows possible adverse events and toxicity in the surrounding tissues. For example, the poorly targeted nature of eye drops leads to extensive systemic exposure, which causes up to 8-53% of glaucoma patients taking topical anti-glaucoma drugs to experience side effects [149, 150]. In case of intravitreal administration of steroids, unwanted contact with lens promotes the formation of cataract in 6.6% of the patients [151]. In addition, delivering sustained release formulation often requires surgical procedures to insert the implants. A novel delivery method that can deliver controlled release formulation around the eye in a non-invasive manner to

maintain high therapeutic levels of a drug in a targeting region of the eye, should provide more effective therapy for many of the vision threatening eye diseases.

Suprachoroidal injection allows an access from space immiditately above ciliary body anteriorly to immediately above the choroid posteriorly. The SCS is a potential space located between sclera and choroid that can expand to accommodate a fluid or drug formulation. The location of the SCS adjacent to the target site for treatment of diseases like glaucoma, wet AMD, diabetic retinopathy, and uveitis may provide higher drug levels in the target tissues. For this reason, the SCS represents a promising new site of administration for treatment many ocular diseases and has become a recent focus of drug delivery research [62-64, 152].

Recently, researchers have shown that there are several ways to access the suprachoroidal space. However, these methods involve using invasive techniques such as catheters or implants that are surgically placed into the eye to access suprachoroidal space [62, 65, 153]. Microneedle's microscopic size makes it an ideal device to deliver materials into suprachoroidal space. Microneedle allows precise placement of the needle tip right at the suprachoroidal space. Previously, microneedles have shown to deliver nanoparticles and microparticles into rabbit, pig, and human cadaver eyes [67]. In vivo study in rabbit model showed microneedle can deliver particles as large as 10 μm to posterior segment [66].

Suprachoroidal space injection provides precise placement of the drugs to the site of action. However, we want to better target within the suprachoroidal space. Using aqueous formulation, the injected polymeric particles covers a portion of the suprachorodial space but not well targeted towards either anteriorly to ciliary body or

posteriorly to the whole layer of the choroid. Anteriorly, injected formulation quickly spreads away from the injection site to target ciliary body [66-69].

To improve on this technique, we have developed formulation to enhance the spreading of the particles or to immobilize the particles at the site of injection. In this study, we tested the hypothesis that particles injected into the suprachoroidal space can be localized at the site of injection or broadly distributed throughout the suprachoroidal space by controlling properties of polymeric formulation such as molecular weight, and rheology. We used properties of non-Newtonian fluids to modulate the movement of both polymers and embedded particles. Many polymers we tested exhibit Non-Newtonian or shear-thinning behavior because of its molecular properties and structure. Non-Newtonian fluids are characterized by increase in viscosity as shear rate decreases or decrease in viscosity as shear rate increases. To widely distribute particles, we used weakly non-Newtonian or shear thinning polymers to prevent polymers and embedded particles to increase its viscosity upon injection into the tissue (e.g. low shear environment). To localize the delivery, we used strongly non-Newtonian (or shear thinning) polymers to significantly increase polymers viscosity upon injection into the tissue (e.g. low shear environment).

We first determined the mobility of particles inside the suprachoroidal space as a function of particle size in a saline formulation. We then examined the extent to which polymeric formulation could affect mobility of particles inside the suprachoroidal space to deliver particles immediately above the ciliary body and around the ocular globe in the suprachoroidal space, which exist immediately above the choroid. For the first time, this study presents methods to deliver polymeric particles to ciliary body and choroid as a

function of properties of polymeric formulation, such as rheology, and molecular weight. Overall, this study shows that the suprachoroidal route of administration can provide targeted delivery of particles to ciliary body and entire surface of choroid in minimally invasive way using a microneedle.

4.2. MATERIALS AND METHODS

4.2.1. Microneedle Fabrication

Microneedles were fabricated from 33-gauge needle cannulas (TSK Laboratories, Tochigi, Japan). The cannulas were shortened to approximately 750 μm in length and the bevel at the orifice was shaped using a laser (Resonetics Maestro, Nashua, NH). The microneedles were electropolished using an E399 electropolisher (ESMA, South Holland, IL) and cleaned with deionized water, as described previously [66]. Microneedles were attached to gas-tight, 100-250 ml glass syringes (Thermo Scientific™ Gas-Tight GC Syringes, Waltham, MA) containing the formulation to be injected.

4.2.2. Formulations

All solutions for injection were prepared by mixing 2 wt% carboxylate-modified FluoSpheres in water (Invitrogen, Grand Island, NY), 0.2 wt% Sky Blue particles in water (Spherotech, Lake Forest, IL) and polymer formulations dissolved in Hank's balanced salt solution (HBSS, Manassas, VA) at a volumetric ratio of 1:1:2. Fluospheres were labeled with red-fluorescent dye and Sky Blue particles were labeled with infrared-fluorescent dye. Particles having diameters of 20 nm, 200 nm, 2 μm or 10 μm were used,

but in a given formulation, only one diameter particle was used and both the FluoSpheres and Sky Blue particles had the same diameter. The polymeric formulations were made using carboxymethyl cellulose (Sigma Aldrich, St. Louis, MO), hyaluronic acid (R&D Systems, Minneapolis, MN), methyl cellulose (Alfa Aesar, Ward Hill, MA), and DiscoVisc® (Alcon, Fort Worth, TX).

4.2.3. Viscosity Measurements

The viscosity (η) measurements were carried out on an MCR300 controlled stress rheometer (Anton Paar, Ashland, VA) equipped with Peltier elements for temperature control and an evaporation blocker that enables measurements of polymer solutions at elevated temperature in a cone-plate geometry. The viscosities of all samples were measured at shear rates from 0.01 s^{-1} to 100 s^{-1}. The viscosity reported for each sample in this study was matched at a shear rate of 0.1 s^{-1}. The measurements were carried out at 39°C to mimic the temperature of the living rabbit eye [154]. Multiple measurements were performed, and their average is reported.

4.2.4. Ex Vivo Injection Procedure

Whole rabbit eyes were purchased (Pel-Freez Biologicals, Rogers, AR) with the optic nerve attached. Eyes were shipped on ice and stored wet at 4°C for up to 2 days prior to use. Before use, eyes were allowed to come to room temperature, and any fat and conjunctiva were removed to expose the sclera. A catheter was inserted through the optic nerve into the vitreous and connected to a bottle of BSS raised to a height that generated

an internal eye pressure of 10 mm Hg, which mimics the lowered intraocular pressure in the rabbit eye under general anesthesia. The microneedle was then inserted perpendicular to the sclera surface 3 mm posterior from the limbus. A volume of 50 μL or 100 μL was injected within 15 s and an additional 30 s was allowed before removing the microneedle from the eye to prevent excessive reflux.

4.2.5. In Vivo Injection Procedure

Microneedle injections were carried out in New Zealand White rabbits (Charles River Breeding Laboratories, Wilmington, MA). All injections were done under systemic anesthesia by subcutaneous injection of a mixture of ketamine/xylazine/acepromazine at a concentration of 17.5/8.5/0.5 mg/kg. A drop of 0.5% proparacaine was given 2 - 3 min before injection as a topical anesthetic. To perform a suprachoroidal injection, the eyelid of the rabbit eye was pushed back and the microneedle was inserted into the sclera 3 mm posterior to the limbus in the superior temporal quadrant of the eye. A volume of 50 μL or 100 μL was injected within 15 s and additional 30 s was allowed before removing the microneedle from the eye to prevent excessive reflux. At terminal study endpoints, rabbits were euthanized with an injection of pentobarbital through the ear vein. The eyes were enucleated after death and processed for further analysis. All animal studies were carried out with approval for the Georgia Institute of Technology Institutional Animal Care and Use Committee (IACUC).

4.2.6. In Vivo Imaging Procedure

Rabbits were anesthetized by subcutaneous injection of a mixture of ketamine/xylazine/acepromazine at a concentration of 6/4/0.25 mg/kg, and suprachoroidal injection was performed as described above. Eyes were then kept open using a lid speculum for the duration of the imaging procedures. The fluorescent signal intensity in the rabbits was measured on a Caliper Xenogen Lumina In Vivo Imaging System (IVIS Lumina, Waltham, MA). Animals were imaged at 680 nm excitation, 720 nm emission and 1 s exposure time. Fluorescence intensity was measured as background-subtracted average efficiency within a fixed region of interest (ROI) centered on the microneedle injection site.

4.2.7. Tissue Processing And Measurement Of Fluorescence Intensity

Immediately after suprachoroidal injection in rabbit eyes ex vivo and immediately after enucleation of rabbit eyes in vivo, eyes were snap frozen in an isopropyl alcohol (2-isopropanol, Sigma Aldrich, St. Louis, MO) bath, which was cooled in dry ice. After the eyes are completely frozen, they were removed and eight radial cuts were made from the optic nerve on the posterior side to the limbus on the anterior side of each eye. Each of the eight pieces of cut tissue was then peeled away outward exposing the chorioretinal surface inside the eye. This made the eyes into a flat mount-like configuration, exposing the injected dyes for imaging. Brightfield and fluorescence images (Fig. 4.3.1.1) were taken using digital camera (Cannon Rebel T1i, Melvile, NY). Green light bulb (Feit Electric, Pico Rivera, CA) was used to excite the florescent particles and red camera filter (Tiffen red filter, Hauppauge, NY) was mounted on a digital camera to visualize the

distribution of particles inside the suprachoroidal space. Obtained images were used to quantify the suprachoroidal space area containing injected particles using Adobe Photoshop (Adobe, Jan Jose, CA). Each of the eight tissue pieces was then divided into additional two pieces. The cuts were made 6 mm antero-posteriorly from the ciliary body, which is the starting point of the suprachoroidal space. From hereafter, we will be refereeing to ocular tissue 0 mm from the ciliary body to 6 mm away from the ciliary body as "anterior SCS". Likewise, ocular tissue 6 mm away from the ciliary body to the rest of the ocular tissue will be hereafter referred to as "posterior SCS". This results in a total of 16 tissue pieces from each eye. Each of the 16 pieces was then put into separate vials containing BSS solution and homogenized (Fisher Scientific PowerGen, Pittsburgh, PA) to extract injected fluorescent particles. The liquid part of the homogenate was pipetted out into 96 well plates to measure fluorescent signal intensity (Synergy Microplate Reader, Winooski, VT). In order to quantify radial distribution of particles, ocular tissue was divided into 2 segments radially: ocular tissue in -90° to 90° from the injection sites (hereafter referred to as "superior SCS") and ocular tissue in 90° to 270° from the injection site (hereafter referred to as "inferior SCS").

4.2.8. Statistical Analysis

Replicate experiments were done for each treatment group, from which the mean and standard deviation were calculated. Experimental data were analyzed using both one and two-way analysis of variance (ANOVA) to examine differences between treatments. In all cases, a value of $p < 0.05$ was considered statistically significant.

4.3. RESULTS AND DISCUSSION

4.3.1.1 Distribution of Nanoparticles and Microparticles in the Suprachoroidal Space

Fluorescently tagged, polystyrene particles with various diameters (20 nm, 200 nm, 2 µm, 10 µm) were suspended in 50 µL of Hank's balanced salt solution (HBSS) and injected into the SCS of New Zealand White rabbit eyes using a hollow microneedle inserted 3 mm posterior to the limbus. The distribution and number of particles in the SCS was determined immediately after injection into rabbit cadaver eyes ex vivo and was determined 14 or 112 days after injection into living rabbit eyes in vivo. Fig. 4.2.8.1. displays images of a representative eye cut open in a flat-mount presentation showing the distribution of fluorescent particles in the SCS. Quantitative analysis of images like these was used to generate the SCS surface area coverage data described immediately below.

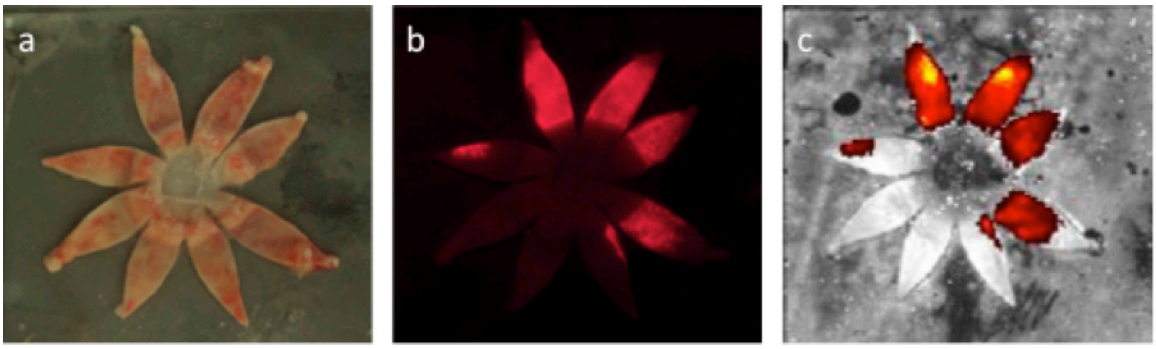

Figure 4.2.8.1. Bright field image of flat mounted eye (a), florescent image of the red fluorescent particles (b), and fluorescent image of near-infrared particles (c).

Immediately after injection, the particles covered 29% - 42% of the SCS surface area (Fig. 4.2.8.2). There was no significant effect of particle size on SCS surface area coverage (one-way ANOVA, $p > 0.10$). Fourteen days after injection, the SCS coverage

area did not significantly change for any of the particle sizes studied. Two-way ANOVA analysis showed no significant difference between the SCS coverage area ($p = 0.75$) and particle size ($p = 0.11$). Likewise, there was no interaction between time and size of the particles ($p = 0.16$). One-way ANOVA was also done, but no significant difference was shown for the individual particle sizes between days 0 and 14.

Between days 14 and 112, there was a significant decrease in the SCS coverage area to 24% - 32% of the SCS. This represents a reduction of 9% - 35% of SCS coverage area. Two-way ANOVA analysis showed a significant difference in SCS coverage area between day 14 and 112 ($p < 0.001$), but there was no significant effect of particle sizes ($p = 0.167$). There was no significant interaction between time and particle size ($p = 0.21$). One-way ANOVA was also done and a significant change in SCS coverage area was shown for 20 nm, 2 μm, and 10 μm particles (but not 200 nm particles) between days 14 and 112.

In addition to measuring SCS coverage area, fluorescent signal intensity of the particles was measured. The fluorescent signal intensity of particles in the SCS between days 0 and 14 showed no significant difference (two-way ANOVA) as a function of time ($p = 0.13$) and particle size ($p = 0.05$). There was also no significant interaction between time and particle size ($p = 0.1$). This suggests that there was no significant clearance of particles during the first 14 days after injection.

However, the number of particles appeared to decrease between days 14 and 112, as shown by fluorescence intensities of 31% - 61% of original values (at day 0). This suggests a 39% - 69% reduction in the number of particles. Two-way ANOVA analysis showed a significant difference in particle fluorescence between days 14 and 112

($p<0.001$), but not as a function of particle size ($p = 0.17$). There was also no significant interaction between time and particle size ($p=0.21$). One-way ANOVA analysis demonstrated a significant decrease of fluorescence intensity for the smaller particle sizes (20 nm, 200 nm and 2 µm), but not for the 10 µm particles.

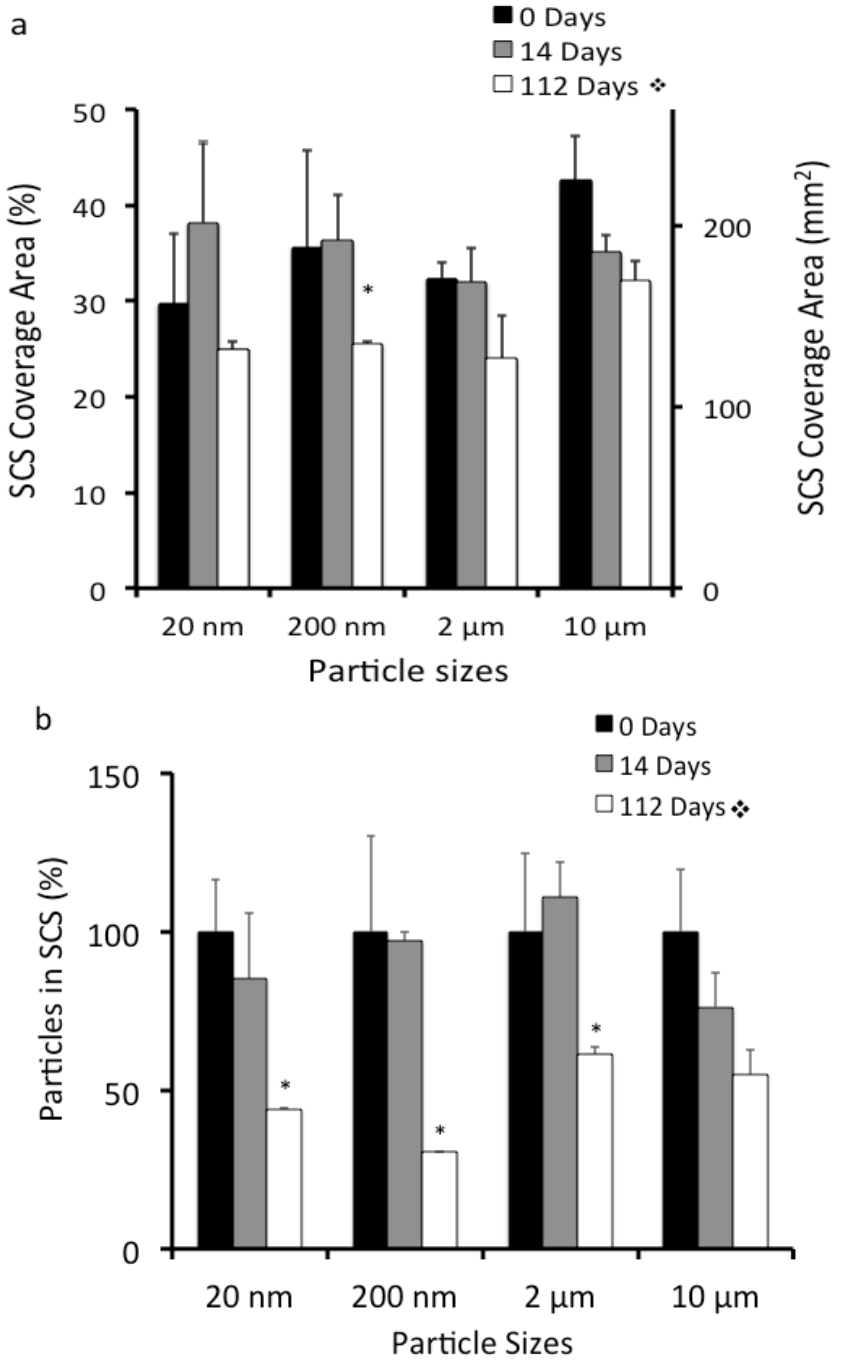

Figure 4.2.8.2. Suprachoroidal space injection of nanoparticles and microparticles. (a) Suprachoroidal surface coverage area as function of time and particle sizes. (b) Mass of particles in suprachoroidal space as a function of time and particle sizes. * - Statistical difference (one-way ANOVA) between day 14 and 112. ❖- Statistical difference (two-way ANOVA) between day 14 and 112.

Overall, these data show that the injected particles spread over a coverage area of about one-third of the SCS. Within 14 days, there was little movement or loss of particles in the SCS, but after 112 days, there was a significant reduction in coverage area to about one-quarter of the SCS and there was a significant reduction in the number of particles in the SCS to about half of the particles originally injected.

We expect that loss of fluorescent particles is either due to removal by macrophages (i.e., true clearance) or a reduction of the fluorescence signal intensity over time (i.e., artifact). To assess the relative roles of these two possible mechanisms, we measured the decrease in fluorescence intensity of 20 nm, 200 nm, 20 μm, and 10 μm particles in HBSS after storage for 112 days in the dark at 39 °C to mimic conditions in the SCS of the rabbit eye. These particles lost 25±6.5% of their fluorescence signal intensity. This suggests that particle clearance from the eye may not be as extensive as reported, but loss of fluorescence signal cannot fully explain the loss.

4.3.2. Polymer characterization

The main objectives for this study were to develop formulation to deliver polymeric particles immediately above the choroid and ciliary body.

In order to target choroid layer, injected particle need to travel around the ocular globe to cover entire layer of the SCS, which is immediately above choroid. For targeting ciliary body, injected particles should be immobilized at the site of the injection and immediately above the ciliary body. To achieve this goal, various polymeric excipient formulations were injected along with particles to decrease or increase the mobility of particles. The hypothesized is that high molecular weight, and weakly non-Newtonian materials rapidly expand its volume along with embedded particles and causes movement of particles inside the suprachoroidal space. Likewise, we hypothesized that strongly non-Newtonian material resists spreading of embedded particles away from the injection site due to its high viscosity at low shear rate.

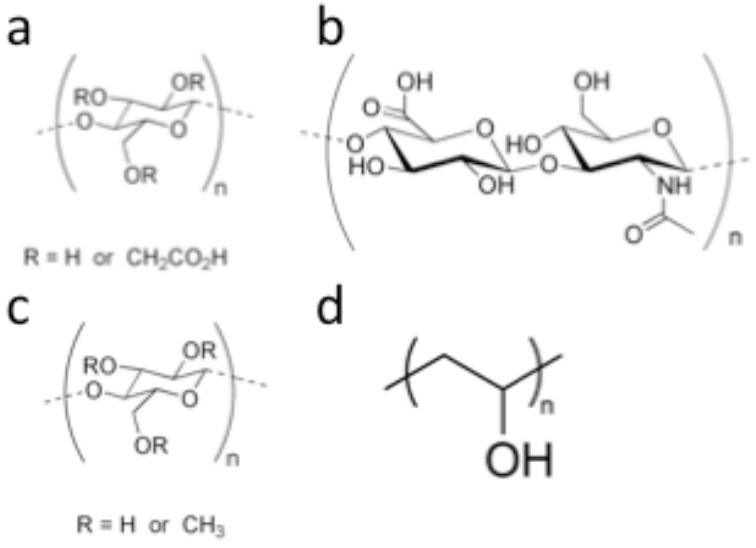

Figure 4.3.2.1. Molecular structure of (a) carboxymethyl cellulose (CMC), (b) hyaluronic acid (HA), (c) methyl cellulose (MC), and (d) poly vinyl alcohol (PVA).

Delivery of polymeric particles were critical parameter that we have considered because of its capability to encapsulate variety of compounds and achieve long-term sustained release that can last many months [155]. We also wanted to use materials that are currently used in pharmaceutical formulation to avoid additional toxicology studies to be readily applicable in human use. We also wanted a system that is simple and easy to use. Many in situ gelling polymers such as solvent removal, temperature, pH, or light mediated did not have characteristics that we were looking for. Solvent removal system involves using organic solvents that denature polymeric particles or proteins. pH or temperature sensitive polymers have very low viscosity before the injection that will quickly spreads away from the injection site before it gels. Furthermore, light sensitive polymers require complex equipment and procedures to be more broadly applicable. We needed a formulation that could resist initial spreading of polymeric particles after the injection and could deliver polymeric particles for a long-term sustained release. For immobilizing particles, we need a formulation that gels to hold the particles in place. But we also need a formulation that has significant viscosity initially to localize the injected formulation during the injection procedure.

In order to promote spreading of particles, we decided to use a polysaccharide as a potential material due to its excellent biocompatibility [156]. Ideal material to should have very hydrophilic characteristic to absorb water to promote spreading of embedded particles. The material should also have high molecular weight to maintain its

concentration within the suprachoroidal space and keep the suprachoroidal space open during swelling process, which will promote movement of embedded particles as polymer swell inside the suprachoroidal space. Furthermore, the ideal material should not exhibit increase in viscosity at low shear rate because we do not want the material to gel. We decided to use hyaluronic acids based material due to its excellent biocompatibility and its favorable characteristics. Rheological analysis showed HA based materials does not increase as its viscosity at low shear rate. Viscosity rapidly plateaus out at shear rate of less than 1 s^{-1}. However, at higher shear rate, the HA exhibits non-Newtonian property to make injection easier.

In addition to HA formulation, we decided to use one additional HA based formulation that are commercially available in the market. Discovisc® (DV) is a viscoelastic material that is used in ophthalmic surgery to protect delicate ocular tissue [157]. DV has contains 17% (w/v) of 1.7 MDa HA formulation in addition to low molecular weight (22 kDa) sodium chondroitin sulfate [157]. We wanted to assess material that is already approved by food and drug administration (FDA). Smaller particles are more likely to be cleared by macrophages, which was also evident in previous aqueous formulation study. Therefore all the experiment was done using 10 μm particles.

In order to study increase the suprachoroidal coverage area we tested the effect of concentration of polymeric excipients on particle's suprachoroidal space coverage area. Considering majority of compound in DV is HA we expected it to have similar rheological characteristics compared to pure HA formulation. Rheological analysis of DV indeed showed similar characteristics to pure HA formulation (Fig. 4.3.2.2.). In addition

to DV formulation, we tested 2 and 4 times the concentration of DV to study the effect of concentration. The hypothesis is that increase in concentration enhances the spreading due to increase swelling of the volume within suprachoroidal space.

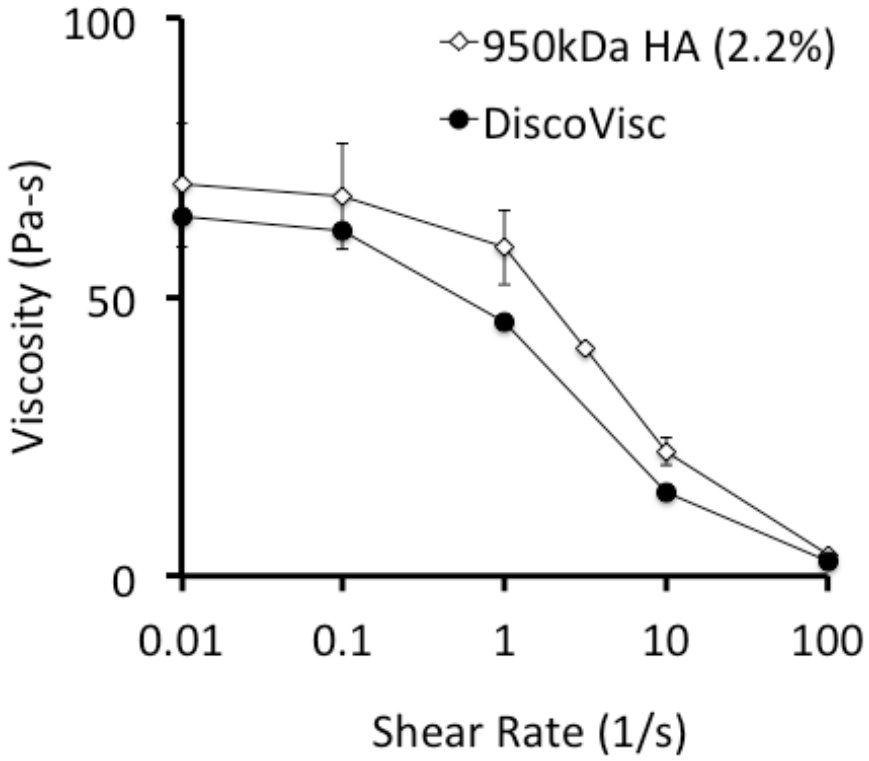

Figure 4.3.2.2. Rheological behavior of hyaluronic acid and Discovisc® showing the viscosity as a function of shear rate (s^{-1}).

We again decided examine polysaccharides as potential formulation to immobilize particles inside the suprachoroidal space due to its excellent biocompatibility [156]. We selected 700kDa carboxymethylcellulose (CMC) and 90kDa methylcellulose (MC) as a potential material to immobilize polymeric particles due to many of its favorable characteristics. Both 700kDa CMC and 90kDa MC are shear thinning material

that has low viscosity at high shear stress but it restores its high viscosity at low shear rate (Fig. 4.3.2.3.). Rheological analysis showed these materials have extremely strong non-Newtonian (Fig. 4.3.2.3.). Upon injection, the materials restores its high viscosity to immobilize the injected particles in SCS. Shear thinning property of the CMC comes from the high molecular weight nature of the material. Rheological analysis of lower molecular weight (90 and 250 kDa) CMC shows this property (Fig. 4.3.2.3.b). In addition, this shear thinning property will lower required pressure to achieve successful injection of a high viscosity material during the injection procedure. In order to experimentally test the hypothesis and its impact on spreading of the embedded particles inside the suprachoroidal space, we also tested 90kDa CMC (12%) that shows relatively weakly non-Newtonian (Fig. 4.3.2.3).

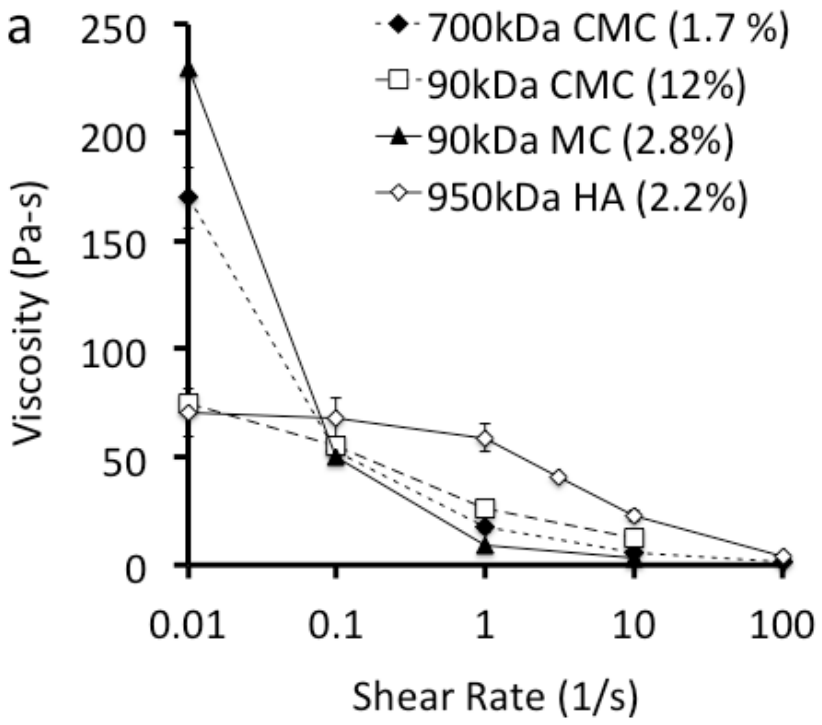

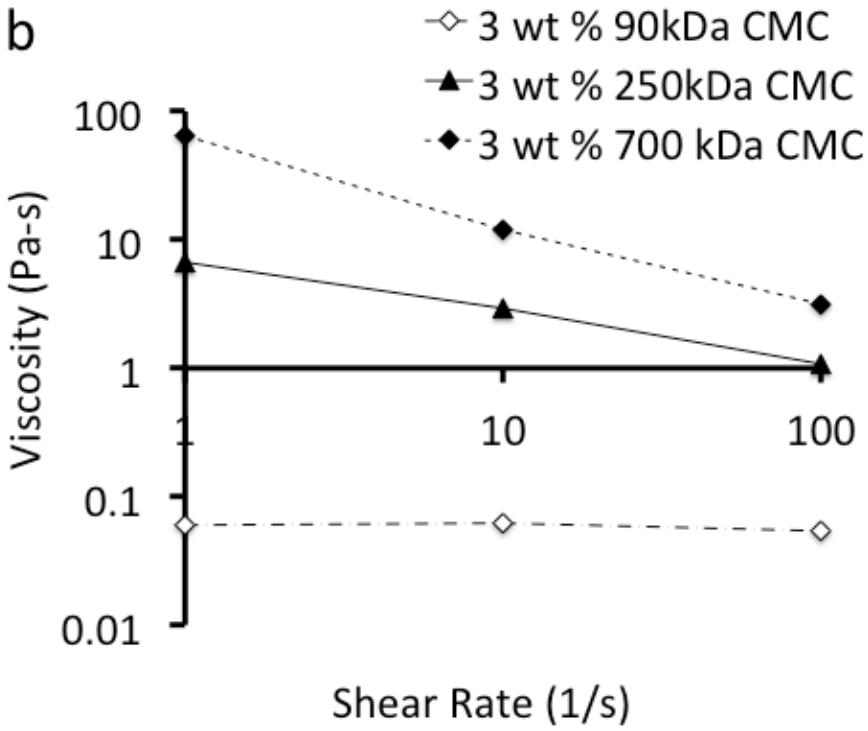

Figure 4.3.2.3. Rheological behavior of CMC, MC, and HA showing the viscosity as a function of shear rate (s^{-1}). (b) Rheological behavior of different molecular weight of CMC (log-log plot).

4.3.3. Formulations to enhance spreading of particles inside the suprachoroidal space

To test spreading of particles inside the suprachroroidal space, we sought to compare suprachoroidal space coverage area immediately after the injection and 14 days after injection. All the initial suprachoroidal space coverage area was done in ex vivo eyes (Pel-Freez Biologicals), as it would not make difference to do the experiment in live rabbit. SCS coverage area of HBSS formulation was also done as a comparison. Immediately after the injection, the particles with polymeric formulations covered 8.3% -

11% of the SCS surface area (Fig. 4.3.3.1.a). This is expected because the formulation is viscous. In contrast HBSS formulation covers 42% of the SCS space initially.

Fourteen days after injection, the SCS coverage area drastically changed for all the HA based formulations. SCS surface coverage areas for 950 kDa HA, 1X, 2X, 4X-DV formulation covered 61% - 85% of the SCS surface (Fig. 4.3.3.1.a). This represents a 5.7- to 8.7-fold increase in SCS coverage area for HA based formulation between days 0 and 14. These significant changes in SCS coverage area showed HA based formulations are capable of enhancing spreading of embedded particles. In comparison to HBSS formulation, the polymeric formulations showed 0.77 – 1.3 fold increase in suprachoroidal space coverage areas after 14 days. One-way ANOVA analysis of between HBSS and polymeric formulations (950kDa HA, 1X, 2X, 4X-DV) showed p-values of 0.018, 0.00052, 0.0094, and 0.0019, respectively. Statistically significant difference was shown for all the HA based formulations. The results also showed the higher concentration of HA formulation resulted in increase in SCS coverage area of the delivered particles. Although there was an increase in coverage area between 1X and 2X-DV formulation, we did not observe any statistically significant increase in coverage area between 2X and 4X-DV formulations. The mechanism behind this needs further studying. In an effort to examine if polymeric formulation could be used to cover entire SCS, we tested increased volume (100µ) of 4X-DV formulation. The results showed the coverage of the entire SCS coverage with single injection after 14 days. In addition to measuring the SCS coverage area 14 days after the injection, we also used IVIS (in vivo imaging system) to get a sense of time scale that this movement of particles is happening. The florescent measurement at the injection site over period of 14 days showed all the

movement of particles happened within 2 days after injection (Fig 4.3.3.1.c). However, further studies are required to fully characterize the movement of particles at different locations within the ocular globe.

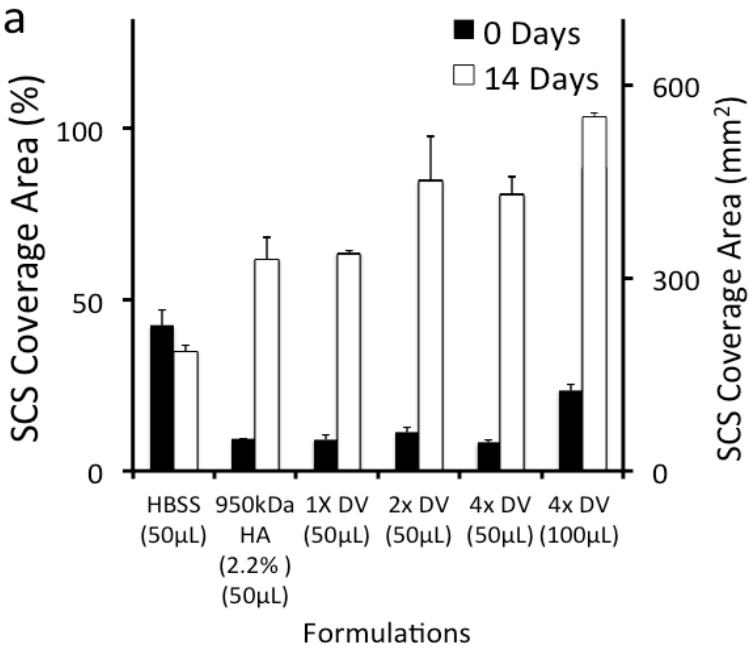

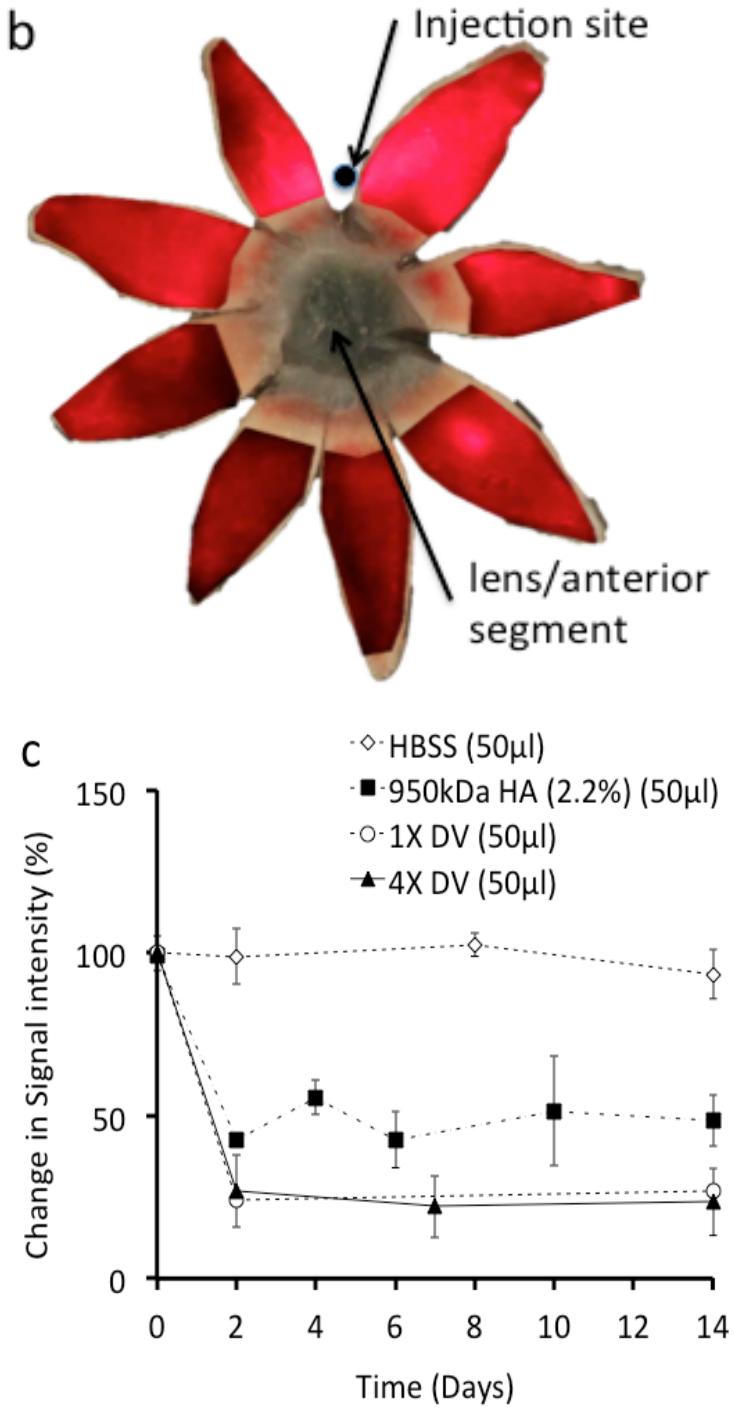

Figure 4.3.3.1. (a) Suprachoroidal surface coverage area for different HA based polymeric compounds between 0 and 14 days. (b) Eyes injected with 4X concentration of DiscoVisc® formulation after 14 days. Merged bright field florescent image showing the

spreading of particles inside the suprachoroidal space. (c) Change in signal intensity at the site of injection over the period of 14 days after the injection for different polymeric formulations.

Physical delivery of particles to the targeting site is important but how much we can deliver is also an important factor to consider. In addition to SCS coverage area, particle weight percent distribution was measured antero-posteriorly to characterize the mobility of particles inside the suprachoroidal space. For the in vivo experiment, the amounts of particles (%) in posterior SCS for 950kDa HA, DV (50 μL), 2X DV (50 μL), 4X DV (50 μL), and 4X DV (100 μL) formulation were 31-49 %. Likewise, amount of particles (%) for HBSS formulation was 29±15%. One-way ANOVA analysis of HBSS and HA formulations showed p-value of 0.69, 0.021, 0.0070, 0.012, and 0.00014, respectively. Statistically significant difference was found for all the DV formulations.

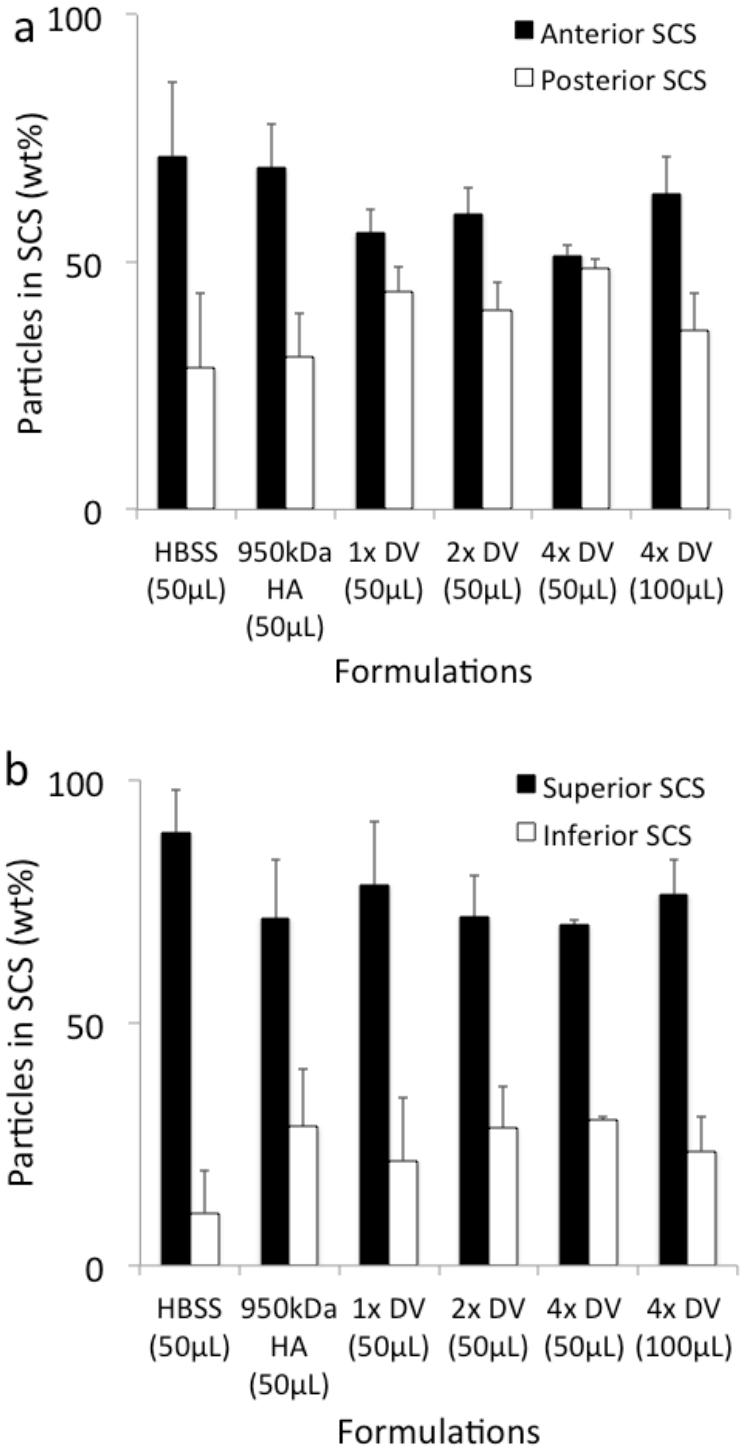

Figure 4.3.3.2. Distribution of particles inside the suprachoroidal space in different locations within the ocular globe. (a) Distribution of particles (wt%) in anterior and

posterior SCS (b) Distribution of particles (wt%) in superior and inferior SCS from the injection site.

Amount of particles (%) radially in superior and inferior SCS was also measured (Fig. 4.3.3.2.b). Amount of particles in the inferior SCS were 22 - 30% of injected particles. Likewise, HBSS formulation showed 11% of the injected particles in superior SCS. One-way ANOVA analysis of HBSS and polymeric formulation showed p-value of 0.05, 0.13, 0.0082, 0.020, and 0.0068 respectively. Statistically significant differences were found for 2X DV (50 µL), 4X DV (50 µL), and 4X DV (100 µL). Particle weight percent analysis showed statistically significant amount in opposite to the injection site and posteriorly compared to HBSS formulation. The HA based formulation failed to achieve an even distribution of particles radially throughout the whole ocular globe. However, we were able to deliver significant amount of particles from the injection site to 180 degrees away from the injection site.

4.3.4. Formulations to immobilize particles inside the suprachoroidal space

To test the hypothesis that strongly non-Newtonian material resists spreading of embedded particles away from the injection site. The main parameter that we measured was the suprachoroidal space coverage area. Viscosity of all the polymers was set at approximately 55 Pa-s at a shear rate of 0.1 s^{-1}. This was viscosity of 90 kDa of carboxymethyl cellulose (12%) at 39 °C. This was chosen because it was high enough viscosity for 90 kDa of carboxymethyl cellulose to inject through microneedles and be able to get accurate volume of injection. All of the initial suprachoroidal space coverage was measured using ex vivo eyes (Pel-Freez Biologicals). Smaller particles are more

likely to get cleared by macrophages, which was also evident in previous aqueous formulation study. Therefore all the experiment was done using 10 μm particles.

Immediately after injection, polymeric formulations (700 kDa CMC, 90 kDa CMC, 90 kDa MC) covered SCS surface area of 7 – 10 %. Likewise HBSS formulation showed SCS coverage area of 42%. Initial suprachoroidal space coverage area of all the polymeric formulation, which had viscosity of 55 Pa-s, was 80% smaller than the HBSS formulation.

Fourteen days after injection, SCS surface coverage area of 700kDa CMC and 90kDa MC did not significantly change except 90kDa CMC formulation. Between days 0 and 14, SCS surface coverage area of polymeric formulations (700kDa CMC, 90kDa CMC, 90kDa MC) increased 0.17 – 4.17 folds. One-way ANOVA showed significant difference in SCS coverage area for 90kDa CMC ($p=0.0007$) but no statistical difference was found for 700kDa CMC and 90kDa MC ($p = 0.16$ and 0.33, respectively). This was expected because of 90kDa CMC showed lower viscosity increase compared (Fig. 4.3.2.3a) to 700kDa CMC and 90kDa MC formulations.

Forty days after injection, SCS surface coverage area of 700kDa and 90kDa CMC was 12 and 36%. SCS surface coverage area of 90kDa CMC between 14 and 40 days did not show significant difference ($p= 0.08$ and 0.9, respectively). Sixty days after injection, SCS surface coverage area of 700kDa increased 0.20 folds. 700kDa CMC between 0 and 60 days showed progressive increase up to 2 folds with statistically significant difference ($p=0.001$).

Overall, this data showed that strongly non-Newtonian material at lower shear rate is capable of slowing down the spreading of particles inside the SCS up to 2 months.

We expect higher concentration of 700kDa CMC will be capable of slowing down the spreading of particles longer periods of time due to higher viscosity at lower shear rate (Fig. 4.3.4.1.). Extremely strongly non-Newtonian property of 700kDa CMC allows reliable injection through microneedles. This is because fluid flowing through the microneedle will experience very high shear stress, which will lower the viscosity of material flowing through the needle. We tested up to 3 wt% of 700kDa CMC solution and able to reliably inject through the microneedles (Data not shown). However, we experienced difficulty injecting reliable volume using concentration higher than 12% for 90kDa CMC.

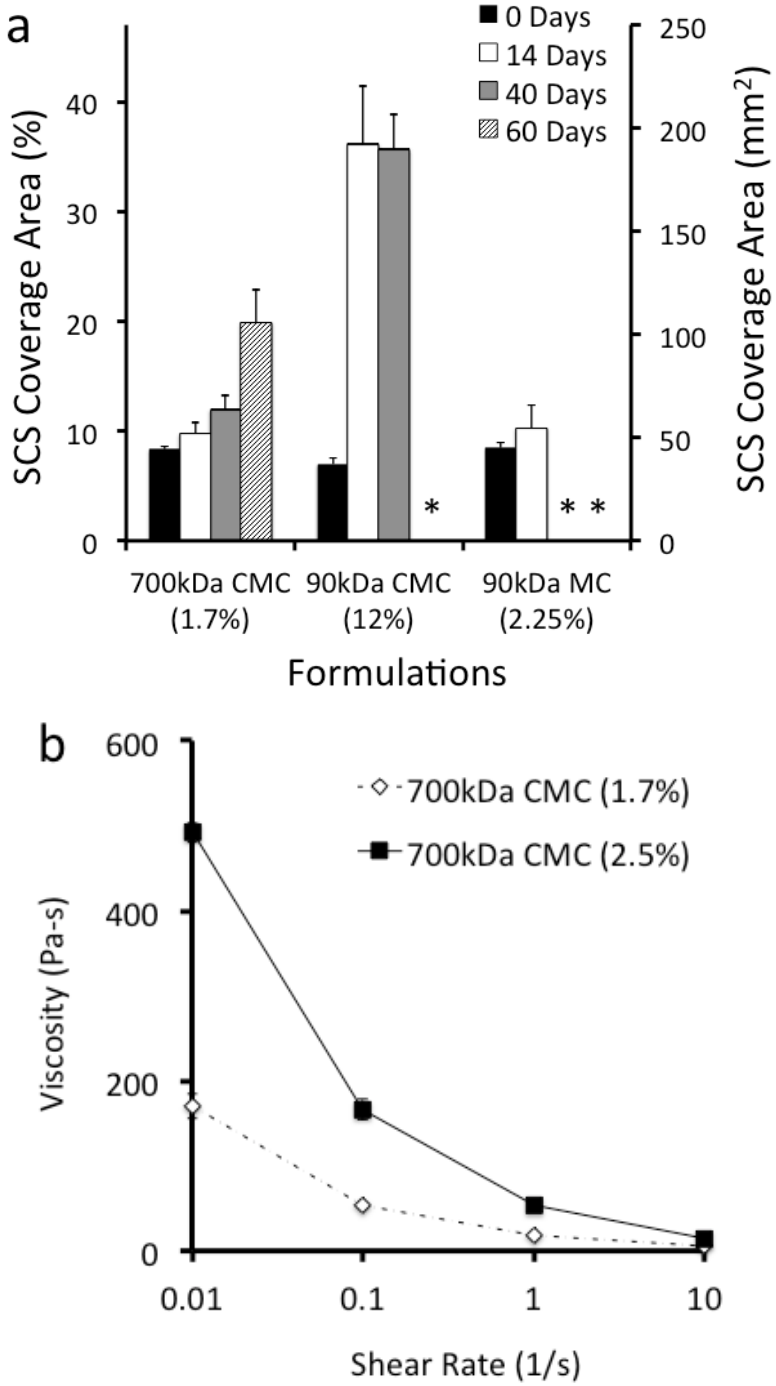

Figure 4.3.4.1. (a) Suprachoroidal space coverage area as a function of polymeric excipient formulation and time. (b) Rheological behavior of different weight percent of 700kDa carboxymethylcellulose. * - indicated no data are available.

4.4. DISCUSSION

Suprachoroidal space (SCS) injection provides access to many unique locations within the ocular globes such as ciliary body and choroid. Microneedle's micron sized tip simplifies the delivery into the suprachoroidal space by designing the tip to just penetrate into but not across the suprachoroidal space. Previous research in this area showed microneedles could be used to inject particles as large as 10 μm into the suprachoroidal space [66]. This study builds on the previous success of using microneedles to deliver materials into suprachoroidal space to enhance targeting ability within the SCS by controlling the movement of the particles.

Suprachoroidal delivery is very attractive method to deliver drugs because it allows us to put therapeutics exactly adjacent to the targeting tissues like ciliary body and choroid, which are the sites of action for serious vision threatening diseases such as glaucoma, wet age related macular degeneration, diabetic retinopathy, and uveitis[147, 148] [11, 12]. Currently, sustained release formulations are delivered as an implant that are placed in vitreous, a chamber at the center of the eye, which often requires surgical procedures to insert the implants.

Microneedle provides simple safe, and reliable way to deliver polymeric controlled release formulations in minimally invasive way. Currently, retinal specialists give millions of intravitreal injections per year at the same site of injection located 2-5 mm from the limbus[158, 159]. This similarity makes the injection procedure straightforward for an ophthalmologist. SCS injection using microneedle also carries less safety concerns because it only penetrates partially into the eye. On the other hand, intravitreal injection requires needle to penetrate across entire layer of the eye.

This study demonstrates for the first time that simple polymeric excipient formulations can be used to target specific regions within the suprachoroidal space using simple polymeric formulations to control the mobility of polymeric particles. This highly targeted delivery reduces the amount of drug administered. This opens up an opportunity for us to deliver longer sustained release formulation, due to reduction in required dosage. This can save money, due to lower drug costs. This can also improve safety and patient acceptance, due to reduced side effects. For example, intravitreal administration of steroids causes unwanted contact with lens and promotes the formation of cataract in 6.6% of the patients [151]. By targeting drug delivery to the targeting site, side effects caused at off-target sites of action can be reduced. SCS delivery could deliver high particles concentration that could potentially deliver many months of sustained release formulation.

Many in situ gelling polymers such as solvent removal, temperature, pH, or light mediated introduces potentially toxic materials (organic solvents), and complexities to the procedure. By simply utilizing non-Newtonian fluids to modulate fluid's viscosity at high shear (when flowing through the needle) and low shear rate (when inside the tissue) provides much simpler pharmaceutical formulations for clinicians to use. Polysaccharides provide excellent biocompatibility and are already used in many pharmaceutical formulations. But most importantly, targeting within the SCS can be easily done by utilizing simple materials that are already approved by FDA. We believe SCS injection can be easily adopted because its similarity to currently used intravitreal administration. Currently, intravitreal injections are done by retinal specialist million times per year at the pars plana located 2-5 mm from the limbus. SCS delivery requires an injection at same site.

This makes the SCS injection procedure very simple and straightforward for an ophthalmologist to perform. In addition, targeting SCS can be easily done by simple polymeric formulation, which does not require any complex process or equipment. Highly reduced dosage requirement and ability to delivery high polymeric concentration using microneedles could potentially deliver many months of sustained release formulation. In related work accessing the suprachoroidal space, microneedles have been used for hundreds of suprachoroidal injections in rabbits and to a lesser extent in pigs, and were recently reported for use in four human subjects[66, 109, 134, 160-162]. We believe ability to target different regions in the uvea could provide more effective therapies for many vision-threatening diseases.

4.5. CONCLUSION

This study demonstrates that polymeric particles as large as 10 μm can be targeted to the site of injection and throughout entire layer of the choroid using simple polymeric excipient formulation. In vivo study showed that materials exhibit strongly non-Newtonian properties at low shear stress can be used to slow down the expansion of the embedded polymeric particles at the site of injection up to 2 months. We also demonstrated that high molecular weight compounds that does not show non-Newtonian properties at lower shear rate are capable of enhancing the spreading of up to 10 μm sized polymeric particles to cover entire layer of the choroid using single injection. This study shows for the first time that simple polysaccharides excipient formulation can to use to target specific regions within the suprachoroidal space using microneedles in minimally invasive way. Further study is required to optimize characteristics of excipient

formulations and injection parameters such as molecular weights, concentration, and injection volume to better-localized injected particles for extended periods of time.

5 TARGETED DELIVERY OF ANTI-GLAUCOMA DRUGS TO THE SUPRACILIARY SPACE USING MICRONEEDLES

5.1. INTRODUCTION

Glaucoma is the second leading cause of blindness worldwide [1, 20], even though well-established pharmacological treatments are available. Poor patient compliance plays a significant role in the loss of the vision in patients with glaucoma. The estimated compliance with use of topical eye drops is as low as 56% [163], which shows that patients cannot manage daily eye drops well. Patients are required to administer eye drops one or more times per day because systemic therapy (e.g., by oral delivery, which typically has higher compliance [163-165]) with most anti-glaucoma drugs causes unacceptable side effects [166, 167].

Although topical drops administer drug to the eye, they nonetheless are poorly targeted to their specific sites of action within the ocular globe [47]. Topical delivery is highly inefficient and requires frequent dosing to overcome poor drug absorption and rapid clearance. Bioavailability of eye drops is typically well below 5%, and what little drug enters the eye is delivered non-specifically throughout the anterior segment with only a small fraction of the drug reaching its site of therapeutic action [45-47]. In the case of many anti-glaucoma drugs, that site of therapeutic action is the ciliary body [110, 111]. Also, the poorly targeted nature of eye drops leads to extensive systemic exposure, which causes up to 8-53% of glaucoma patients taking topical anti-glaucoma drugs to experience side effects [149, 150]. This poor patient compliance and low bioavailability of glaucoma drugs creates the need for a better delivery method [3].

In this study, we introduce supraciliary delivery to target drug administration adjacent to the ciliary body to maintain high therapeutic drug levels at the site of pharmacologic action in the targeted tissue. This targeting of the ciliary body can be accomplished by administering drug into the supraciliary space, which is a potential space located below the sclera and above the choroid and ciliary body that can expand to accommodate a fluid or drug formulation. We and others have previously reported on the use of the suprachoroidal space for drug targeting to the choroid and adjacent retina to reach posterior segment targets [62, 65, 67, 109, 134, 168-170]. Here, we access the ciliary body in the anterior segment by injecting drug into the most anterior portion of the suprachoroidal space, which we are calling the supraciliary space. By localizing the drug in the supraciliary space, we expect to achieve high drug levels locally in the adjacent ciliary body.

Previous studies have accessed the suprachoroidal space to demonstrate highly targeted and reliable delivery to this space and effective drug treatment with no major safety concerns in animal models and human subjects [62, 65, 67, 109, 134, 168-170]. Researchers have accessed the suprachoroidal space using surgically introduced catheters and conventional hypodermic needles, but more recently our group introduced the use of microneedles as a simple and reliable method of suprachoroidal injection that is expected to be suitable for use as a rapid office procedure [67]. A first-in-humans study recently demonstrated injection of bevacizumab into the suprachoroidal space of four human eyes using a microneedle [109]. In the present study, we have adapted this method to target injection into the supraciliary space, as the first study exploring the use of this potential

space to deliver therapeutics immediately adjacent to the ciliary body and the first study to examine pharmacodynamics of this delivery method.

This study seeks to assess the efficacy of supraciliary delivery using a hollow microneedle in the rabbit and compare that to conventional topical delivery. We carried out this assessment by delivering anti-galucoma drugs to the supraciliary space and measuring reduction in intraocular pressure (IOP) over time compared to topical delivery of the same drugs. The drugs used in this study – sulprostone and brimonidine – both have sites of action in the ciliary body [110, 111], which suggests that supraciliary targeting should be beneficial.

Sulprostone is a prostaglandin analogue that has been shown to lower IOP in the rabbit [171-174], but is not used in humans to treat glaucoma. Latanoprost, travoprost, and bimatoprost are prostaglandin analogues in common human clinical use [175, 176], but rabbits respond poorly to these drugs [177-183]. We therefore used sulprostone as a model prostaglandin analogue with similar pharmacological properties to other prostaglandin analogues [110, 111]. Our other drug, brimonidine, is in common clinical use for anti-glaucoma therapy and is active in the rabbit eye too. In this study, we measured IOP in the New Zealand White rabbit after bolus injection of sulprostone and brimonidine at a range of different doses and compare their responses to topical eye drops to test the hypothesis that highly targeted delivery of anti-galucoma drugs to the supraciliary space using a hollow microneedle allows dramatic dose sparing of drug compared to topical eye drops.

5.2. MATERIALS AND METHODS

5.2.1. Microneedle Fabrication and Formulation

Microneedles were fabricated from 33-gauge stainless steel needle cannulas (TSK Laboratories, Tochigi, Japan). The cannulas were shortened to approximately 700-800 μm in length and the bevel at the orifice was shaped using a laser (Resonetics Maestro, Nashua, NH), as described previously [66, 69]. The microneedles were electropolished using an E399 electropolisher (ESMA, South Holland, IL) and cleaned with deionized water. Sulprostone (Cayman Chemical, Ann Arbor, MI) and 0.15% brimonidine tartrate ophthalmic solution (Alphagan® P, Allergan, Irvine, CA) were diluted in Hank's Balanced Salt Solution (HBSS, Cellgro, Manassas, VA). For topical delivery, the final concentration was 0.05 mg/ml sulprostone or 1.5 mg/ml brimonidine tartrate. For supraciliary injection, the solution was diluted to a range of drug concentrations and included 2% carboxymethylcellulose (CMC, Sigma–Aldrich, St. Louis, MO) to increase viscosity and thereby improve localization of the drug at the site of injection.

5.2.2. Anesthesia and Euthanasia

All studies used New Zealand White rabbits of mixed gender weighing between 3-4 kg (Charles River Breeding Laboratories, Wilmington, MA). All of the animals were treated according to the ARVO statement for the Use of Animals in Ophthalmic and Vision Research. For supraciliary injections and for application of topical eye drops, rabbits were anesthetized using 0.5 – 3.0% isoflurane, unless otherwise noted. The isoflurane percentage was slowly increased from 0.5% up to 2.5% or 3.0% for 15 min. To

achieve longer-lasting anesthesia for the supraciliary and intravitreal safety studies measuring IOP immediately after injection, anesthesia was achieved using subcutaneous injection of a mixture of ketamine (25 mg/kg) and xylazine (2.5 mg/kg). This ketamine/xylazine dose was also used during initial studies screening suitable anesthetics for this study. Proparacaine (a drop of 0.5% solution) was given 1 – 3 min before each injection to locally numb the ocular surface. Animals were euthanized with an injection of 150 mg/kg pentobarbital into the ear vein.

5.2.3. Pharmacodynamics studies

For supraciliary injection, a microneedle was attached to a 50 µl gas-tight glass syringe containing either (i) a placebo formulation of HBSS or (ii) a drug formulation containing a specified concentration of either sulprostone or brimonidine tartrate. The eyelid of the rabbit was pushed back and the microneedle was inserted into the sclera 3 mm posterior to the limbus in the superior temporal quadrant of the eye. A volume of 10 µl was injected within 5 s and the microneedle was removed from the eye 15 s later to reduce reflux of the injected formulation. Topical delivery of sulprostone and brimonidine was achieved by administering an eye drop into the upper conjunctival sack. IOP was measured hourly for 9 h after drug administration, as described below. Each treatment involved application of just one dose of one drug either topically or by supraciliary injection in one eye. After a recovery period of at least 7 days, rabbits were used for additional experiments, alternating between the left and right eyes.

5.2.4. Safety Studies

Supraciliary injections of either 10 µl or 50 µl of HBSS were performed as described above. Intravitreal injection was performed by inserting a 30-gauge hypodermic needle across the sclera 1.5 mm posterior to the limbus in the superior temporal quadrant of the eye. A volume of 50 µl HBSS was injected within 5 s and the needle was removed from the eye 15 s later to reduce reflux. IOP was measured periodically for 1 h after injection, as described below.

5.2.5. Intraocular Pressure Measurement

IOP was measured with a hand-held tonometer (TonoVet, icare, Vantaa, Finland) in the awake, restrained rabbit. Topical anesthesia was not necessary for the measurement and no general anesthetic or immobilizing agent was used because the procedure is not painful. We made every effort to avoid artifactual elevation of IOP by avoiding topical anesthesia and by careful and consistent animal handling during each measurement. Each rabbit was acclimatized to the IOP measurement procedure for at least 3 days to obtain a stable background IOP reading.

5.2.6. Calculation of Area Under the Curve And Equivalent Dosage

The pharmacodynamic effect of each treatment was characterized by determining the area under the curve of the temporal profile of intraocular pressure by numerically integrated using the trapezoidal rule[184]. This pharmacodynamic area under the curve (AUC_{PD}) is a measure of the strength and duration of the treatment on IOP. To make the

AUC_{PD} calculation, IOP readings were normalized to the IOP reading prior to the treatment. The obtained value of AUC_{PD} had units of mm Hg-hr and a negative value (because the drugs under study all lowered IOP). However, the negative values were changed to positive values for better representation of the data.

$$AUC_{PD} = \sum_{i=1}^{9} \left[-(t_i - t_{i-1}) \left[\frac{IOP(t_{i-1}) + IOP(t_i)}{2} \right] \right] \quad (1)$$

Where $IOP(t_i)$ in mm Hg represents the IOP value measured at time t_i in seconds. An equivalent dosage comparison between topical and supraciliary delivery was made using the following equation, where D is the dose administered and the subscripts SC and $topical$ mean suprachoroidal injection and topical administration, respectively.

$$Equivalent\ dosage = \left[\frac{AUC_{PD,SC} / D_{PD,SC}}{AUC_{PD,topical} / D_{PD,topical}} \right] \quad (2)$$

5.2.7. Statistical Analysis

Three replicate pharmacodynamics and safety experiments were done for each treatment group, from which the mean and standard error of mean were calculated. Experimental data were analyzed using two-way analysis of variance (ANOVA) to examine the difference between treatments. In all cases, a value of $p < 0.05$ was considered statistically significant.

5.3. RESULTS

5.3.1. Effect Of Anesthesia On Transient IOP Change

Before studying the effect of supraciliary targeting of anti-glaucoma drugs, we needed to identify a general anesthetic that does not create artifactual changes in rabbit IOP over the time scale of the experiment. We first tested subcutaneous injection of ketamine/xylazine, which produced deep anesthesia for approximately 2 h. This anesthetic also produced significant ocular hypotension that lasted for 4 – 5 h, with a peak IOP decrease of approximately 5 mm Hg at 1 h after injection of the anesthetic, which was followed by a slow recovery of IOP over time (Fig 5.3.1.1.).

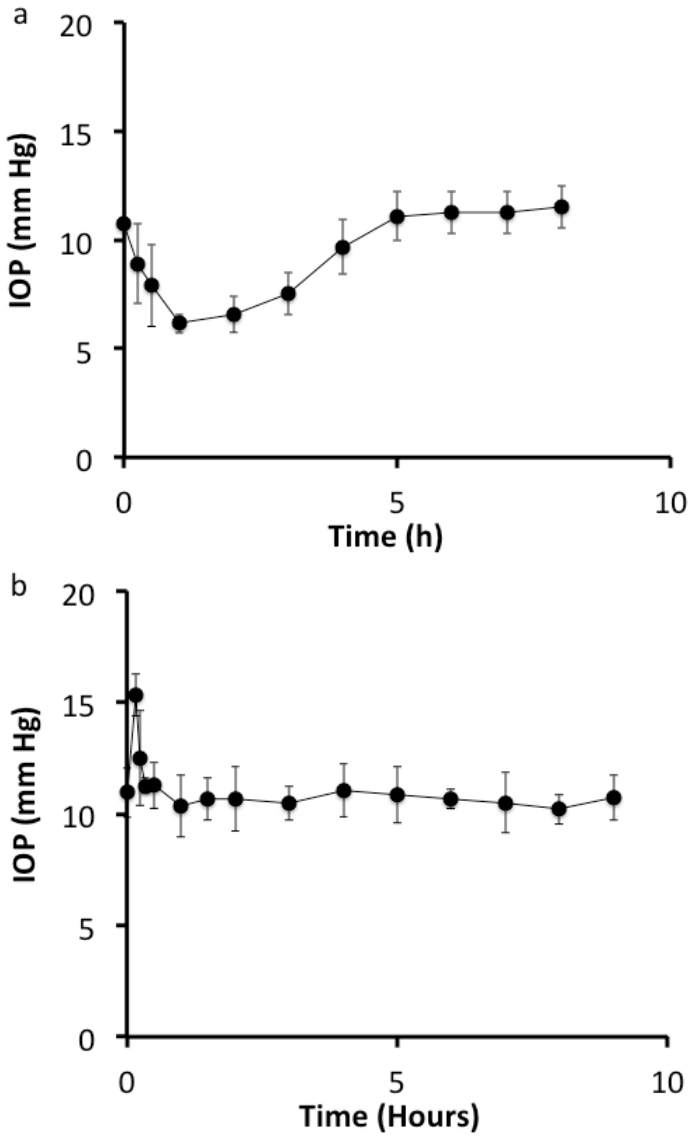

Figure 5.3.1.1. Effect of general anesthetics on IOP in the rabbit eye. (a) Ketamine/xylazine (25/2.5 mg/kg) was administered by subcutaneous injection. (b) Isoflurane (up to 3%) was administered by inhalation for 15 min. IOP was measured in both eyes periodically for up to 9 h. Data points represent the average ± SEM (n = 4-6).

We then tested isoflurane, which was administered by inhalation of an escalating dose over 15 min. Anesthesia quickly set in upon initiation of the isoflurane dose and quickly reversed upon discontinuation of the isoflurane dose. During the 15 min of isoflurane administration, IOP was elevated by almost 5 mm Hg, but quickly returned to normal after isoflurane administration was stopped, and remained unchanged for 9 h after that (Fig. 5.3.1.1.b). We believe the initial, transient ocular hypotension may have been due to both the pharmacological effect of the anesthetic, as well as the psychological effect (i.e., startling the rabbit) of administering the inhaled anesthetic.

We conclude from these studies that isoflurane is a suitable anesthetic for the pharmacodynamic experiments in this study, because isoflurane's effects on IOP reversed within 15 – 30 min, which is fast enough to permit hourly measurements of IOP without significant artifact from the anesthetic. However, for the safety experiments in this study in which IOP is measured multiple times within 1 h, the rapidly changing effects of isoflurane on IOP would significantly affect IOP measurements. For that reason, we used ketamine/xylazine for the safety study, because the effect of the anesthetic on IOP was relatively small during the first 10 min when the most critical IOP measurements were made in the safety study.

5.3.2. Anti-Glaucoma Drugs in the Normotensive Rabbit Model

To test our hypothesis regarding drug targeting via the supraciliary space, we next needed to identify anti-glaucoma drugs that have pharmacological action at the ciliary body and reduce IOP in the normotensive rabbit model. Our candidates were prostaglandin analogues, adrenergic agonists and beta-blockers that have their

pharmacological site of action at the ciliary body [110, 111, 166]. Our first choice was prostaglandin analogues because they are widely used in human clinical medicine [175, 176], including for glaucoma treatment [166]. Latanoprost, travoprost, and bimatoprost are commonly used prostaglandin analogues [175, 176], but rabbits respond poorly to these drugs [177-183]. We tested latanoprost in our rabbit model, but observed no change in IOP at the standard human dose of 2.5 μg (data not shown).

We therefore used sulprostone as a model prostaglandin analogue with its site of pharmacological action to the ciliary body [110, 111] and an ocular hypotensive effect well documented in literature [172, 174]. A single topical eye drop of 2.5 μg of sulprostone gave a maximum IOP decrease of almost 5 mm Hg at approximately 2 h after drug administration (Fig 5.3.2.1.). Ocular hypotension in the treated eye lasted up to 5 h. We did not observe changes in IOP in the contralateral (i.e., untreated) eye. Responses of the contralateral eyes were statistically insignificant compared to the negative control (isoflurane only) with ($p = 0.242$).

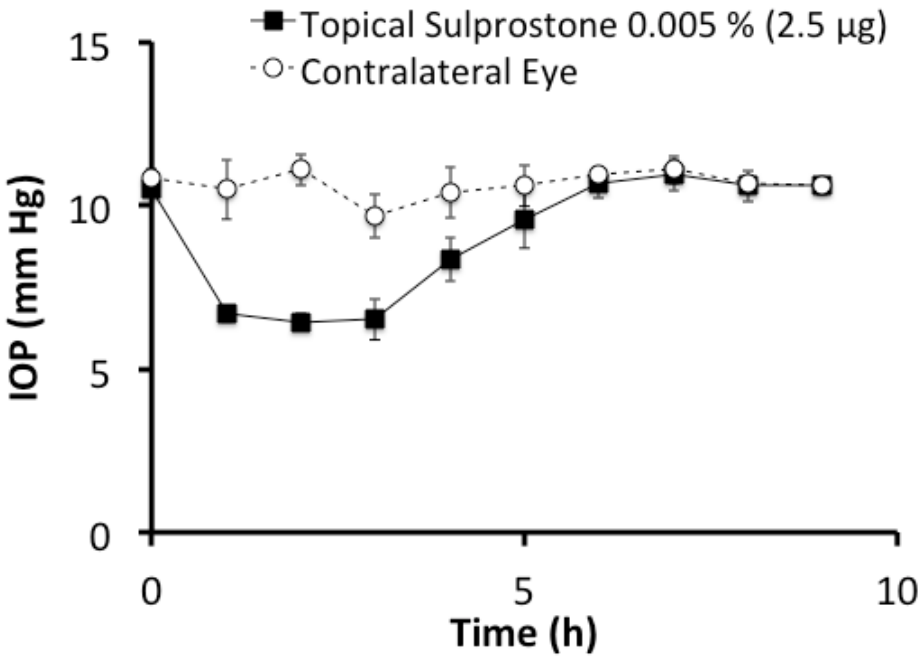

Figure 5.3.2.1. Effect of topical sulprostone administration on IOP in the rabbit eye. A single drop containing 2.5 µg sulprostone was administered to one eye. IOP was then followed for 9 h in both the treated eye and the untreated/contralateral eye. Data points represent the average ± SEM (n = 4).

To more fully test our hypothesis, we decided to study a second drug that lowers IOP by a different mechanism in the ciliary body as well, and selected brimonidine, an adrenergic agonist that is widely used in clinical glaucoma therapy. While the pharmacology and site of action causing an IOP response to brimonidine is species dependent [185], adrenergic agonists have a site of action in the ciliary body in both the rabbit [185] and human [186-188]. A previous study demonstrated α_2-adrenoceptor agonism by showing that pretreating the eye with α_2-selective antagonists inhibited the IOP response to brimonidine in rabbits [189].

We found that topical administration of a single drop (75 µg) of brimonidine produced a peak IOP reduction of approximately 5 mm Hg at 3 h after drug administration, which slowly returned to normal within 7 h (Fig. 5.3.2.2. a). Topical administration of three drops (225 µg) of brimonidine initially increased IOP, but then reduced it by approximately 6 mm Hg at 2 h after drug administration, which slowly returned to normal within 9 h (Fig. 5.3.2.2. b). This initially elevated IOP response can be explained by the known effect of brimonidine to increase IOP at high concentrations and lower it at more moderate concentrations [185].

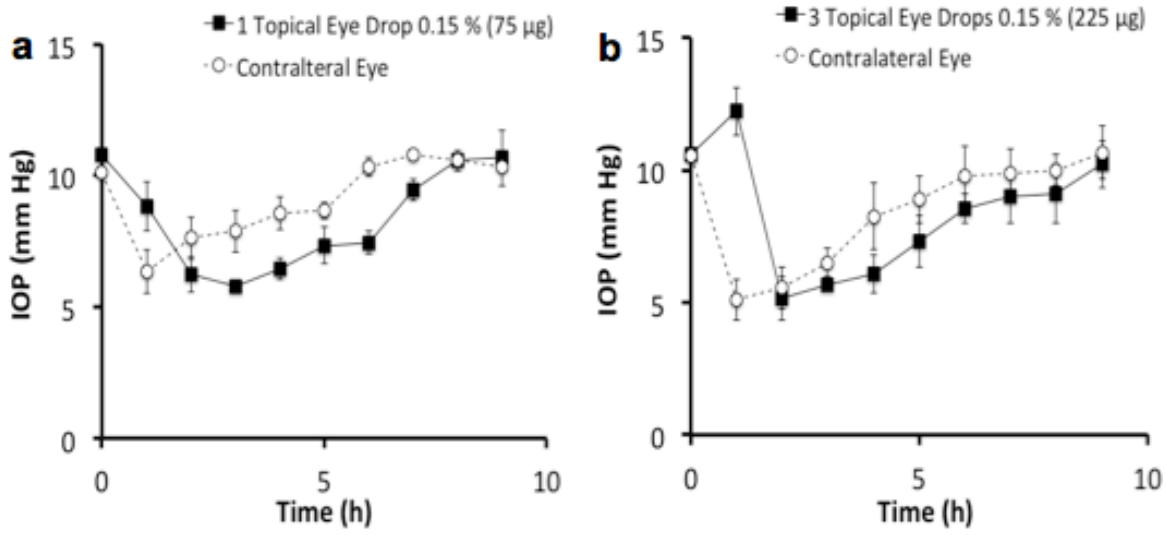

Figure 5.3.2.2. Effect of topical brimonidine administration on IOP in the rabbit eye. A single drop containing (a) 75 µg or (b) 225 µg brimonidine was administered to one eye. IOP was then followed for 9 h in both the treated eye and the untreated/contralateral eye. Data points represent the average ± SEM (n = 3).

It is notable that the contralateral (untreated) eye also experienced elevated IOP with faster kinetics and similar magnitude (Fig. 5.3.2.2.), presumably due to systemic distribution of brimonidine. The slower kinetics in the treated eye could be explained by a local brimonidine concentration that was initially too high and only after some clearance of the drug reached the optimal concentration for IOP reduction, whereas the contralateral eye had lower brimonidine concentration from the start due to the non-targeted systemic delivery route. Previous research also showed decreased IOP in the contralateral eye in rabbits, which was produced due to systemic administration after administering brimonidine at high concentrations in the treated eye and was reflected by plasma concentrations high enough to activate central α_2-adrenoceptors [190] and cardiovascular changes [185].

5.3.3. Microneedles For Targeted Delivery To the Supraciliary Space

Our next step was to demonstrate targeted injection into the supraciliary space using a microneedle. Because the thickness of sclera above the suprachoroidal space in the rabbit is ~500 μm [191], we prepared microneedles measuring 700 – 800 μm to be inserted to the base of the sclera and in that way target injection into the suprachoroidal space. The needles were longer than the thickness of the sclera to account for the overlying conjunctiva and for the expected deformation of the sclera during insertion of the microneedle. Fig. 5.3.3.1. shows a representative microneedle prepared for supraciliary injection next to a typical eye drop used for topical administration.

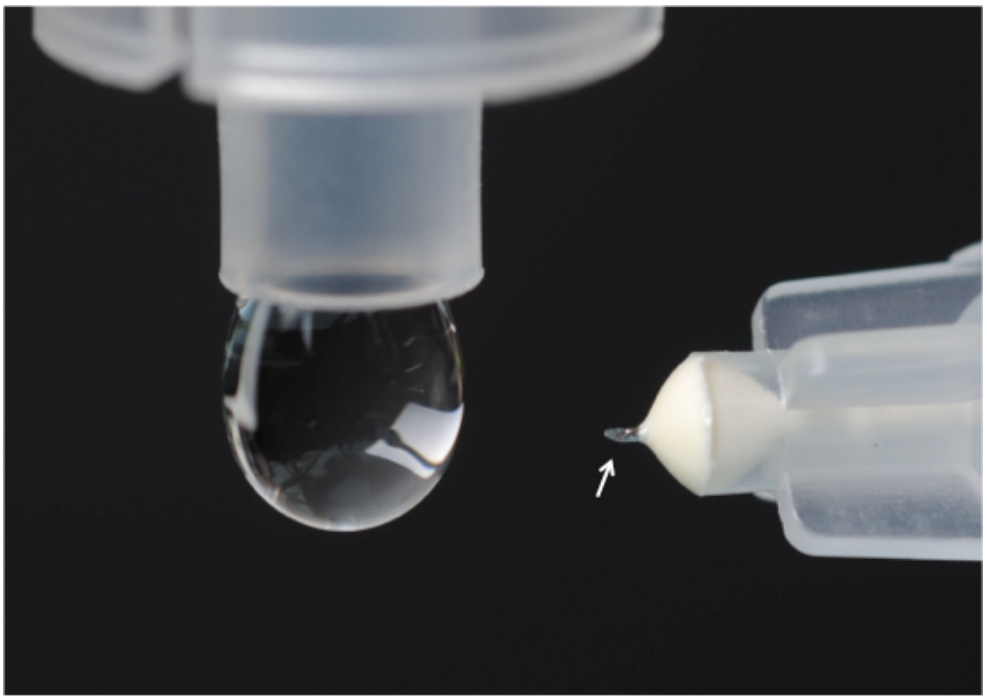

Figure 5.3.3.1. Hollow microneedle (at arrow) measuring 720 μm in length shown next to a liquid drop of approximately 50 μl volume from a conventional eye dropper.

Previous studies making injections in this way have targeted the suprachoroidal space with the objective of having the injected formulation flow away from the site of injection and travel circumferentially around the eye for broad coverage of the choroidal surface, especially toward the posterior pole. In this study, we had the opposite objective. Our goal was to localize the injected formulation at the site of injection immediately above the ciliary body and minimize flow to other parts of the eye.

To accomplish this goal, we increased the viscosity of the injected formulation by adding 2% w/v CMC. The viscosity of this solution at rabbit body temperature of 39°C was 80.5 ± 3.7 Pa-s at a shear rate of 0.1 s^{-1}, which is approximately 80,000 times more viscous than water at room temperature. Injection of this high-viscosity formulation into the rabbit eye using a microneedle was able to localize the injection near the site of

injection. As shown in Fig 5.3.3.2.a, the dye injected in this way spread over an area within just a few millimeters from the site of injection. The degree of this spread depended on the amount of fluid injected, such that there was more spread when larger volumes were used (data not show).

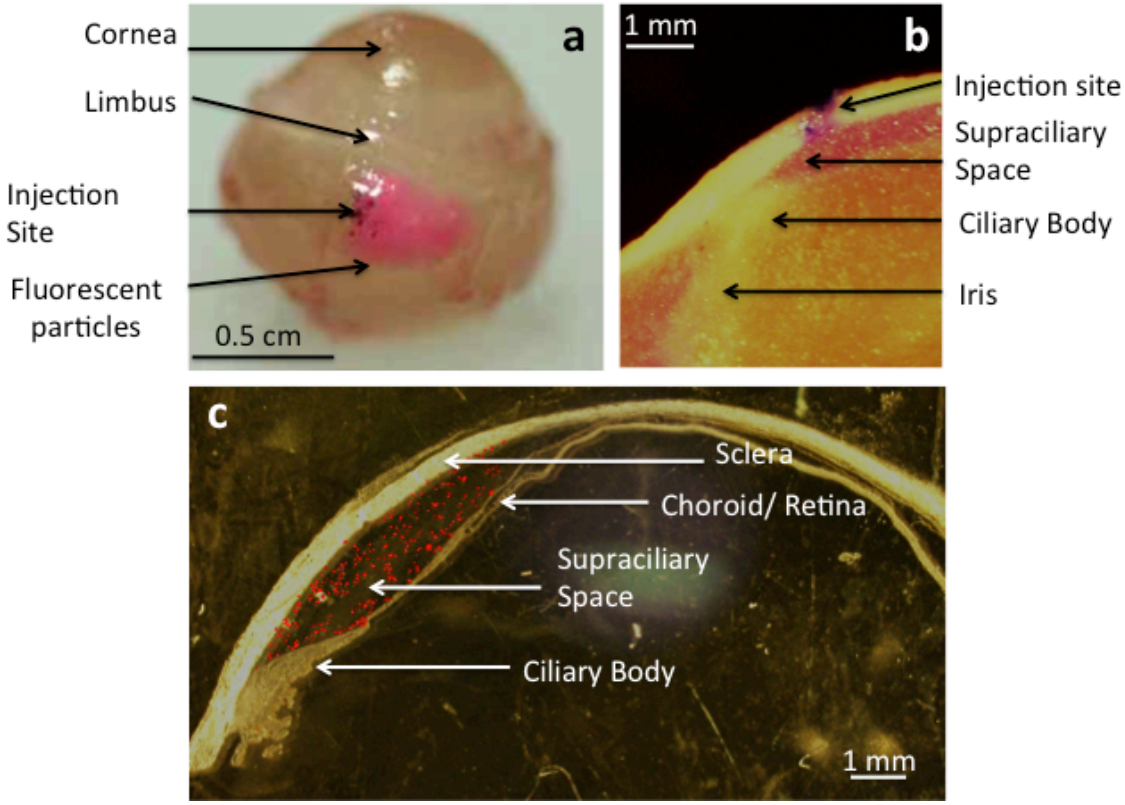

Figure 5.3.3.2. Supraciliary targeting of injections using a high-viscosity formulation injected using a microneedle. (a) Injection of 10 µl of red-fluorescent particles (1 µm diameter, 0.5% w/v) into the rabbit eye ex vivo spread only a few millimeters from the site of injection. The whole eye was imaged by a digital camera 60 min after injection. (b) Injection of 50 µl of red-fluorescent particles (1 µm diameter, 0.5% w/v) into the rabbit eye ex vivo was localized to the supraciliary space, directly above and adjacent to the ciliary body. The eye was frozen immediately after injection, prepared as frozen sections and

imaged by brightfield microscopy. (c) Injection of 30 µl of red-fluorescent microparticles (10 µm diameter, 0.5% w/v) into a human cadaver eye was localized to the supraciliary space. The eye was fixed in formalin immediately after injection, prepared as frozen sections and imaged by overlaying a brightfield microscopy image to show ocular anatomy with a fluorescent microscopy image of the same histological section showing fluorescent particles.

Histological examination demonstrated that the injection was localized to the supraciliary space. As shown in Fig. 5.3.3.2. b, the injected dye can be seen in the expanded supraciliary space bounded by the ciliary body on the lower anterior boundary, the choroid on the lower central and posterior boundary and the sclera on the upper boundary of the rabbit eye. In Fig 5.3.3.2. c, a similar experiment was conducted in a human eye, which similarly shows supraciliary localization of the injected fluorescent particles. While the supraciliary space is significantly expanded immediately after injection when these tissues were frozen for analysis, we believe that this space closes down again as fluid is absorbed, based on our unpublished data on suprachoroidal injections and other data discussed further below.

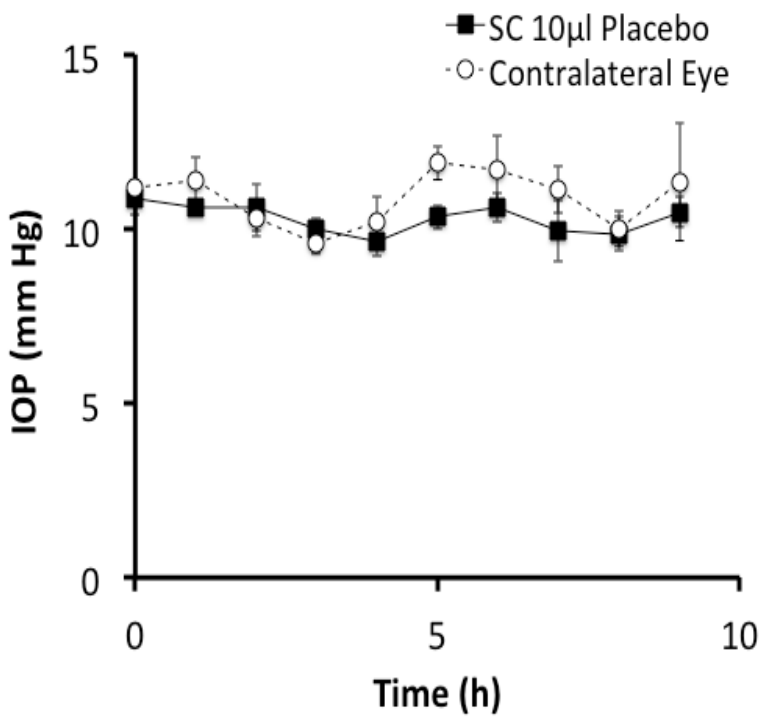

Figure 5.3.3.3. Effect of supraciliary injection on IOP in the rabbit eye. A single injection of 10 µl of a 2% w/v solution of CMC was administered to one eye. IOP was then followed for 9 h in both the treated eye and the untreated/contralateral eye. Data points represent the average ± SEM (n = 3).

We also determined the possible effect of supraciliary injection of 2% CMC on IOP over the course of our experiments. As shown in Fig. 5.3.3.3., there was no apparent effect of this injection on IOP at the hourly timepoints over the course of a 9 h study. A two-way ANOVA comparing the isoflurane-only group (Fig. 5.3.1.1.) to the data in Fig. 5.3.3.3. showed no statistically significant difference with p-values of 0.885 and 0.084 for treated and contralateral eyes, respectively.

5.3.4. Pharmacodynamics of Sulprostone After Supraciliary Delivery

Having completed the initial experiments on anesthesia, topical delivery and supraciliary targeting, we were now able to test the central hypothesis of this study regarding the effects of anti-glaucoma drugs targeted to the supraciliary space. We therefore injected sulprostone into the supraciliary space over a range of doses (0.05 µg – 0.0005 µg) in rabbits. Starting with a pre-treatment IOP of 10-11 mm Hg, supraciliary delivery of sulprostone at a dose of 0.05 µg (i.e., a dose 50 times lower than the topical dose shown in Fig. 5.3.2.2.) produced an IOP decrease of ~6 mm Hg within 1 h that persisted at that level for at least 9 h (Fig. 5.3.4.1. a). IOP was similarly decreased in the contralateral eyes, but to a lesser extent. At this dose, responses of the contralateral eyes were significantly different compared to placebo treatment ($p = 0.006$). Supraciliary delivery of 0.005 µg sulprostone (i.e., a dose 500 times lower than the topical dose) produced a peak IOP drop of ~4.5 mm Hg at 1 h after drug administration (Fig. 5.3.4.1. b). IOP increased over time, but ocular hypotension persisted for the full 9 h in the treated eye. Responses of the contralateral eyes were not significantly different from placebo treated eyes ($p = 0.53$). Supraciliary delivery of 0.0005 µg sulprostone (i.e., a dose 5,000 times lower than the topical dose) did not produce a significant reduction in IOP in the treated eyes ($p = 0.68$) or the contralatereral eyes ($p = 0.18$) (Fig. 5.3.4.1. c).

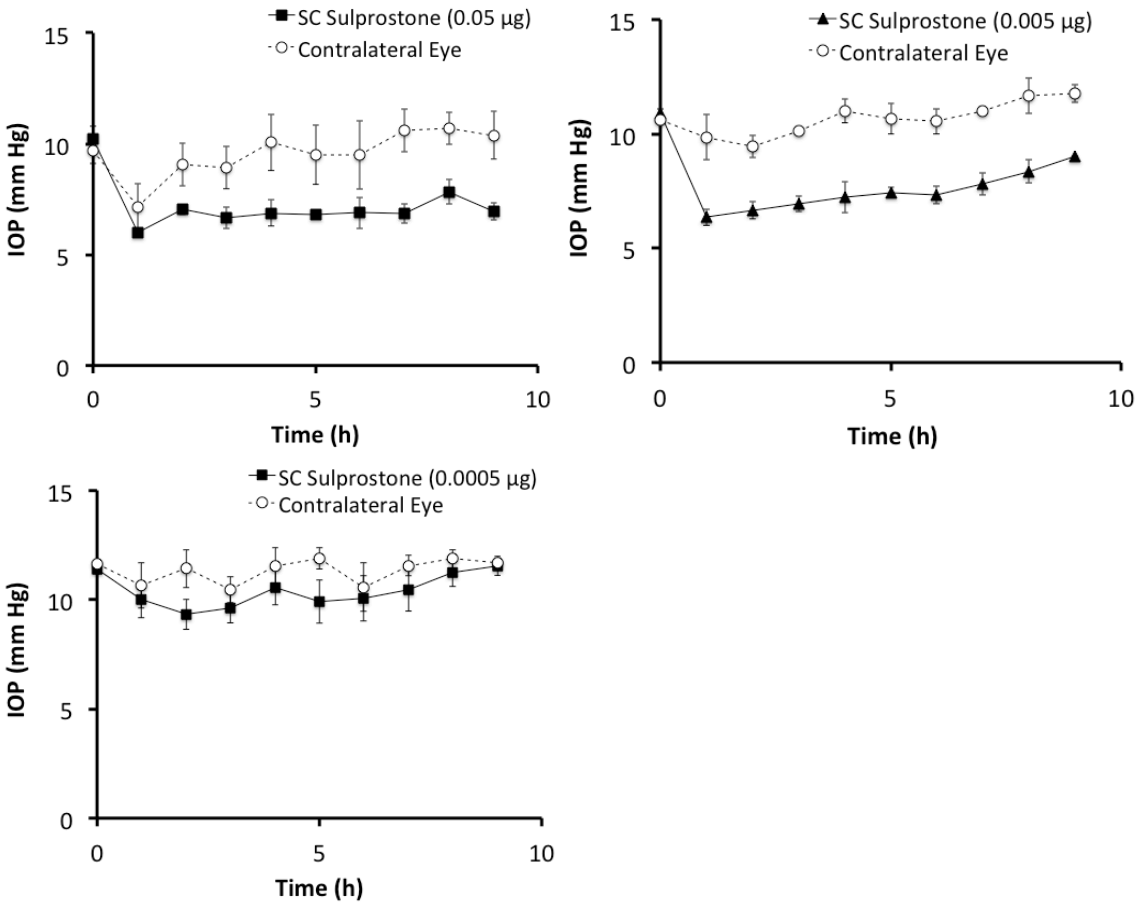

Figure 5.3.4.1. Effect of supraciliary injection of sulprostone on IOP in the rabbit eye. A single injection of (a) 0.05 µg, (b) 0.005 µg and (c) 0.0005 µg sulprostone was administered to one eye. IOP was then followed for 9 h in both the treated eye and the untreated/contralateral eye. Data points represent the average ± SEM (n = 3-4).

Overall, sulprostone was found to lower IOP in a dose-dependent manner (Fig. 5.3.4.1.a). Based on a rough comparison, topical delivery of 2.5 µg sulprostone and supraciliary delivery of 0.005 µg sulprostone showed similar levels of initial IOP reduction, although the effect lasted longer after supraciliary delivery. To provide a more quantitative measure of the supraciliary dose equivalent to topical delivery, we determined and compared the AUC_{PD} for the pharmacodynamic data in the topical and

supraciliary treated eyes (Fig. 5.3.4.2. b). Comparison of these values gave a ratio of 1122, which indicates that the supraciliary dose needed to achieve a similar pharmacodynamic response was ~1100 fold less than for topical delivery. We believe that this dramatic dose sparing was achieved by highly targeted delivery of sulprostone to its site of action in the ciliary body.

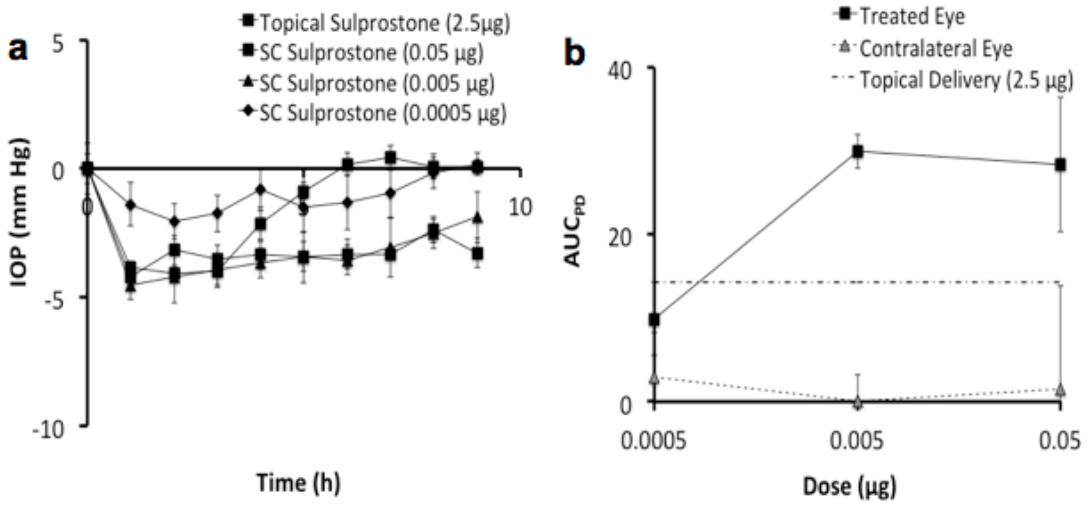

Figure 5.3.4.2. Comparison of IOP drop caused by supraciliary delivery versus topical delivery of sulprostone. (a) Data from Figs. 5.3.2.1. and 5.3.4.1. are graphed together to show the dose-response relationship after supraciliary delivery and to facilitate comparison with topical delivery in the treated eyes. (b) Pharmacodynamic area under the curve (AUC_{PD}) after supraciliary delivery in treated and contralateral eyes, and in comparison with topical delivery. Data are from Figs. 5.3.2.1. and 5.3.4.1. AUC_{PD} was calculated using Eq. 1.

5.3.5. Pharmacodynamics Of Brimonidine After Supraciliary Delivery

To assess the generality of dose sparing by targeting anti-glaucoma drugs to the supraciliary space, we carried out similar experiments to study supraciliary delivery of brimonidine over a range of concentrations (0.0015 μg – 0.15 μg) in rabbits. Similar to sulprostone, brimonidine produced a concentration-dependent drop in IOP at doses much lower than used for topical delivery. Supraciliary delivery of brimonidine at a dose of 15 μg (i.e., a dose 5 times lower than the topical dose shown in Fig. 5.3.2.2. a) produced an IOP decrease of ~5 mm Hg within 1 h that persisted at that level for about 9 h (Fig. 5.3.51. a). IOP was similarly increased in the contralateral eye, but to a lesser extent.

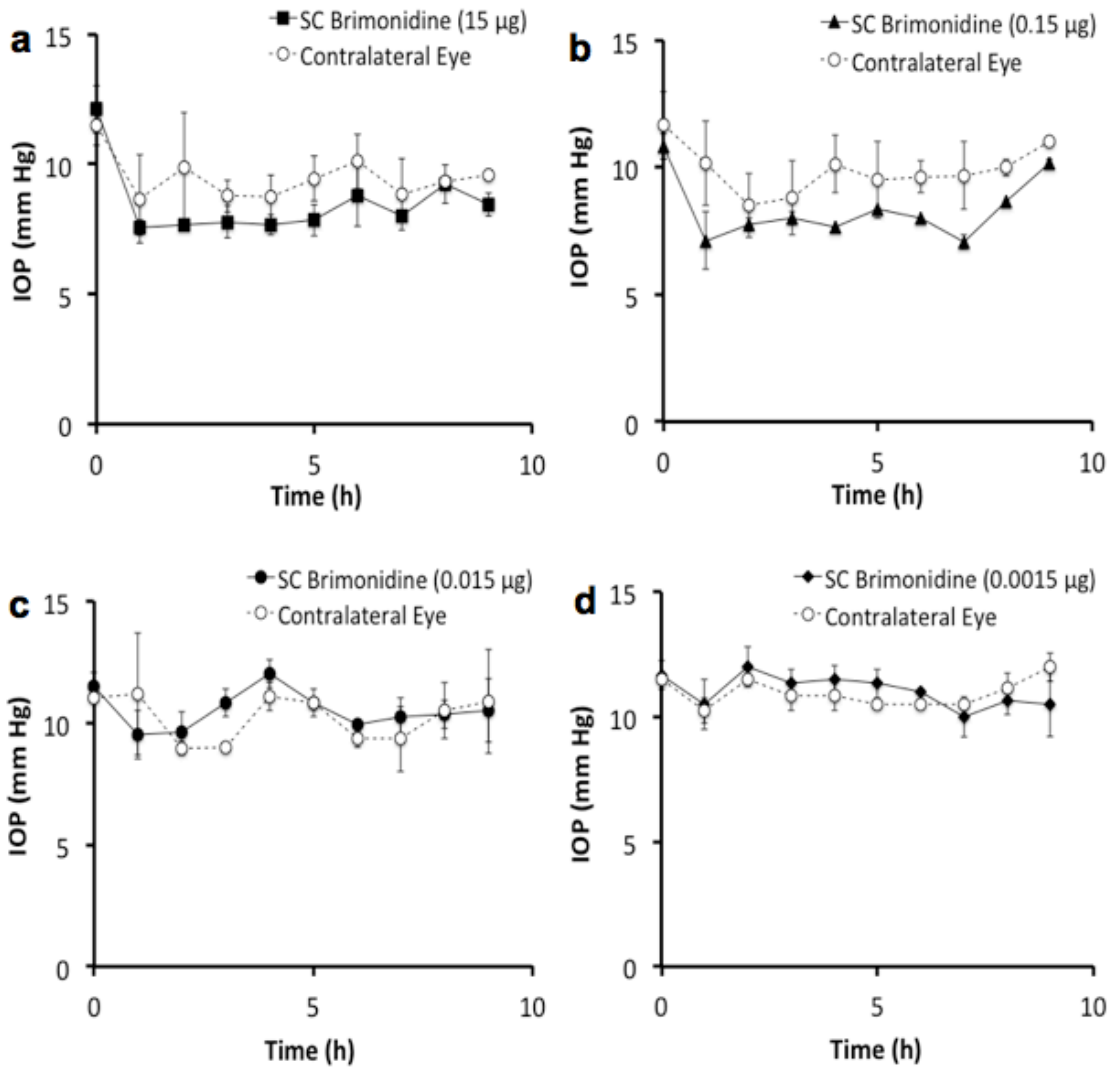

Figure 5.3.5.1. Effect of supraciliary injection of brimonidine on IOP in the rabbit eye. A single injection of (a) 15 µg, (b) 0.15 µg, (c) 0.0015 µg and (d) 0.00015 µg brimonidine was administered to one eye. IOP was then followed for 9 h in both the treated eye and the untreated/contralateral eye. Data points represent the average ± SEM (n = 3).

Supraciliary delivery of 0.15 µg brimonidine (i.e., a dose 500 times lower than the topical dose) produced a peak IOP drop of ~3.5 mm Hg at 1 h after drug administration that persisted at that level for about 7 h (Fig. 5.3.5.1. b). The contralaterial eye showed a

similar, but smaller drop in IOP. Supraciliary delivery of both 0.015 µg and 0.0015 µg brimonidine (i.e., doses 5,000 and 50,000 times lower than the topical dose, respectively) showed no significant IOP changes in treated ($p=0.91$) and contralateral eyes ($p=0.056$). Supraciliary delivery of brimonidine reduced IOP in a dose-dependent matter (Fig. 5.3.5.1. a). Compared to topical delivery of 75 µg of brimonidine, a 500-fold lower dose of 0.15 µg of brimonidine by supraciliary delivery showed a similar duration and magnitude of ocular hypotension (Fig. 5.3.5.1. a). By calculating AUC_{PD} values (Fig. 5.3.5.1. b), we estimated the supraciliary dose needed to get a similar pharmacodynamic response was 504-fold less than topical delivery. It is notable that in the rabbit model studied here, decreased IOP was seen both in the treated eyes and to a lesser extent in the contralateral eyes (Fig. 5.3.5.1.). Ocular hypotension in contralateral eyes is believed to be due to systemic absorption [192]. Similar contralateral responses were also observed after topical delivery of brimonidine both by us (Fig. 5.3.2.1.) and others [185].

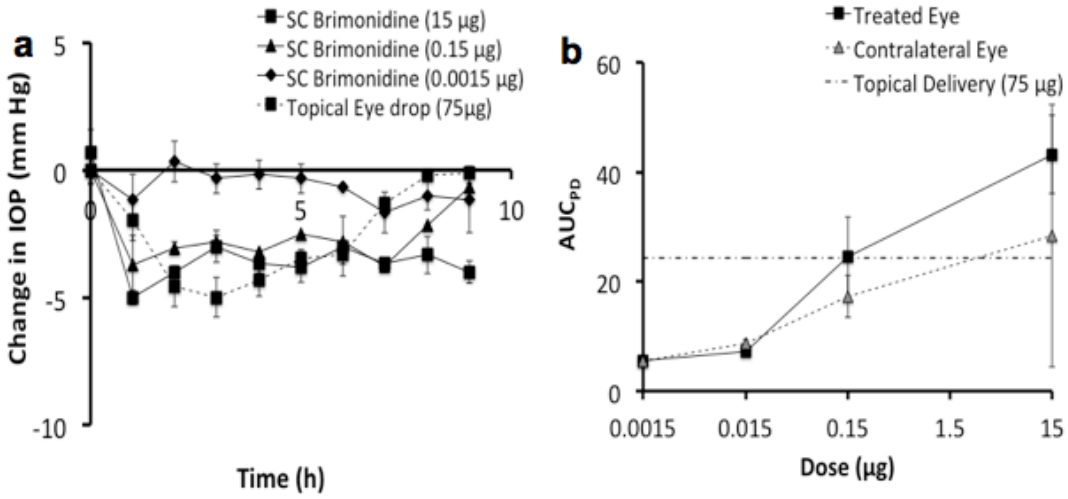

Figure 5.3.5.2. Comparison of IOP drop caused by supraciliary delivery versus topical delivery of brimonidine. (a) Data from Figs. 5.3.2.2.a and 5.3.5.1. are graphed together to show the dose-response relationship after supraciliary delivery and to facilitate comparison with topical delivery in the treated eyes. (b) Pharmacodynamic area under the curve (AUC_{PD}) after supraciliary delivery in treated and contralateral eyes, and in comparison with topical delivery. Data are from Figs. 5.3.2.2. a and 5.3.5.1. AUC_{PD} was calculated using Eq. 1.

5.3.6. Safety of Microneedle Injection into the Supraciliary Space

Injections into the supraciliary space using microneedles were well tolerated and no injection-related complications were observed, such as bleeding or squinting. After injection, the needle insertion site was not visually apparent on the conjunctival surface, indicating only very minor trauma (Fig. 5.3.6.1.). We did not observe any inflammation, redness, or pain-related response after the injection. No apparent vision loss was observed in any of the rabbits. To further assess safety, we measured IOP elevation associated with supraciliary and intravitreal injection. Note that this is the short-lived elevation in IOP

caused by the injection itself (as opposed to the longer-term IOP reduction caused by the anti-glaucoma drugs presented above). For this study, ketamine/xylazine was used for general anesthesia because it provides a relatively steady IOP between 1 h and 2 h after injection (Fig. 5.3.1.1.). Rabbits given an intravitreal injection of 50 µl of HBSS 1 h after induction of anesthesia were found to have a peak IOP increase 36±1 mm Hg due to the injection (Fig. 5.3.6.2.). IOP then decreased exponentially until it stabilized after 30-40 min after the injection. This is similar to what is seen in human patients, where intravitreal injection can increase IOP by ~30 mm Hg [193]. Considering intravitreal injection is well tolerated in human patients using just topical anesthesia and is safely performed millions of times per year [194], we expect that this temporary increase in IOP is safe and well tolerated.

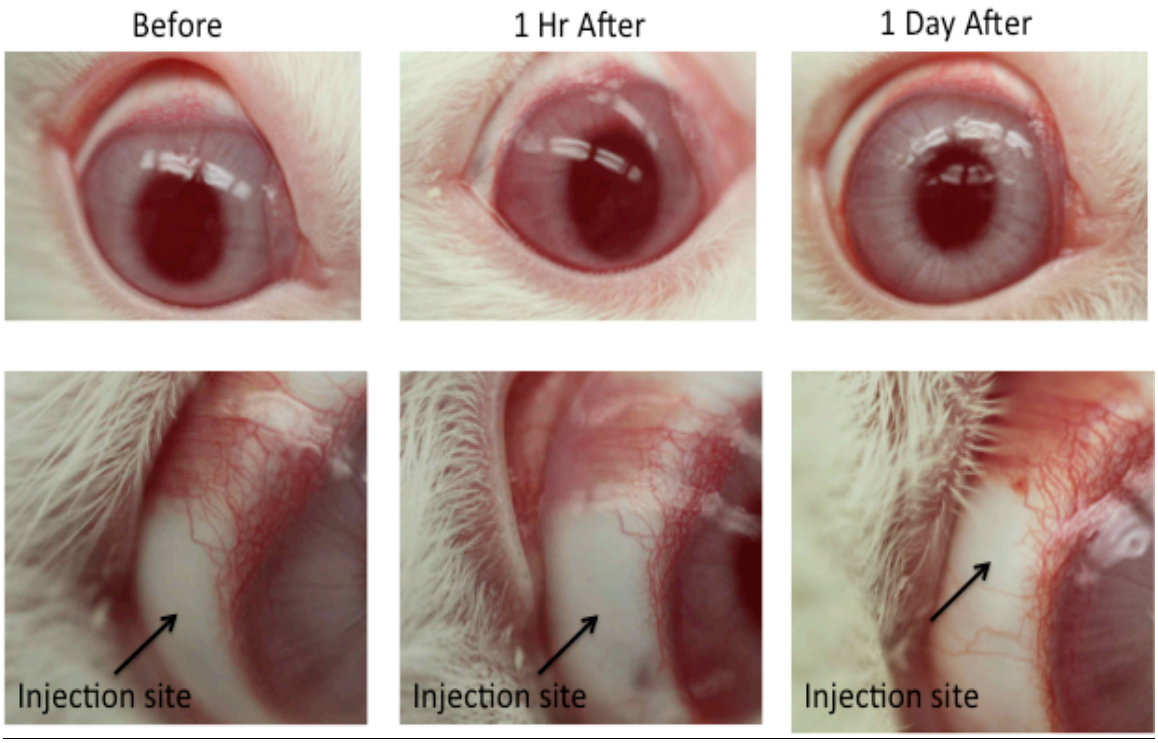

Figure 5.3.6.1. Representative images of a rabbit eye (a) before (b) 1 hour after and (c) on day after supraciliary injection of the placebo formulation (2% CMC). All images are of the same rabbit eye. The lower row of images shows magnified views of the injection site of the eyes shown in the upper row of images.

We similarly injected 50 µl of a 2% CMC formulation into the supraciliary space of the rabbit eye and observed a transient increase in IOP that peaked at 35±3 mm Hg and decayed in under 1 h, which is similar to the effects of conventional intravitreal injection (Fig. 5.3.6.2.). We also injected 10 µl of formulation into the supraciliary space and found the peak IOP increase was 5±1 mm Hg, which then disappeared within 20 min. Considering the similar magnitude and kinetics of IOP change by these intravitreal and supraciliary injection, we hypothesize that the safety profile of supraciliary delivery may be similar to that of intravitreal injection. In fact, supraciliary injection may be safer than

intravitreal injection, considering that intravitreal and supraciliary injections are performed at the same site of the eye (i.e., pars plana) [194], but supraciliary injection uses a needle that penetrate an order of magnitude less deeply into the eye.

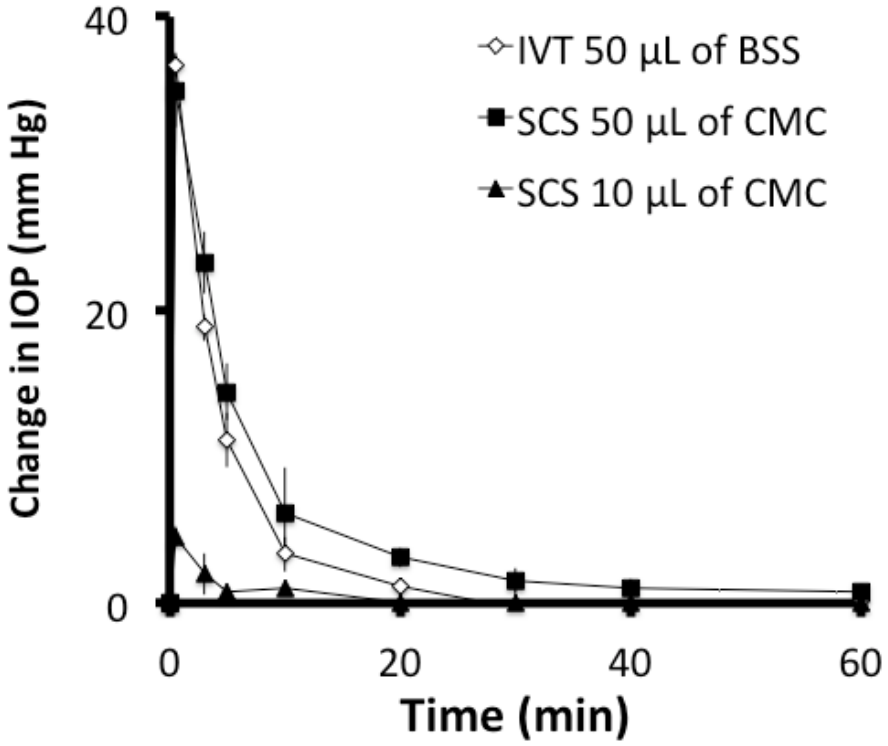

Figure 5.3.6.2. IOP increase due to injection of 50 µl of HBSS into the intravitreal space (IVT) and 10 µl and 50 µl of 2% carboxymethylcellulose placebo formulation (CMC) into the supraciliary space (SCS).

5.4. DISCUSSION

In current therapy, anti-glaucoma drugs with a site of action in the ciliary body are almost always given by topical eye drops. This approach has a very low bioavailability, with typically less than 5% of the applied drug being absorbed into the

eye and only a tiny fraction of that reaching its therapeutic target in the ciliary body [195, 196]. As a result, eye drops must be given at least daily and there can be side effects from systemic delivery of the poorly absorbed drug [197, 198]. This study introduces the idea of targeting the ciliary body by injection into the adjacent supraciliary space. We accessed this space located just a few hundred microns below the conjunctival surface by using a hollow microneedle designed to be just long enough to penetrate to the base of the sclera. Injection at this site filled the supraciliary space with a formulation designed with high viscosity that inhibited its flow away from the site of injection, thereby creating a depot next to the ciliary body. When anti-glaucoma drugs – sulprostone and brimonidine – we injected in this way, they were able to reduce IOP at doses three orders of magnitude lower than those required for similar pharmacodynamics using topical eye drops. These results show the highly targeted nature of supraciliary delivery and suggest opportunities to improve glaucoma therapies. Targeted delivery reduces the amount of drug administered. This can save money, due to lower drug costs. This can also improve safety and patient acceptance, due to reduced side effects. For example, incidence of iris darkening in patients receiving prostaglandin analogues is as high as 35% [199, 200] and brimonidine causes dry mouth in 33% of patients [167]. By targeting drug delivery to the ciliary body, side effects caused at off-target sites of action can be reduced.

Targeted delivery also facilitates development of sustained-release therapies that eliminate the need for patients to comply with daily eye-drop regimens. For example, brimonidine is used clinically at a daily topical dose of 75 μg given 3 times per day [201]. The daily dose of brimonidine administered to the supraciliary space appears to be approximately 500 times less than the topical dose. This means that the supraciliary daily

dose is believed to be 0.45 μg and a six-month supply would be 81 μg. A six-month polymeric sustained-release system with a 5% drug loading would have a mass of 1,620 μg, which corresponds to a volume of 1.6 μl (assuming a density of 1 g/ml). A 10% w/v suspension of microparticles containing a six-month supply of sustained-release brimonidine would have a volume of 16 μl. This small volume can easily be injected into the supraciliary space, given that much larger volumes were successfully injected in this study.

If this vision for sustained-release drug therapy can be realized, it could have a dramatic effect on patient compliance with glaucoma therapy. Current therapy requires many patients to administer eye drops on at least a daily basis. Compliance with such dosing schedules is very low, in the range of 56% [163]. Many glaucoma patients visit their ophthalmologists every six months for routine exams. In this way, glaucoma patients could receive supraciliary injections of sustained-release medication during their regular doctor's visits and thereby eliminate the need for compliance with topical eye drop therapy.

From a practical standpoint, we believe that supraciliary injections could be relatively easily introduced into clinical practice. Currently, retina specialists give millions of intravitreal injections per year at the pars plana located 2-5 mm from the limbus [158, 159]. Supraciliary targeting requires placement of microneedles at the same site, which should be straightforward for an ophthalmologist to do. Assuring microneedles go to the right depth at the base of the sclera is determined by microneedle length, which is designed to match scleral thickness. In related work accessing the suprachoroidal space, microneedles have been used for hundreds of suprachoroidal

injections in rabbits and to a lesser extent in pigs, and were recently reported for use in four human subjects [66, 109, 134, 160-162].

5.5. CONCLUSION

This study provides the first demonstration of supraciliary injection that targeted delivery of anti-glaucoma drugs to their site of action in the ciliary body. Choice of the right anesthetic facilitated these studies, as both isofluorane and ketamine/xylazine affected IOP, but with different pharmacodynamics. Choice of the right drug was also important; we studied sulprostone, which is a model prostaglandin analogue drug that works in rabbits, and brimonidine, which is an α2-adrenergic agonist drug that works in both rabbits and humans, and shows significant effects in the contralateral eye after unilateral drug administration in the rabbit. We found that microneedles enable targeted injection into the supraciliary space and that anti-glaucoma drugs administered in this way show three-order-of-magnitude reduction in dose for similar reductions in IOP compared to topical delivery. The rabbits tolerated supraciliary injections well, with no adverse events or notable findings regarding safety. We conclude that targeted drug delivery to the supraciliary space using a microneedle enables dramatic dose sparing of anti-glaucoma therapeutics compared to topical eye drops.

6 PARTICLE-STABILIZED EMULSION DROPLETS FOR GRAVITY-MEDIATED TARGETING IN THE POSTERIOR SEGMENT OF THE EYE

6.1. INTRODUCTION

Age related macular degeneration (AMD) is the third leading cause of blindness. It is estimated that more than 1.8 million individuals in United States are afflicted by wet age-related macular degeneration (AMD) and that number expected to grow to almost 3 million by 2020 [21, 22]. Only within the past decade many revolutionary therapeutics agents became available to effectively mange chorioretinal diseases [29, 30]. However, there are no clinically used methods to deliver therapeutics to the targeting part of the eye to obtain best treatment efficacy. Currently, free drug formulations are administered by intravitreal injection, a hypodermic needle injection in the center of the eye. And sustained release formulations are delivered as an implant that are placed in vitreous, a chamber at the center of the eye. However, it is often overlooked that the targeting sites for many of the posterior diseases are not at the center but at the back of the eye in the layer of choroid, mid layer in the back of the eye [147, 148]. Furthermore the non-targeted nature of intravitreal administration allows possible adverse events and toxicity in the surrounding tissue. For example, intravitreal administration of steroids causes unwanted contact with lens and promotes the formation of cataract in 6.6% of the patients [151]. In addition, delivering sustained release formulation often requires surgical procedures to insert the implants. A novel delivery method that can deliver controlled release formulation in a non-invasive manner specifically to the back of the eye to

maintain high therapeutic levels of a drug in the choroid, a targeting region of the eye, should provide more effective therapy for back of the eye diseases.

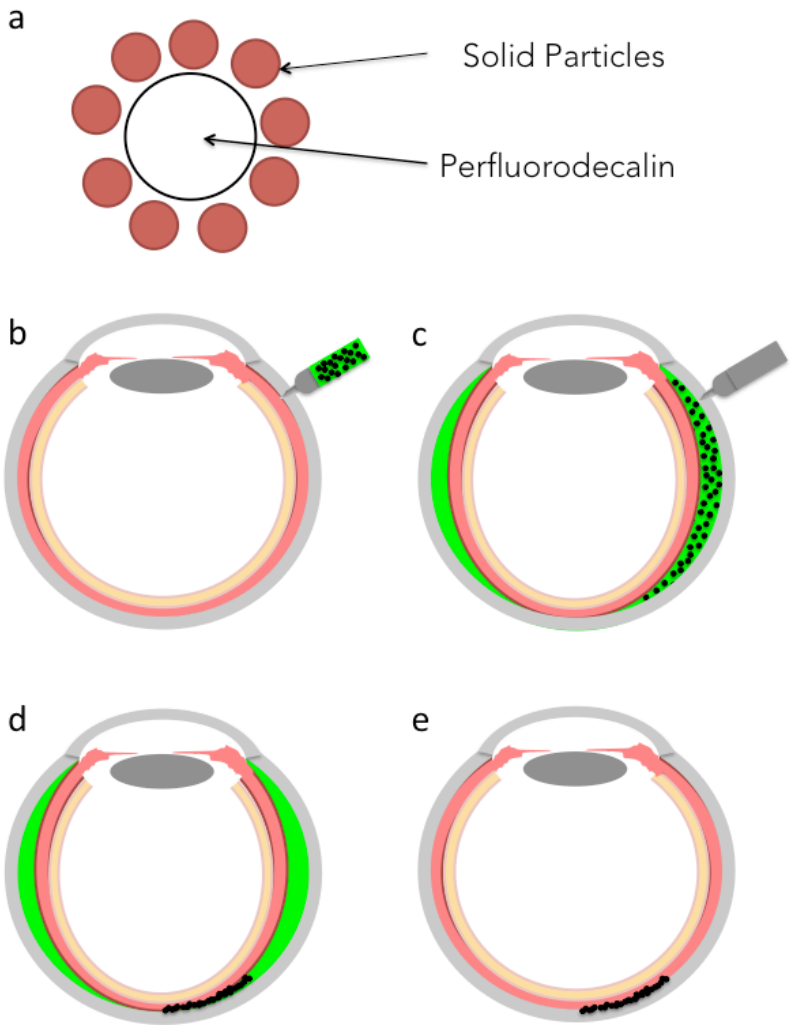

Figure 5.3.6.1. Schematic showing the structure of PEDs (a). Schematics showing injection of PEDs into suprachoroidal space of the eye. Prior to injection procedure, suprachoroidal space is collapsed and does not exist (b). Following the injection, suprachoroidal space expand (c) and give space or PEDs to migrate towards back of the eye (d). After several minutes suprachoroidal space will clear aqueous phase to hold the PEDs in place (d).

The targeting within the eye can be accomplished by administering drugs into the suprachoroidal space (SCS). The SCS is a potential space located between sclera and choroid that can expand to accommodate a fluid or drug formulation. The location of the SCS adjacent to the target site for treatment of chorioretinal diseases like wet AMD and diabetic retinopathy may provide higher drug levels in the target tissues. For this reason, the SCS represents a promising new site of administration for treatment many ocular diseases.

Microneedle's microscopic size makes it an ideal device to deliver materials into suprachoroidal space. Microneedles allows precise placement of the needle tip right at the suprachoroidal space. The suprachorodal space is right above the choroidal blood bed, which is targeting site for many uveoretinal diseases. Suprachoroidal space can expand to incorporate large amount of polymeric particle formulations [66]. This method can potentially used to deliver many months of controlled release formulation. Using just aqueous formulation, the injected micro and nanoparticles covers a portion of the suprachorodial space but not well targeted to specific regions within suprachoroidal space.

To improve on this technique, we have developed formulation to deliver the nanoparticles specifically to posterior segment of the eye using emulsion droplets. These emulsion droplets have high-density perflurodecalin liquid at the core and are stabilized using nanoparticles. Perfluorodecalin has approximately twice the density of water and this density difference will be used to create mobility inside the suprachoroidal space in the direction of gravity. The nanoparticles have a dual purpose to carry drugs and stabilize the emulsion droplets. For the first time, this study presents a method to target

particles specifically to the back of the eye using particle stabilized emulsion droplets (PEDs).

The concept of using gravity and density differences to enhance targeting ability of injected particles has been previously studied before in creating floating particles for to enhance gastric retention, and pulmonary delivery [70-72]. Both approaches are similar in a sense that the key parameter that was considered was density difference between particle and the carrier fluid. To our knowledge this is first study to create and study high-density emulsions for ophthalmic drug delivery to the posterior of the eye. We examined the capabilities and critical parameters of stabilized emulsion droplets (PEDs) that could affect the mobility of PEDs inside the suprachoroidal space. Overall, this study shows that the gravity-mediated delivery can provide targeted delivery of nanoparticles to the ciliary body and macula using minimally invasive microneedle device.

6.2. MATERIALS AND METHODS

6.2.1. Microneedle fabrication

Metal microneedles were fabricated from 30-gauge needle cannulas (Becton Dickinson, Franklin Lakes, NJ). The cannulas were shortened to approximately 600-700 μm in length and the bevel at the orifice was shaped using a laser (Resonetics Maestro, Nashua, NH). The microneedles were electropolished using an E399 electropolisher (ESMA, South Holland, IL) and cleaned with deionized water.

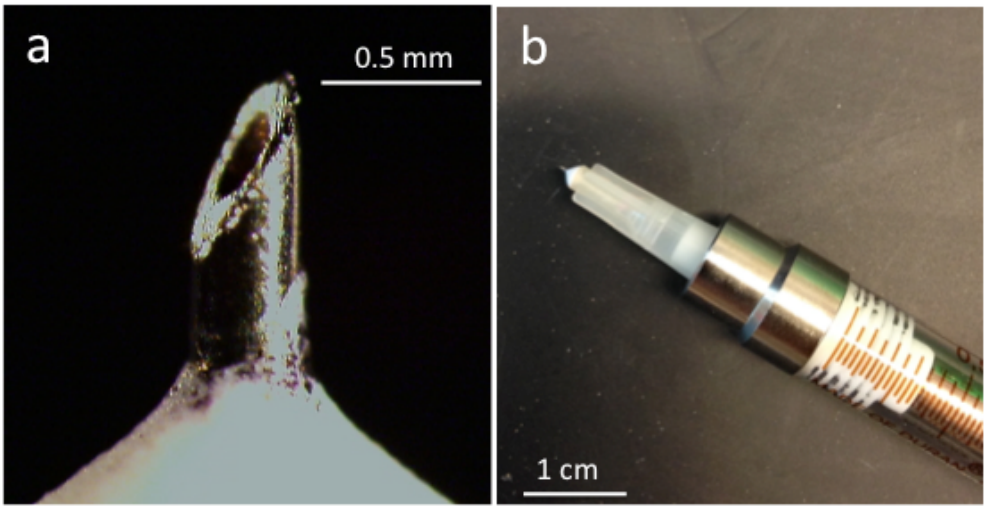

Figure 6.2.1.1. Hollow microneedle (a) and a hollow microneedle mounted on a leur adapter attached to a syringe (b)

6.2.2. Ex vivo injection procedure

Whole rabbit eyes were purchased (Pel-Freez Biologicals, Rogers, AR) with the optic nerve attached. Eyes were shipped on ice and stored wet at 4°C for up to 2 days prior to use. Eyes were allowed to come to room temperature, and any fat and conjunctiva were removed to expose the sclera. A catheter was inserted through the optic nerve into the vitreous and connected to a bottle of Hank's Balanced Salt Solution (HBSS, Corning Cellgro, Manassas, VA) raised to a height to generate internal eye pressure of 10 mmHg. 10 mm Hg was used to mimic the lowered intraocular pressure in rabbit with general anesthesia. The microneedle was attached to a gas tight glass syringe containing the formulation to be injected. Microneedle was then inserted perpendicular to the sclera tissue 3 mm posterior from the limbus. Volume of 200 µL was injected within 3 seconds and additional 30 seconds was allowed before removing the microneedles from the eye to prevent excessive reflux.

6.2.3. In vivo microneedle injection

Microneedle injection was done under systemic anesthesia (subcutaneous injection of a mixture of ketamine/xylazine/ace promazine - 17.5/8.5/0.5 mg/kg). Proparacaine (a drop of 0.5% solution) was given two to three minutes before microneedle injection as a temporary analgesia. The microneedle was attached to a gas tight glass syringes containing the formulation to be injected. For an SCS injection, the eyelids of the rabbit were pushed back and the microneedle was inserted into the sclera 3 mm past the limbus in the superior temporal quadrant of the eye. Volume of 200 µl was injected within 5 seconds and additional 60 seconds was allowed before removing the microneedles from the eye to prevent excessive reflux. Both eyes on each animal were used for the experiment. We waited 30 minutes after the injection to give enough time for the PEDs to completely settle down and all the aqueous formulation to dissipate out of the suprachoroidal space. After waiting 30 minutes, if needed injection to other side of the eye was done. All experiments were carried out using New Zealand white rabbits and animals were euthanized with an injection of pentobarbital through the ear vein.

6.2.4. Particle stabilized emulsion droplet Formulation

Carboxylate-modified non-biodegradable, fluorescently tagged, 2 wt. % of 200 nm diameter polystyrene nanoparticles (Invitrogen, Carlsbad, CA) was diluted in BSS to obtain 0.6%, 0.4%, and 0.2% solution. Obtained solution was then mixed at 7:3 ratio by volume with perfluorocarbon (perfluorodecalin, Sigma-Aldrich, St. Louis, MO) and it

was homogenized (PowerGen 700, Fisher Scientific Pittsburgh, PA) at setting 5 for 20 seconds to form particle stabilized emulsion droplets (PEDs). After forming PEDs, aqueous phase was removed and replaced with 1% polyvinyl alcohol (PVA, Sigma-Aldrich) in BSS solution. The solution was then filtered through various sizes (11, 20, 30, 41 μm) of nylon net filters (Millipore, Billerica MA) to obtain desired emulsion droplet sizes. Multiple images of the PEDs were taken using microscope and the PEDs size distribution was measured using ImageJ (US National Institutes of Health, Bethesda, MD). The concentration of the PEDs was determined by volume of settled PEDs per volume of aqueous phase (1% PVA). All the particle size were prepared using the concentration of 50 μl of PEDs/1 mL of solution.

6.2.5. Tissue processing and measurement of florescent intensity

After the suprachoroidal injection, eyes were snap frozen in an isopropyl alcohol (2-isopropanol, Sigma Aldrich) bath, which was cooled in dry ice. After the eyes were completely frozen, they were removed and eight radial cuts were made from the posterior side towards anterior segment to the cornea. After making eight cuts around the ocular globe, each of cut was peeled away outward exposing the inside of the eye. This makes eyes into flat mount like configuration visually exposing the inner side and the injected dyes in naked eyes. Bright field and florescent images of the inside of the eyes were imaged to visualize the distribution of fluorescent nanoparticles. Brightfield images were taken using digital camera (Cannon Rebel T1i, Melvile, NY) and florescent images were taken using a fluorescence microscope (Olympus SZX16, Center Valley, PA). Each of the eight pieces was then divided into additional four pieces. Approximate distance from

the pars plana to back of eye ranged from 1.2 – 1.4 mm. The cuts were made 3, 6, and 9 mm away from the pars plana, where suprachoroidal space starts, and resulting total of 32 pieces from each eye. Individual pieces were paired into 4 quadrants resulting in 16 vials containing 2 pieces of the tissue and BSS solution. Ocular tissues were then homogenized (Fisher Scientific PowerGen) to extract injected non-biodegradable florescent nanoparticles. Aqueous part of the solution was pipetted out into 96 well plates to measure fluorescent signal intensity (Synergy Microplate Reader, Winooski, VT).

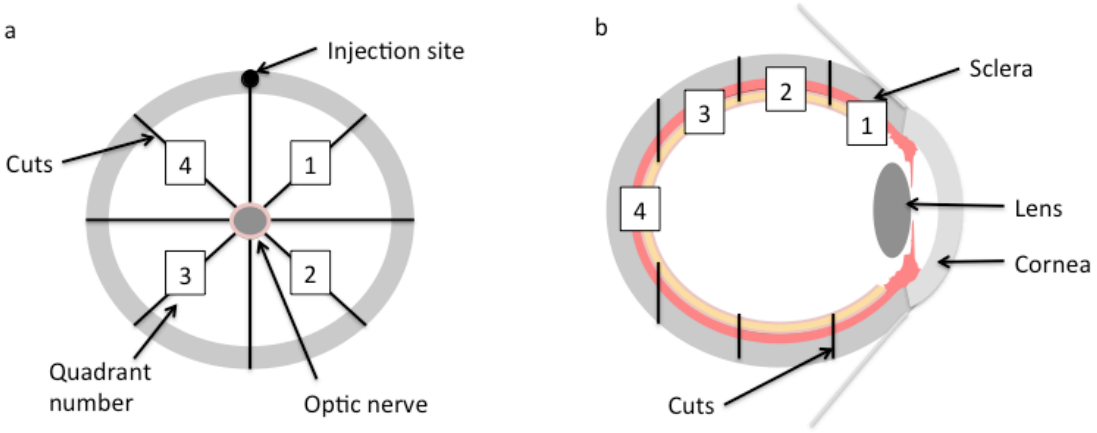

Figure 6.2.5.1. (a). Picture of posterior segment of the eye showing the radial cuts and how ocular tissues were divided into 4 radial quadrants. Picture of an ocular globe showing the 3 mm cuts from the anterior to posterior segment (b).

6.2.6. Particle Stabilized Emulsion droplet Fall Time Measurement

Prepared PEDs were put into the clear glass vial and vigorously shaken before the start of recording the movement of PEDs using digital camera (Cannon Rebel T1i). Green light bulb (Feit Electric, Pico Rivera, CA) was used to excite the florescent nanoparticles surrounding the PEDs and red camera filter (Tiffen red filter, Hauppauge, NY) was

mounted on a digital camera to visualize the movement of PEDs. Height of the solution was measured and the time it takes for all the PEDs to submerge to the bottom of the vial was measured.

6.2.7. Particle Stabilized Emulsion droplet Fall Time Modeling

$$F_{net} = F_g - F_B - F_D \quad (1)$$

$$\rho_o V_o \, x''(t) = \rho_o V_o g + \rho_f V_f g + 6\pi\eta r x'(t) \quad (2)$$

Where, F_D is Stokes drag force, F_B is buoyancy force, F_g is gravitational force, F_{net} is the net force, ρ_o is density of the PED, ρ_f is density of a carrier fluid (i.e., water), V_o is the displacement volume of a PED, V_f is the displacement volume of the carrier fluid, g is gravitation acceleration, η is the viscosity of the carrier fluid, r is the radius of a PED, and $x(t)$ is height as a function of time.

6.2.8. Ultrasound measurement

Ultrasound scanner (UBM Plus, Accutome, Malvern, PA) was used to monitor the expansion of the suprachoroidal space. Ultrasound scanning probe was positioned 45 degrees away from the injection site radially was constantly measured for before and 10 minutes after the injection procedure.

6.2.9. Statistical Analysis

Three replicate pharmacodynamics and safety experiments were done for each treatment group, from which the mean and standard deviation were calculated. Experimental data were analyzed using one-way analysis of variance (ANOVA) was used to examine the difference between treatments. In all cases, a value of $p < 0.05$ was considered statistically significant.

6.3. RESULTS

6.3.1. Fabrication and characterization of particle-stabilized high-density emulsion droplets (PEDs)

We sought to create high-density particles that enables targeting posterior of the eye by gravity. In order to advance currently available treatment of once a month hypodermic needle injection in to the center of the eye, we wanted deliver sustained release formulation. Therefore, we sought to deliver polymeric particles for long-term release of a drug. It would be ideal if we could design a polymeric particle that have a high density and also capable of encapsulating and releasing drugs. However, it could be a difficult task to creating such a novel material and additional toxicology studies are required to be applicable in human use. It would be beneficial to create formulation based on existing FDA approved materials to avoid possible toxicity associated with novel biomaterial. Therefore, we decided to create a particle with two different materials for independently optimizing the density and drug encapsulation and release. We sought to create emulsion droplets with high-density liquid core and polymeric particles as a

stabilizer for drug encapsulation (Fig. 5.3.6.1.a). We wanted to use polymeric particles as a drug carrier because its capability to easily tailor properties, release profile, and has been studied extensively in a literature. And we selected a high gravity material as perfluorodecalin due to its high density (1.9 g-cm^{-3}) and is considered as a most commonly used perfluorocabons in vitreoretinal surgeries [202]. Instead of conducting studies using drug-loaded particles, we decided to use commercially available non-biodegradable polystyrene florescent particles to easily trace and quantify targeting efficiency of the injected PEDs. It is well cited in literature that hydrophilic surfaces are necessary for stabilizing the oil in water emulsion droplets [203]. Although pure polystyrene nanoparticles are hydrophobic, we used particles with carboxylate modification on the surface of the particles with a zeta potential of -47.5±6.07mV, which is essential to form oil in water emulsion droplets [204]. We aimed to create PEDs using largest size of particles to maximize the loading of a drug. However, we failed to create emulsion droplets using nanoparticles larger than 200 nm.

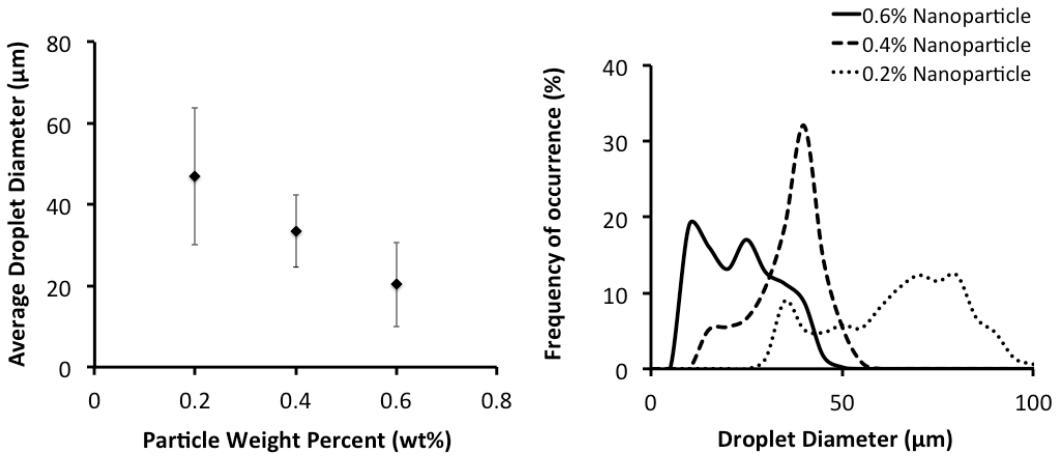

Figure 6.3.1.1. (a) Diameter of the emulsion droplet as a function of nanoparticle concentration in aqueous phase. (b) Size distribution of emulsion droplet as a function of nanoparticle concentration in aqueous phase.

Next, we wanted to make PEDs of different sizes in order to optimize size for gravity-based targeting in the eye. We achieved this by varying the concentration of nanoparticles in the solution when fabricating the PEDs. As shown in Fig. 6.3.1.1.a PED size decreased with increasing nanoparticle concentration, which is consistent with observations by others [205]. Increase in nanoparticle's concentration allows higher surface area coverage of the emulsion droplets resulting smaller size of PEDs. However, PED populations produced in this way were highly poly-disperse (see Fig. 6.3.1.1.b). To provide more uniform particle size distributions, we separated the PEDs into size fractions by passing sequentially through nylon net membrane filters of 11, 20, 30 and 40 µm pore size, which produced PED populations of 14 ± 4.3 µm, 25 ± 6.0 µm and 35 ± 7.5 µm diameter (Figs. 6.3.1.2.a - 6.3.1.2.c). As shown in Fig. 5.3.6.1., each PED contained a non-fluorescent interior composed of perfluorodecalin and a film of red-fluorescent nanoparticles around the outer surface. The high-density of the PEDs was

demonstrated by rapid settling under gravity, as shown in Fig. 6.3.1.2.d. The ability to separate the different PED sizes by filtration shows that the PEDs were mechanically strong enough to withstand the separation process.

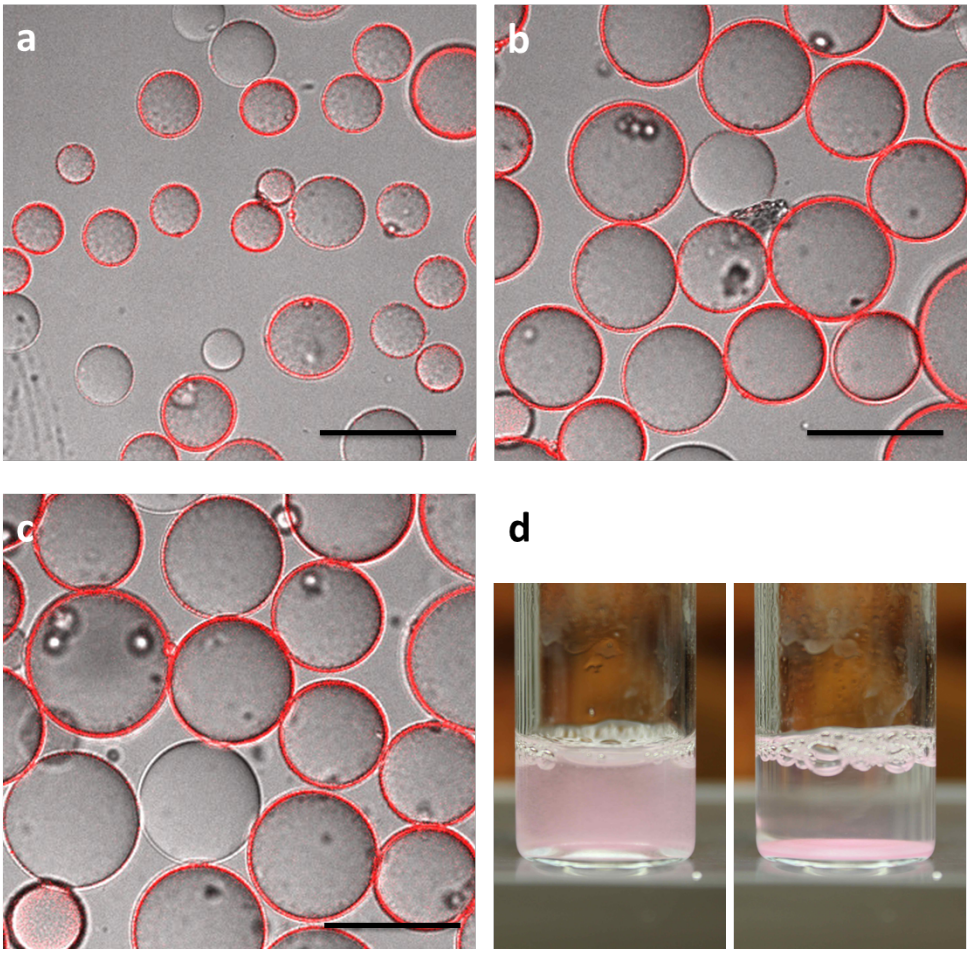

Figure 6.3.1.2. Confocal microscope image of 14 µm (a), 25 µm (b), and 35 µm (c) PEDs. The scale bar indicates 40 µm. Florescent image of 35 µm PEDs immediately after violently shaking the vial and 30 seconds after (d).

PEDs were designed to fall quickly in the eye due to gravity, where larger particles should fall faster than smaller particles due to their increased mass. To determine the fall time of the PEDs in water, which provides an initial estimate of fall time inside the eye after injection, both experimental measurements and theoretical calculations were performed. The measured time for PEDS of 14 μm, 25 μm and 35 μm diameter to fall to the bottom of a vial filled with water to a height of 1 cm (see Materials and Methods) was 93±3 s, 54±5 s, and 31±2.4 s, respectively. A simple force balance to model the process predicted fall times of 104 s, 32 s and 16 s, respectively. The discrepancies between measured and calculated values may be due to variation of the size of and interaction between the PEDs, as well as the subjective nature of experimentally determining when all PEDs settled to the bottom by visualization. In any case, settling times by measurement and calculation were fast, i.e., on the order of 1 min.

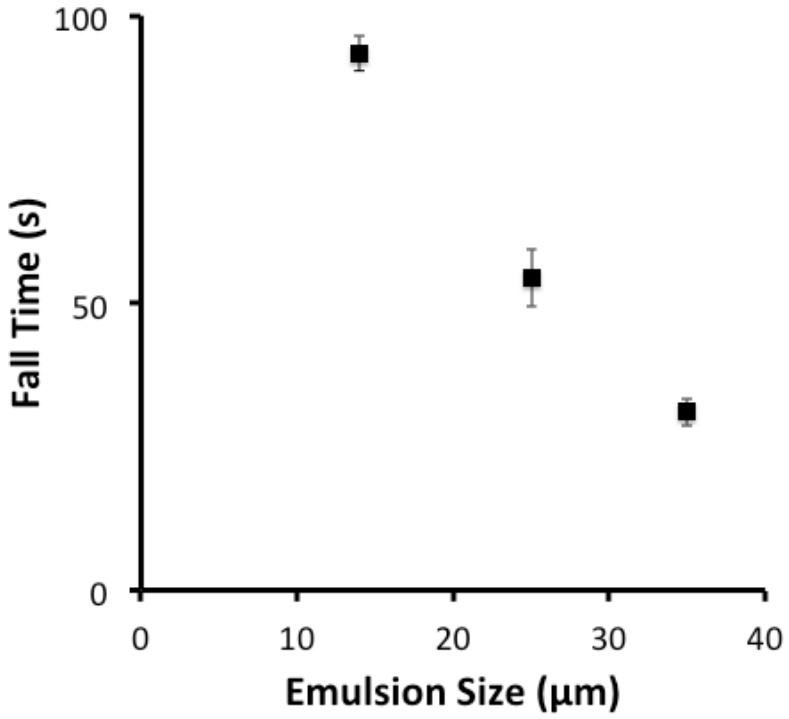

Figure 6.3.1.3. Measured time it take for the emulsion droplets to fall 1 cm in 1% PVA solution.

6.3.2. Use of gravity to target PEDs within the rabbit eye ex vivo

Before conducting *in vivo* experiments, we tested our hypothesis that deposition of PEDs in eye can be directed by gravity by injecting PED suspension in the suprachoroidal space of the rabbit eye *ex vivo* and changing orientation of the eye with respect to gravity. We first targeted delivery to the anterior portion of the suprachoroidal space by positioning the eye with the cornea facing down. The distribution of PEDs after injection was determined by dividing the suprachoroidal space into four antero-posterior quadrants (Fig. 6.2.5.1.a). We found that 59% of the injected PEDs were targeted to the most anterior quadrant, located between the limbus and the site of injection 3 mm back

from the limbus (Fig. 6.3.2.1.b and 6.3.2.1.d). Particle concentration decreased further back in the eye, with just 2.3% of PEDs in the most posterior quadrant located 9 mm or further back from the limbus. There was a statistically significant decrease in PED concentration moving posteriorly within the suprachoroidal space (one-way ANOVA, $p = 0.0002$). This shows significant targeting of the PEDs to the anterior portion of the suprachoroidal space.

We next targeted delivery to the posterior portion of the suprachoroidal space by positioning the eye with the cornea facing up. In this case, 73% of the injected PEDs were located in the two most posterior quadrants and just 8.1% was in the most anterior quadrant (Fig. 6.3.2.1.c and 6.3.2.1.d). There was a statistically significant increase in PED concentration moving posteriorly within the first three quadrants of the suprachoroidal space (one-way ANOVA, $p = 0.02$). This shows significant targeting of the PEDs to the posterior portion of the suprachoroidal space and, when compared with the anteriorly targeted data, demonstrates the gravity-mediated mechanism of the targeting.

Finally, we were interested to characterize the radial distribution of PEDS to the left and right of the injection site. As shown in Fig. 6.3.2.1.e, the large majority of the particles were located in the upper radial quadrants immediately to the left and right of the injections site (i.e., between -90° to 0° and 0° to 90°) and very little reached the lower radial quadrants (i.e., between -180° to 90° and 90° to 180°). There was no significant difference between the particle concentration in each of these quadrants as a function of eye orientation (i.e., cornea up versus cornea down, $p > 0.10$). This is expected, because

radial movement is in the direction perpendicular to the gravitational field, meaning that gravity should not influence radial movement.

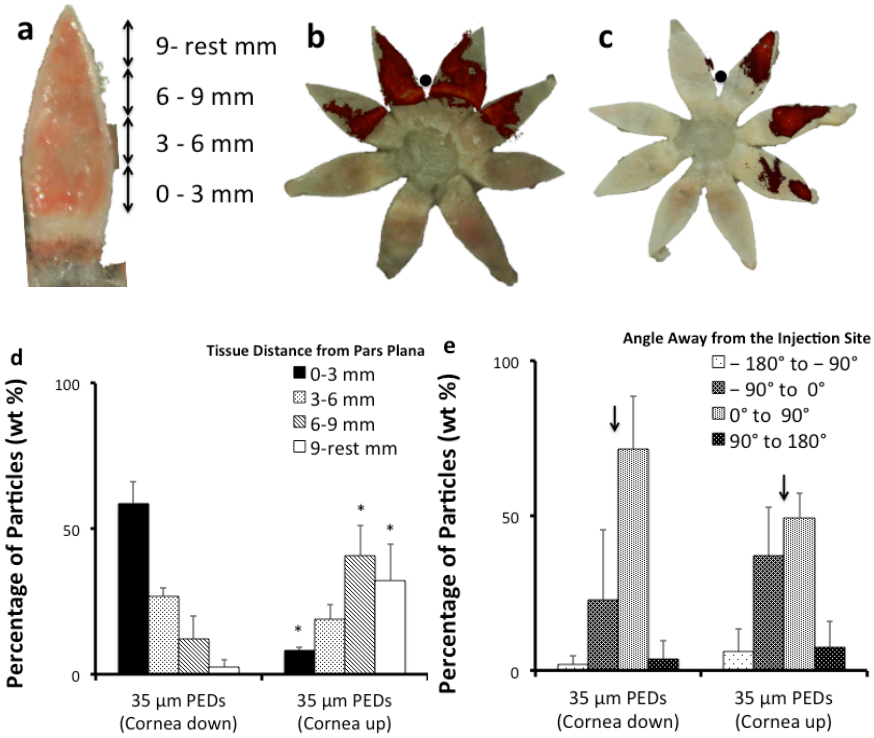

Figure 6.3.2.1. Image showing how the ocular tissue was dissected (a). Injection of 35 µm of PEDs into a rabbit eyes showing localization to the anterior segment (b) and posterior segment (c) by changing orientation of the eye. The eyes were enucleated and frozen immediately and imaged by overlaying a brightfield microscopy image to show ocular anatomy with a fluorescent microscopy image of the same eye showing fluorescent nanoparticles. (e) Distribution of percentage of particles towards posterior segment for two different orientations (cornea down and up). (e) Radial distribution of percentage of particles away from the injection site. The arrow indicates the injection site. * - Indicates statistical significance between two different orientations.

6.3.3. 2.2. Use of gravity to target PEDs within the rabbit eye in vivo

Next, that we repeated the injection of 35 μm PEDs in *in vivo* to verify if *ex vivo* results can be translated *in vivo* eyes. Comparison between the PEDs in each antero-posterior quadrant (0 – 3, 3 – 6, 6 – 9, and 9 – rest mm) of the suprachoroidal space after injection *in vivo* was insignificantly different from injection *ex vivo* (one-way ANOVA, $p > 0.8, 0.7, 0.9, 0.7$, respectively see Fig. 6.3.3.1.). The radial distributions (–180° to –90°, –90° to 0°, 0° to 90°, and 90° to 180°) for *in vivo* and *ex vivo* eyes also showed no significant differences (one-way ANOVA, $p > 1, 0.8, 0.9, 0.9$, respectively). These data show a good correlation between ex vivo and in vivo injections and demonstrate the use of gravity to target PEDs within the living rabbit eye. Gravity-based targeted relies on the use of PEDs with a density greater than water. Therefore, to further assess the role of gravity to target movement of PEDs inside the suprachoroidal space, we carried out an identical experiment using fluorescently tagged polystyrene microparticles with a 32 μm diameter and a density of 1.05 g-cm^{-3} in comparison to PEDs with a 35 μm diameter and perflurodecalin density of 1.92 g-cm^{-3}. The injection conditions in both cases were the same, such as volume (200 μL), concentration (50 μl / 1 ml) and cornea up. As shown in Fig. 6.3.3.2., injection of 32 μm polystyrene fluorescent microparticles resulted in 13±5% of polystyrene particles reaching the most posterior quadrant. In contrast, 2.5 times more of the PEDs reached the most posterior quadrant (i.e., 32±12%). One-way ANOVA analysis shows a statistically significant increase in PED concentration moving posteriorly within the first three quadrants of the suprachoroidal space (one-way ANOVA, $p = 0.0020$). In contrast, there was no statistically significant change in concentration of the polystyrene microparticles within the first three antero-posterior

quadrants (one-way ANOVA, p = 0.99). The radial distributions (–180° to –90°, –90° to 0°, 0° to 90°, and 90° to 180°) showed no significant differences (one-way ANOVA, p = 0.34, 0.34, 0.026, and 0.14, respectively) between PEDs and polystyrene microparticles.

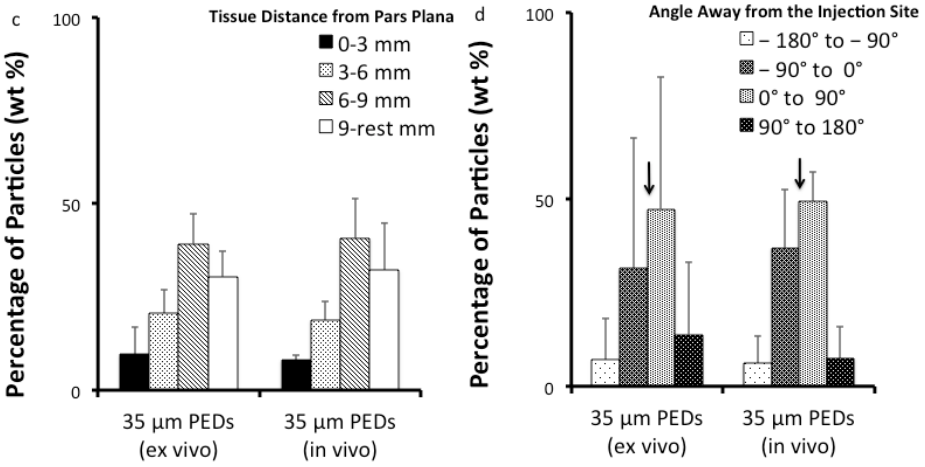

Figure 6.3.3.1. (c) Distribution of percentage of PEDs towards posterior segment. (d) Radial distribution of percentage of PEDs away from the injection site. The arrow indicates the injection site.

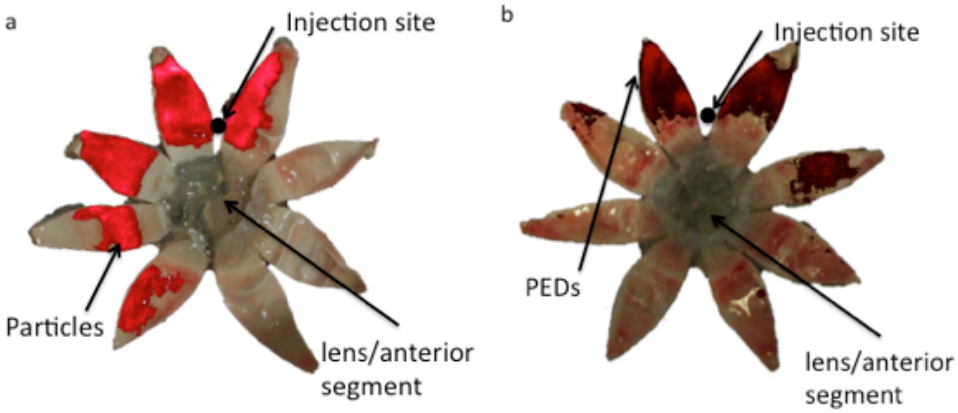

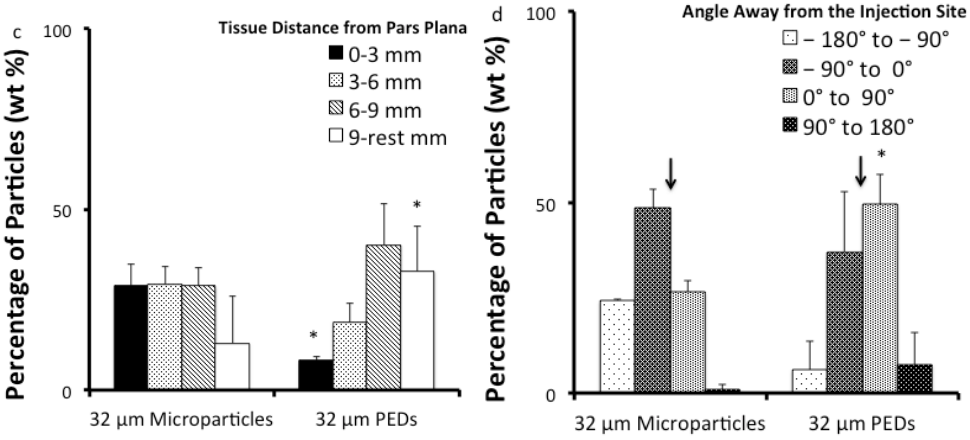

Figure 6.3.3.2. (a) Injection of 32 µm of polystyrene microparticles into a rabbit eyes showing distribution of microparticles. The eyes were enucleated and frozen immediately and imaged by overlaying a brightfield microscopy image to show ocular anatomy with a fluorescent microscopy image of the same eye showing fluorescent nanoparticles. (b) Injection of 35 µm of PEDs into a rabbit eyes showing localization to the posterior segment. The eyes were enucleated and frozen immediately and imaged by overlaying a brightfield microscopy image to show ocular anatomy with a fluorescent microscopy image of the same eye showing fluorescent nanoparticles. (c) Distribution of percentage of microparticles towards posterior segment. (d) Radial distribution of percentage of PEDs away from the injection site. The arrow indicates the injection site. *- Indicates statistical significance between 32 µm micronparticles and PEDs.

6.3.4. Retention of PEDs at the site of targeted delivery

To be most valuable, PEDs should not move around inside the eye after the targeted injection. We hypothesized suprachoroidal space will immediately expand after the injection but will collapse back to its normal position as fluid dissipates and this will immobilize the PEDs. To test this hypothesis, we injected 35 µm PEDs to left eyes and

waited 5 days and immediately before sacrificing the rabbits, we injected PEDs to the right eyes to compare the distribution of PEDs to left eyes of the same animal. As shown in Fig. 6.3.4.1., the distribution of the particles showed similar trend of increase in amount of PEDs towards the posterior segment. Statistical analysis (one-way ANOVA) between each tissue segments (0 – 3, 3 – 6, 6 – 9, and 9 – rest mm) showed significant difference only in 6 – 9 mm segment with p-values of 0.79, 0.89, 0.032, and 0.11, respectively. The radial distributions (–180° to –90°, –90° to 0°, 0° to 90°, and 90° to 180°) for eyes at 0 days and 5 days after injection showed no statistical (one-way ANOVA) difference with p-value of 0.27, 0.36, 0.27, and 0.32, respectively. We therefore conclude PEDs can be targeted to regions of the suprachoroidal space during injection and then can be retained at the site of targeted delivery afterwards. Additional studies will be needed to further assess this retention of PEDs over longer times and, eventually, in humans.

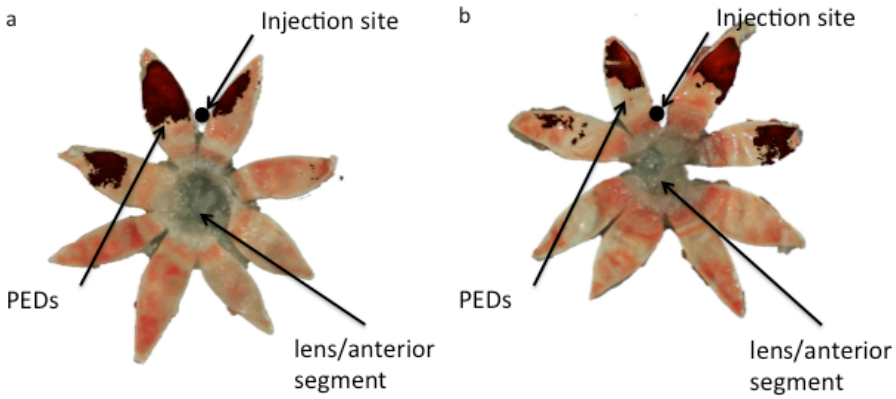

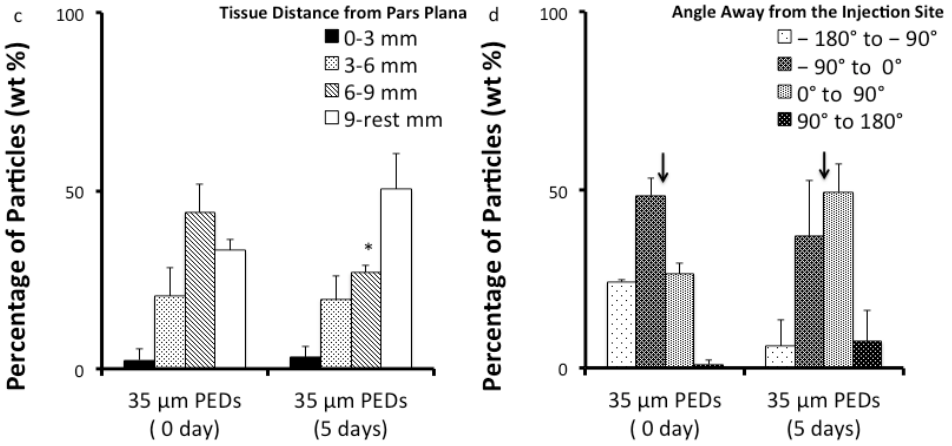

Figure 6.3.4.1. Injection of 35 µm PEDs into a rabbit eyes in vivo showing localization to the posterior segment after 0 day (a) and 5 days (b). The eyes were enucleated and frozen immediately and imaged by overlaying a brightfield microscopy image to show ocular anatomy with a fluorescent microscopy image of the same eye showing fluorescent nanoparticles. (n = 3-4) (c) Distribution of percentage of PEDs towards posterior segment. (d) Radial distribution of percentage of PEDs away from the injection site. The arrow indicates the injection site. *- Indicates statistical significance between day 0 and 5.

6.3.5. Effect of PED size on gravity-mediated targeting

Next we sought to measure the mobility of PEDs inside the suprachroidal space as a function of PED size. We therefore injected PEDS of 14 µm, 25 µm and 35 µm diameter (Fig. 6.3.1.2.) into the suprachoroidal space and measure the extent of posterior targeting with the cornea facing up in the rabbit eye *in vivo*. Our data indicate that the larger PEDs are better in targeting posterior segment (Fig. 6.3.5.1.). We believe this variation is due to variation of the fall time for different size of the PEDs (Fig. 6.3.1.3.). Although the trends suggest the 35 µm particles have a better targeting ability towards

the macula, statistical analysis (one-way ANOVA) showed no significance. The radial distributions for 14 and 25 µm only showed statistical (one-way ANOVA) difference in –90° to 0° and 0° to 90°, segment with p-value of 0.005 and 0.01, respectively. However, no significance in radial distribution was found between 35 µm PEDs and other sizes. We conclude that 35 µm PEDs are optimal for gravity-mediated targeting among the PED sizes tested. It is possible that still-larger PEDS would provide even better targeting by gravity. However, if the PEDs become too large their movement in the suprachoroidal space may be hindered.

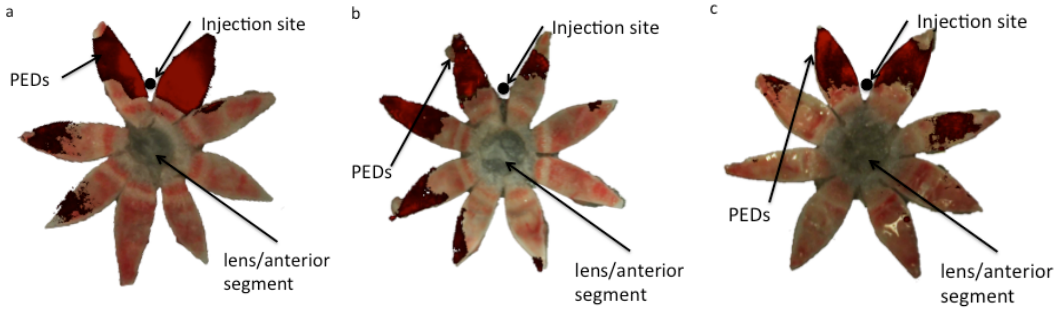

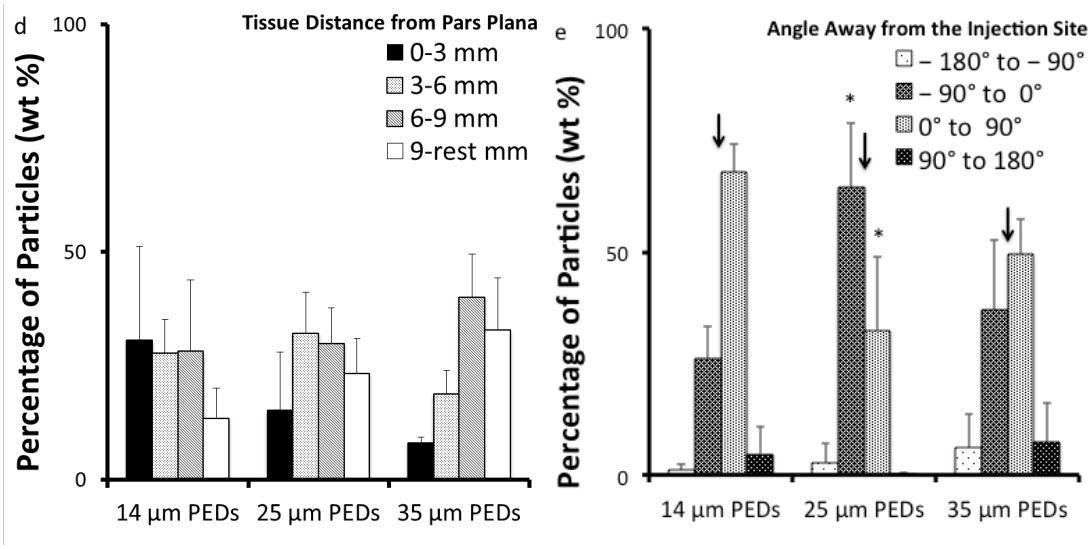

Figure 6.3.5.1. Injection of 14 (a), 25 (b), and 35 μm (c) of PEDs into a rabbit eyes showing distribution. The eyes were enucleated and frozen immediately and imaged by overlaying a brightfield microscopy image to show ocular anatomy with a fluorescent microscopy image of the same eye showing fluorescent nanoparticles. (d) Distribution of percentage of PEDs towards posterior segment. (e) Radial distribution of percentage of PEDs away from the injection site. The arrow indicates the injection site. *- Indicates statistical significance between 14 and 25 μm PEDs.

6.3.6. Kinetics of suprachoroidal space expansion and collapse

An important parameter that could affect the movement of PEDs in suprachoroidal space is the time it takes for suprachoroidal space to collapse down after the injection. Since the time-required PEDs to migrate to posterior segment strongly depend on spatial expansion and collapse time of suprachoroidal space after the injection, therefore we sought to further explore the physical changes to understand the movement of PEDs inside the suprachoroidal space. The targeting efficiency of the PEDs of different particle suggests that particle size has an impact on the mobility of the PEDs inside the suprachoroidal space. In another word, the drop time of the PEDs will impact the targeting efficiency (Fig. 6.3.5.1.). We hypothesized that after the injection into suprachoroidal space, it temporarily expands to incorporate injected fluid until the fluid quickly dissipates away within 30 seconds (approximate drop time for 35 μm PEDs).

We therefore determined the time it takes for fluid to dissipate from suprachoroidal space by two methods. First, we measured IOP over time after injection as an indirect measure of suprachoroidal space expansion. As shown in Fig. 6.3.6.1.a, IOP

increased by 72 mm Hg upon injection, substantially dropped within 5 min and then returned to baseline IOP within 20 min. The initial increase in IOP is believed to be due to introduction of additional fluid into the eye. This effect is seen after intravitreal injection as well [206]. The decay in IOP is believed to be due to clearance of the fluid from the eye. These data therefore suggest that fluid that is injected into the suprachoroidal space is cleared from that space largely within 5 min and completely within 20 min. This provides an estimate for the time window during which PEDS can be targeted by gravity within the suprachoroidal space before that space closes down and entraps the PEDs.

The second method we used to assess the kinetics of suprachoroidal space expansion and collapse used ultrasound imaging to directly measured the height of the suprachoroidal space over time at a single location. Measurements by ultrasound at a location 45° away radially from the injection site showed immediate expansion and substantial collapse within tens of seconds. We believe this rapid collapse of the suprachoroidal space could explain why 35 μm PEDs showed better movement towards the posterior segment of the eye compared to 14 μm PEDs (Fig. 6.3.5.1.). The 35 μm PEDs showed as much as 50% injected PEDs 9 mm away from the ciliary body 5 days after the injection (Fig. 6.3.4.1.).

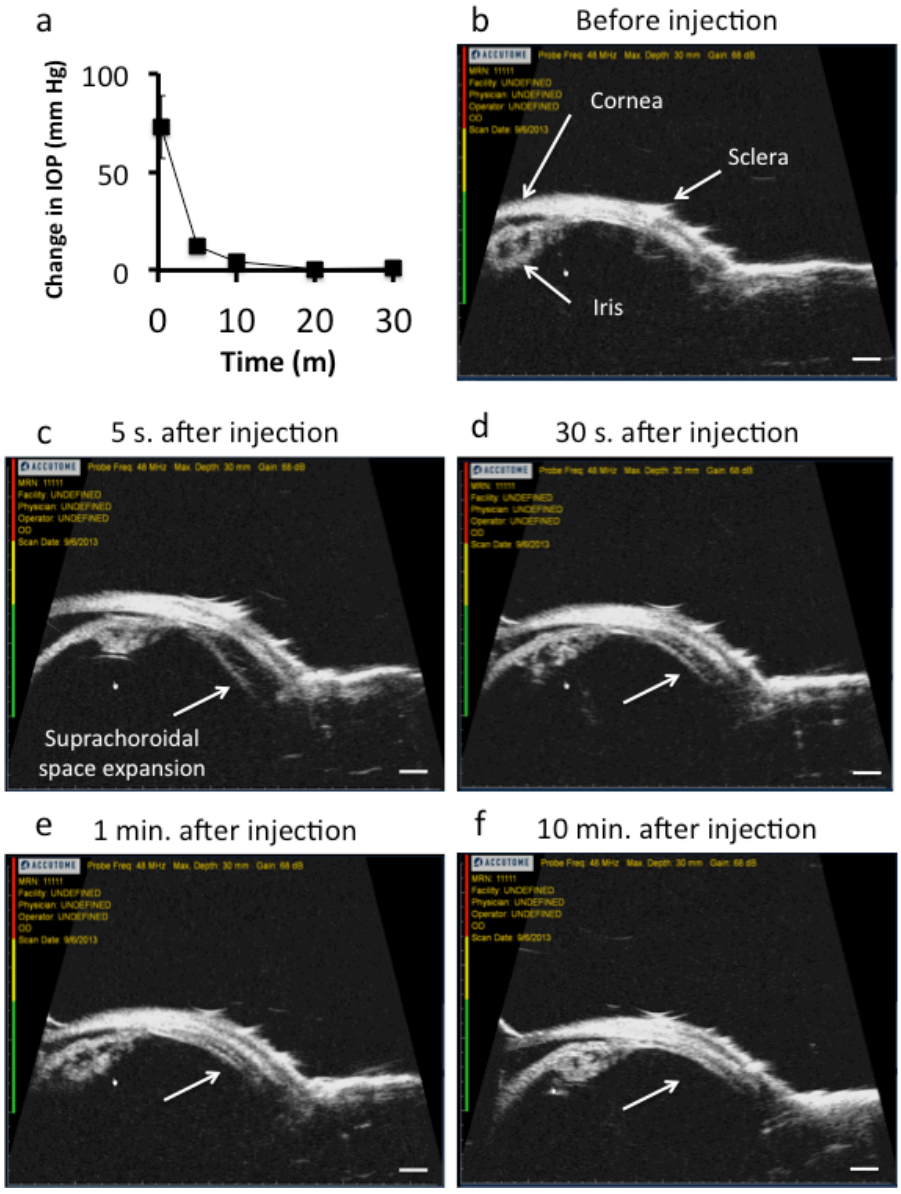

Figure 6.3.6.1. Intraocular pressure change after injecting 200 µl of BSS into suprachoroidal space (a). Ultrasound images of the rabbit eye showing kinetics of the suprachoroidal space expansion and subsequent collapse after injecting 200 µl of BSS into suprachoroidal space (b-f). The ultrasound probe was positioned 45 degrees away from the injection site radially in the superior side of the eye. The scale bar indicates 1mm.

6.4. DISCUSSION

The idea of creating density differences to enhance drug delivery has been used before in creating floating particles to enhance gastric retention and pulmonary delivery [70-72]. Both approaches are similar in a sense that the key parameter that was considered was density difference between particle and the carrier fluid. Creating emulsion droplet using solid particles has been studied since the Pickering [82] originally recognized the role of insoluble solid particles in stabilizing emulsion droplet. Since then, many investigators have studied the stability of particle-stabilized emulsion droplets [83-85]. Particle stabilized emulsion droplet has many uses in food industry, cosmetic industry, pharmaceutical industry, petroleum industry, and in agricultural industry [83]. Particle stabilized emulsion droplets could be stabilized using particles such as silica, clays, titanium dioxide, latex and many others [87-90]. Previously, particle stabilized emulsion droplets has been studied in drug delivery applications [86]. To our knowledge this is the first study to use gravity and particle stabilized emulsion droplets to enhance targeting in the eye.

Currently, the conventional drug delivery methods, such as topical and intravitreal administration, cannot target specific locations within the ocular globe and that is especially the case for delivering controlled release formulation. Suprachoroidal space is a unique space that gives us an ability to deliver large amount of therapeutic formulations in a confined space within the ocular globe. The targeting ability of PEDs will provide us with power to deliver polymeric nanoparticles into posterior segment.

Age related macular degeneration is a disease affects older generation and results in a vision loss due to damage in central part of the retina called the macula. Age related

macular degeneration is the third leading cause of blindness. It is estimated that more than 1.8 million individuals in United States are afflicted by wet age-related macular degeneration (AMD) and that number expected to grow to almost 3 million by 2020 [21, 22]. Choroidal neovascularization (CNV) is the underlying disease of age-related macular degeneration and diabetic retinopathy. However, there are no clinical used methods to deliver therapeutics to the targeting tissue layer, which is choroid. Currently pharmacological treatment for age-related macular degeneration requires once a month injection into anterior chamber of the eye for six months or as a necessary basis. Suprachoroidal injection of allows extremely targeted delivery method to deliver therapeutics to the site of action. The combination of suprachoroidal injection and PEDs will allow delivery of controlled release formulation in an extremely targeted manner. This targeted approach should lead to significant amount of dose sparing, which in turn, reduces side effect due to low required dose.

For targeting posterior segment of the eye, we envisioned, patients receiving the injection lying down on a bed and wait certain period of time for the PEDs to settle and the suprachoroidal space to collapse to hold the PEDs at the posterior segment. Emulsions could be made using various emulsifiers such as amino acids, phospholipids, or solid particles. Using solid particles loaded with drug as an emulsifier simplifies the design of the emulsion droplets compared to using phospholipids and allows controlled release of a drug. In addition, unnecessary excipient formulation could be avoided by using only essential materials that could act both as emulsifier and drug carrier. Perfluorocarbons is the material that has been used in the food and drug administration (FDA) approved ultrasound contrast agents [207] and ophthalmic vitreoretinal

surgeries[208]. Since the introduction by Haidt in 1982 [209] perfluorocarbons have been widely used in ophthalmic surgeries [202]. Perfluorodecalin, the material that is used in this study, is considered as most commonly used perfluorocabons in vitreoretinal surgeries along with perfluorohexyloctane and perfluoroperhydrophenanthrene, and octafluoropropane [202].

In current clinical practice, retina specialists give millions of intravitreal injections per year at the pars plana located 2-5 mm from the limbus [158, 159]. Suprachoroidal injection requires placement of microneedles at the same site, which should be straightforward for an ophthalmologist to do. Assuring microneedles go to the right depth at the base of the sclera is determined by microneedle length. While scleral thickness varies among eyes, experience in rabbits, pigs and humans shows that for a given species, a single microneedle length generally works in all eyes to target the suprachoroidal space. Ocular anatomy is accommodating because shallow injections can punch through scleral tissue to reach the supraciliary space and deep injections do not enter choroid because of its deformability. Microneedles have been used for hundreds of suprachoroidal injections in rabbits, a dozen in pigs and four in human subjects with extremely reliable targeting [66, 109, 134, 160-162]. Highly targeted delivery into suprachoroidal space could enable us to deliver single dosing of anti-VEGF therapeutics every 3-6 months or more, which could dramatically increase patient compliance.

Our research group at Georgia Institute of Technology used microneedles for injection into the suprachoroidal space for delivery to the posterior segment in >200 rabbits. All injections were successfully targeted to the suprachoroidal space and there were no significant adverse reactions [66-68, 134, 161]. Clearside Biomedical, a company that has

licensed our technology, has received IND approval from FDA based on a published 90-rabbit GLP study of safety, which likewise showed no significant adverse effects or lasting IOP changes [162]. The company has also published data from four human patients receiving suprachoroidal injection of Avastin using a microneedle, which was well tolerated with no serious adverse events over a two-month monitoring period[109]. Based on this experience with suprachoroidal injection to the posterior segment, we believe that supraciliary injection to the anterior segment will be safe and can be simply and reliably performed.

6.5. CONCLUSION

This study demonstrates that polymeric nanoparticles can be targeted to the posterior of the ocular globe using gravity mediated delivery methods via suprachoroidal delivery using hollow microneedles. In vivo study showed that 35 μm particle stabilized emulsion droplets can specifically target 73% of injected particles towards back of the ocular globe. We also demonstrated that by orienting the eyes in different orientation, allows us to mobilize emulsion droplets in the direction of gravity to target different locations within the ocular globes. Orienting the eye's visual direction in the same direction as the gravity (e.g. surface of the cornea facing downward) allows more than 85% of injected particles to stay within 6 mm of the pars plana. This study shows for the first time that gravity mediated method can be used to target specific locations within the ocular globe using microneedles in minimally invasive way. Future study is required to optimize many injection parameters such as injection volume, optimize size of emulsion droplets, and concentration to improve this technique.

7 CONCLUSIONS

Current treatment of ocular disorders in the eye is constrained by inefficient drug delivery methods, since topical application and even intraocular injection is not targeted enough to the site of action. In addition, many intraocular injections lead to safety concerns. It is especially challenging if the molecules we want to deliver are macromolecules such as protein or sustained release formulation. It makes the treatment much more challenging if the targeting tissue is at the back of the eye such as in age related macular degeneration (AMD). In this study, microneedles were tested in conjunction with novel formulations to provide targeted drug delivery into the eye guided by the previous advancement in ocular drug delivery.

The first part of the work introduced a minimally invasive strategy for delivering protein therapeutics to the cornea. In this work, we showed that highly targeted intracorneal delivery of bevacizumab using a coated microneedle allowed dramatic dose sparing compared to subconjunctival and topical delivery in an injury-induced neovascularization model. Eyes treated with 4.4 μg of bevacizumab using microneedles reduced neovascularization compared to the untreated eye by 65% (day 10) to 44% (day 18). Eyes treated with 2500 μg of bevacizumab using subconjunctival injection gave the same results as the eyes treated with 4.4 μg of bevacizumab-coated microneedles. While eyes treated with 52500 μg of bevacizumab by eye drops three times per day for 14 days reduced neovascularization area compared to the untreated eye by 44% (day 10) to 6% (day 18). Safety study showed microneedle did not affect corneal transparency and microanatomical structures. As a result, these data could be used to design an effective device for delivering bevacizumab and other protein therapeutics into the cornea.

In second part the study, we developed novel formulations to immobilize or to enhance the spreading of injected polymeric particles. Study showed stronly non-Newtonian materials were capable of slowing down the movement of particles inside the suprachoroidal space for period of 60 days. Study also showed that the high molecular weight polymers and weakly non-Newtonian materials generated movement of imbedded particles inside the suprachoroidal space and were capable of covering 100% of the suprachoroidal space using a single injection. Overall, this study demonstrates for the first time that simple polymeric excipients could be used to control the movement of polymeric particles inside the suprachoroidal space.

In the third part of the study, we showed that highly targeted delivery of anti-glaucoma drugs to the supraciliary space using a hollow microneedle allows dramatic dose sparing of the drug compared to topical eye drops. The supraciliary space is the most anterior portion of the suprachoroidal space located below the sclera and above the choroid and ciliary body. We showed that isoflurane, rather than ketamine/xylazine as the anesthetic, did not effect the IOP change in the time scale of an hour, thereby minimizing artifacts from anesthesia. We showed supraciliary delivery of sulprostone reduced IOP unilaterally in a dose-related response. Pharmacodynamics analysis showed approximately 1100-fold dose sparing of sulprostone by supraciliary injection in comparison with topical administration at the conventional human dose. We also showed supraciliary delivery of brimonidine reduced IOP bilaterally in a dose-related response. Pharmacodynamics analysis showed approximately 500-fold dose sparing of brimonidine by supraciliary injection in comparison with topical administration at the conventional human dose. A safety study showed that the kinetics of IOP elevation immediately after

supraciliary and intravitreal injection of placebo formulations were similar. Overall, we demonstrated targeted delivery in this way could increase patient compliance and safety by achieving significant dose sparing which allow a single injection to contain enough drugs for long-term sustained delivery and reduces side effects.

In the fourth and final part of the study, we showed particle stabilized high-density emulsion droplets (PEDs) could be used to enhance targeting of various locations within the eye via suprachoroidal space injection. Microneedles were shown to deliver nanoparticles preferentially towards the posterior of the eye using high-density PEDs into the suprachoroidal space of rabbits. Up to 35 μm sized PEDs were injected into suprachoroidal space of the eye and were able to deliver particles preferentially towards back of the eye by showing 2.5 times increase in particle concentration at the posterior of the eye compared to 32 μm polystyrene particles. In addition, by comparing the eyes immediately and 5 days after the injection, we demonstrated that the PEDs stay at the posterior segment up to 5 days. We were able to confirm the expansion of the suprachoroidal space immediately after the injection, to incorporate the injected fluid but then collapse down within several minutes by looking at real time ultrasound images. This study demonstrates for the first time that high-density PEDs could be used to preferentially deliver nanoparticles to posterior of the eye.

Overall, this work introduces novel approaches to enhance targeting of macromolecules to cornea, ciliary body, choroid, and back of the eye using microneedles as a drug delivery platform. This work showed methods to effectively deliver macromolecules to the targeted tissues and demonstrated that the highly targeted drug delivery method using microneedles provided the following expected advantages: (i)

bioavailability approaching 100% by delivering drugs directly to the targeting tissue, (ii) reduce side effects due to low dosage requirement by delivering more drugs to the targeting site, (iii) improved patient compliance by administering longer controlled-release formulation which is not possible without highly targeted delivery, (iv) in a minimally invasive way using microneedles.

Studies in this thesis show some of the first methods to achieve targeted delivery of sustained-release formulation at various locations within the eye. We believe this work can provide an alternative modality to deliver pharmacotherapies and controlled release formulations in a highly targeted way to reduce side effects and increase patient compliance. We expect clinicians to make sound decision to utilize both existing and microneedle based delivery to tailor the treatments to fit the need for different patients' life style and symptoms. We also believe this work could provide a tool for both present and future research to develop new pharmacotherapies that might require significant targeting to achieve its full efficacy. Blindness results in devastating impact on peoples' lives and we believe microneedle based drug delivery methods could one day be used to enhance treatment for many vision-threatening diseases.

8 RECOMMENDATIONS

The research presented here represents some of the first studies to develop novel techniques to deliver dugs to specific locations within the eye. In addition, studies here demonstrate the advantages of highly targeted ocular drug deliver using microneedles. Conventional ocular drug delivery methods often deliver drugs to the whole ocular globe and are not capable of delivering drugs to specific locations within the ocular globe. The results from this work demonstrate the capabilities of microneedle-based drug delivery methods to deliver therapeutics to various locations within the eye in minimally invasive and highly targeted way. However, there are still many unanswered questions that need exploring before the full potential of these strategies can be understood.

In the first part of the study, we introduced a minimally invasive strategy for delivering protein therapeutics into the cornea. In this work, we showed that highly targeted intracorneal delivery of bevacizumab using a coated microneedle allows dramatic dose sparing compared to subconjunctival and topical delivery in an injury-induced neovascularization model. The further studies are required to test the capability of delivering other therapeutics with different properties and formulations into intrastromal space of the cornea. Experiments should be designed to understand the relationship between different properties of molecules and pharmacokinetics of intrastromal injection. In addition, further studies to examine how the changes in formulations could influence the pharmacokinetics within the intrastromal space. For example, lipophilic drugs, such as steroids, may have prolonged residence times because of their low solubility in aqueous environments. In addition, formulation changes could be used to control diffusion of a molecule within the intracorneal space. In addition,

biodegradable particles with encapsulated drugs need to be evaluated within the intracorneal space to demonstrate sustained release. Understanding the diffusion of the drugs in the intraocular tissues as a function of properties of a molecule will help determine the potential of the intracorneal delivery.

There are many hurdles that we have to overcome for this technology to be available for treating corneal neovascularization in the clinic. Even before starting human clinical trials, there are few things that we have to address. First, a viable product should have a long shelf life. Therefore, long-term stability of bevacizumab in a dried state needs be studied. Optimum parameters that impact the stability of bevacizumab must be studied to create a suitable packaging environment for coated microneedles. Second, a new pen-like device to hold the microneedle and to make the insertion procedure easier has to be designed.

For the second part of the study, we developed novel formulations to immobilize or to enhance the spreading of injected polymeric particles. Future work needs to focus on understanding the mechanism of the immobilization and the spreading of the polymeric particles by observing the movement of excipient formulations. Moreover, further experiments are needed to understand the pharmacokinetics of described suprachoroidal targeting and how different properties of injected drug impact the biodistribution. In addition, biodegradable particles with encapsulated drugs need to be evaluated within the suprachoroidal space to demonstrate sustained release.

In order for this technology to be available in clinic, there are many additional hurles that we have to overcome. First, the anatomical differences in the suprachoroidal space of different species must be studied before starting the human clinical trial. It is

possible that physiological barriers might exist inside the suprachoroidal space to block the spreading of injected steroid particles. Second, often times, posterior and pan-uveitis involve inflammation in the layer of both choroid and retina. Further studies have to be carried out to determine if suprachoroidal delivery alone is capable of reducing inflammation in both choroid and retina. If suprachoroidal delivery alone cannot reduce retinal inflammation, the minimal intravitreal dose that could be used in conjunction with suprachoroidal delivery should be studied.

In the third part of the study, we showed highly targeted delivery of anti-glaucoma drugs to the supraciliary space using a hollow microneedle allowed dramatic dose sparing of the drug compared to topical eye drops. Future work needs to focus on understanding the pharmacokinetics of supraciliary targeting and how different properties of injected drugs impact the biodistribution. In addition, biodegradable particles with encapsulated drugs need to be evaluated within the supraciliary space to demonstrate sustained release. We believe this study can contribute to the development of novel therapies for glaucoma.

In order for this technology to be available in the clinic, there are many additional hurdles that we have to overcome. We still know very little about safety of injected biodegradable particles in the suprachroidal space. Further safety studies are required to see if polymeric formulation cause adverse events. One critical drawback of delivering controlled release formulations is that we cannot stop the medication in case adverse events occurs in a patient. Therefore it is crucial to make sure that patients are free from adverse events before administering controlled release formulations.

In the fourth and final part of the study, we showed particle-stabilized high-density emulsion droplets (PEDs) could be used to enhance targeting of various locations in the eye via suprachoroidal space injection. Future work is needed to optimize the injection volume, PED concentration, and polymeric particle sizes for better mobility or targeting inside the suprachoroidal space. Experiments should be designed to understand how surface properties of PEDs change the interactions between the tissue and PEDs within the suprachoroidal space. Future work also needs to focus on understanding the intraocular pharmacokinetics of drug loaded PEDs. In addition, pharmacodynamics study to demonstrate dose sparing of this highly targeted delivery method will help determine the potential that these injections have on treating eye diseases.

There are many additional hurdles that we need to overcome for this technology to be available for treating age-related macular degeneration in the clinic. First, the anatomical differences in the suprachoroidal space of different species must be studied before starting the clinical trials. It is possible that physiological barriers might exist inside the suprachoroidal space to block the spreading of injected PEDs. Second, there are some additional concerns with the formulation of PEDs. Biodegradable particles, and aqueous formulation too, have to be in a separate container because particles will dissolve inside the aqueous formulation during storage. Because particles cannot be stored in aqueous formulation, additional formulation studies are required to keep dried form of PEDs to be separated from aqueous formulation.

Overall, these studies offer exciting opportunities to target various locations within the eye enabled by microneedle technology. Studies in this thesis demonstrate and show many advantages of delivering drugs within specific locations of the eye in a

minimally invasive way. A successful treatment requires effective combination of a pharmacological therapy and a delivery method. Recent advancement in biotechnology is allowing more macromolecular therapeutics to be in the market but conventional delivery methods are not efficient in delivering macromolecules to the targeted site of action and achieve full potential of the developed pharmacological therapies. Microneedle-based delivery methods could provide required delivery methods to support new and existing drug development.

APPENDIX A

A.1. Mathematical Modeling And In Vivo Imaging Of Bevacizumab (Chapter 3)

Diffusion of immunoglobulin G (IgG) in stroma was modeled by modifying the previous work in literature[210], which combines an expression for 2-dimensional radial diffusion from a bolus source in cylindrical coordinates with a term to account for loss in the z dimension across epithelium and endothelium (k) to describe concentration, C, of a solute molecule in stroma. Following equation was used to evaluate the concentration of injected bevacizumab around the delivery site as a function of time. An amount, M_0, of protein is injected at time 0, and it can be considered diffusing radially in the stroma. After time, t, the concentration of protein is given by following equation. Where D is effective solute diffusivity in stroma, r is distance from insertion site, a is radius of insertion bolus, and u and k are constants. Analytical solution is given by Crank [211]. Mathematical modeling of drug diffusion after intrastromal delivery will predict concentration profiles as a function of time and radius from the insertion site.

$$C(t) = \left[\frac{M_0}{2Dt} e^{\frac{-r^2}{4Dt}} \int_0^a e^{\frac{-u^2}{4Dt}} I_0\left(\frac{ru}{2Dt}\right) u\partial u\right]_{Diffusion\ in\ Stroma} [e^{-kt}]_{Loss\ through\ epithelium\ and\ endothelium} \quad (1)$$

Since our experimental measurements were fluorescent signal intensity in a fixed region of interest (ROI) over time (t), the above equation can be integrated with respect to distance R from the center of the insertion site to yield the following equation. Diffusivity and the endothelium diffusion constant was obtained from literature [210]. Quantitative

measurements of the pharmacokinetic of labeled bevacizumab in stroma will be measured periodically for up to 8 days using in vivo florescence measurement. Image analysis was calibrated against coating formulation with known concentrations. The dynamic range we were able to obtain was 66.64 ~0.02 mg/mL. The concentration of be bevacizumab was verified using ELISA. Insertion was made on the superior side of the eye using 4 microneedles 1mm away from the limbus.

$$C(t)_{Ave} = \frac{\int_0^R \frac{M_0}{2Dt} e^{\frac{-r^2}{4Dt}} e^{-kt} \left[\int_0^a e^{\frac{-u^2}{4Dt}} I_0\left(\frac{ru}{2Dt}\right) u \partial u \right] 2\pi r dr}{\int_0^R 2\pi r dr} \quad (2)$$

Prior to insertion and imaging procedure, rabbits were anesthetized with ketamine (6 mg/kg) and xylazine (4 mg/kg) and acepromazine (0.25 mg/kg) subcutaneously. Eyes were kept open using lid speculum for the whole duration of the imaging procedures. The fluorescent signal intensity in the rabbits was measured on a Caliper Xenogen Lumina In Vivo Imaging System (IVIS) at 0, 2, and 4 days post insertion. Animals were imaged at 745 nm excitation, 780 nm emission and 1 second exposure time. Fluorescence intensity was measured as background-subtracted average efficiency within a fixed region of interest (ROI) centered on the insertion site.

A.1.1. Intracorneal Bevacizumab Diffusion Modeling

We sought to better understand the diffusion of the IgG molecules inside the corneal stoma after microneedle insertion using mathematical model. Aside from the diffusion of molecules radially, molecules can diffuse through the endothelium and

epithelium. The loss through the epithelium could be significant due to the hole created by inserting microneedle into the corneal stroma. The loss through the both endothelium and epithelium are represented by the unknown constant (*k*). Furthermore, there could be a variation in the radius of the instantaneous source (*a*) because the microneedle was inserted into the cornea not perpendicular but at an angle.

Theoretical model was fitted with given initial value and by varying the value of *k* and *a* using least square analysis method. An exponential decline in signal intensity of the labeled bevacizumab delivery was observed, with 97% of the signal lost by 4 days after the delivery. The experimental and theoretical value of labeled bevacizumab was compared and showed decent fit. The percent difference between experimental and theoretical values were in as low as 0.29 % and as high as 100 %. The obtained value of *a* and *k* was 100 μm and 0.41 h^{-1}, respectively. The rate of the loss through the endothelium was previously measured by Allensmith et al [212] to be 0.00104 h^{-1}. The large difference between the two values indicates the significant loss through the hole what was made by the inserting the microneedle. In addition, sensitivity analysis showed a value lower than 100 μm does not impact the calculated concentration profile.

Time (h)	Experimental Conc. (ug/mL)	Theoretical (μg/ml)	Difference (%)
0	731.88684	731.88684	0
3	319.9323475	319	0.291420204
48	67.90161	1.69E-06	99.99999751
96	20.130244	3.37E-15	100

REFERENCES

1. Resnikoff, S., et al., *Global data on visual impairment in the year 2002.* Bull World Health Organ, 2004. **82**(11): p. 844-51.

2. Congdon, N., et al., *Causes and prevalence of visual impairment among adults in the United States.* Archives of Ophthalmology, 2004. **122**(4): p. 477-485.

3. Lee, D.A. and E.J. Higginbotham, *Glaucoma and its treatment: a review.* Am J Health Syst Pharm, 2005. **62**(7): p. 691-9.

4. Ferrara, N., et al., *Targeting VEGF-A to treat cancer and age-related macular degeneration.* Annu Rev Med, 2007. **58**: p. 491-504.

5. Fatt, I. and B.A. Weissman, *Physiology of the eye : an introduction to the vegetative functions*. 2nd ed. ed. 1992: Butterworth-Heinemann. xi, 275 p.

6. Kaufman, P.L., A. Alm, and F.H.P.o.t.e. Adler, *Adler's physiology of the eye : clinical application*. 10th ed. / edited by Paul L. Kaufman, Albert Alm. ed. 2003, St. Louis ; London: Mosby. xvii, 876 p.

7. Lens, A., *Ocular anatomy and physiology*. The basic bookshelf for eyecare professionals. 1999, Thorofare, NJ: SLACK. xi, 147 p.

8. Alm, A. and S.F. Nilsson, *Uveoscleral outflow--a review.* Exp Eye Res, 2009. **88**(4): p. 760-8.

9. Bachmann, B., R.S. Taylor, and C. Cursiefen, *Corneal Neovascularization as a Risk Factor for Graft Failure and Rejection after Keratoplasty An Evidence-Based Meta-analysis.* Ophthalmology, 2010. **117**(7): p. 1300-U42.

10. Folkman, J. and Y. Shing, *Angiogenesis.* J Biol Chem, 1992. **267**(16): p. 10931-4.

11. Ferrara, N., H.P. Gerber, and J. LeCouter, *The biology of VEGF and its receptors.* Nat Med, 2003. **9**(6): p. 669-76.

12. Dorrell, M., et al., *Ocular neovascularization: basic mechanisms and therapeutic advances.* Surv Ophthalmol, 2007. **52 Suppl 1**: p. S3-19.

13. Ferrara, N., *Vascular endothelial growth factor: basic science and clinical progress.* Endocr Rev, 2004. **25**(4): p. 581-611.

14. *FDA Approval for Bevacizumab - National Cancer Institute*, 2010, National Cancer Institute.

15. Holash, J., et al., *VEGF-Trap: a VEGF blocker with potent antitumor effects.* Proceedings of the National Academy of Sciences of the United States of America, 2002. **99**(17): p. 11393-8.

16. Heier, J.S., et al., *Intravitreal aflibercept (VEGF trap-eye) in wet age-related macular degeneration.* Ophthalmology, 2012. **119**(12): p. 2537-48.

17. Bachmann B, T.R., Cursiefen C, *Corneal neovascularization as a risk factor for graft failure and rejection after keratoplasty: an evidence-based meta-analysis.* Ophthalmology. , 2010. **117**(7): p. 1300-U42.

18. Panda, A., et al., *Corneal graft rejection.* Surv Ophthalmol, 2007. **52**(4): p. 375-96.

19. Inoue, K., et al., *Risk factors for corneal graft failure and rejection in penetrating keratoplasty.* Acta Ophthalmol Scand, 2001. **79**(3): p. 251-5.

20. Quigley, H.A. and A.T. Broman, *The number of people with glaucoma worldwide in 2010 and 2020.* Br J Ophthalmol, 2006. **90**(3): p. 262-7.

21. Friedman, D.S., et al., *Prevalence of age-related macular degeneration in the United States.* Arch Ophthalmol, 2004. **122**(4): p. 564-72.

22. Saaddine, J.B., et al., *Projection of diabetic retinopathy and other major eye diseases among people with diabetes mellitus: United States, 2005-2050.* Arch Ophthalmol, 2008. **126**(12): p. 1740-7.

23. Nowak, J.Z., *Age-related macular degeneration (AMD): pathogenesis and therapy.* Pharmacol Rep, 2006. **58**(3): p. 353-63.

24. Lafaut, B.A., et al., *Clinicopathological correlation in exudative age related macular degeneration: histological differentiation between classic and occult choroidal neovascularisation.* Br J Ophthalmol, 2000. **84**(3): p. 239-43.

25. Lafaut, B.A., et al., *Clinicopathological correlation of retinal pigment epithelial tears in exudative age related macular degeneration: pretear, tear, and scarred tear.* Br J Ophthalmol, 2001. **85**(4): p. 454-60.

26. Hughes, P.M., et al., *Topical and systemic drug delivery to the posterior segments.* Adv Drug Deliv Rev, 2005. **57**(14): p. 2010-32.

27. Fattal, E. and A. Bochot, *Ocular delivery of nucleic acids: antisense oligonucleotides, aptamers and siRNA.* Adv Drug Deliv Rev, 2006. **58**(11): p. 1203-23.

28. Steinbrook, R., *The price of sight--ranibizumab, bevacizumab, and the treatment of macular degeneration.* N Engl J Med, 2006. **355**(14): p. 1409-12.

29. Chappelow, A.V. and P.K. Kaiser, *Neovascular age-related macular degeneration: potential therapies.* Drugs, 2008. **68**(8): p. 1029-36.

30. Peyman, G.A., E.M. Lad, and D.M. Moshfeghi, *Intravitreal injection of therapeutic agents.* Retina, 2009. **29**(7): p. 875-912.

31. Otsuji, T., et al., *Initial non-responders to ranibizumab in the treatment of age-related macular degeneration (AMD).* Clin Ophthalmol, 2013. **7**: p. 1487-90.

32. Nigam, N., J. Hedaya, and W.R. Freeman, *Non-responders to bevacizumab (Avastin) therapy of choroidal neovascular lesions.* Br J Ophthalmol, 2008. **92**(6): p. 864-5; author reply 865-6.

33. Lux, A., et al., *Non-responders to bevacizumab (Avastin) therapy of choroidal neovascular lesions.* Br J Ophthalmol, 2007. **91**(10): p. 1318-22.

34. Klein, R., et al., *The Wisconsin Epidemiologic Study of Diabetic Retinopathy: XVII. The 14-year incidence and progression of diabetic retinopathy and associated risk factors in type 1 diabetes.* Ophthalmology, 1998. **105**(10): p. 1801-15.

35. Wong, T.Y., et al., *Diabetic retinopathy in a multi-ethnic cohort in the United States.* Am J Ophthalmol, 2006. **141**(3): p. 446-455.

36. Avery, R.L., et al., *Intravitreal bevacizumab (Avastin) in the treatment of proliferative diabetic retinopathy.* Ophthalmology, 2006. **113**(10): p. 1695 e1-15.

37. Chun, D.W., et al., *A pilot study of multiple intravitreal injections of ranibizumab in patients with center-involving clinically significant diabetic macular edema.* Ophthalmology, 2006. **113**(10): p. 1706-12.

38. Gaudana, R., et al., *Ocular drug delivery.* The AAPS journal, 2010. **12**(3): p. 348-60.

39. Barar, J., A.R. Javadzadeh, and Y. Omidi, *Ocular novel drug delivery: impacts of membranes and barriers.* Expert opinion on drug delivery, 2008. **5**(5): p. 567-81.

40. Hughes, P.M., et al., *Topical and systemic drug delivery to the posterior segments.* Advanced drug delivery reviews, 2005. **57**(14): p. 2010-32.

41. Kaur, I.P., et al., *Acetazolamide: future perspective in topical glaucoma therapeutics.* International journal of pharmaceutics, 2002. **248**(1-2): p. 1-14.

42. Coppens, M., L. Versichelen, and E. Mortier, *Treatment of postoperative pain after ophthalmic surgery.* Bulletin de la Societe belge d'ophtalmologie, 2002(285): p. 27-32.

43. Kampougeris, G., et al., *Penetration of moxifloxacin into the human aqueous humour after oral administration.* The British journal of ophthalmology, 2005. **89**(5): p. 628-31.

44. Chong, D.Y., et al., *Vitreous penetration of orally administered famciclovir.* American journal of ophthalmology, 2009. **148**(1): p. 38-42.e1.

45. Burstein, N.L. and J.A. Anderson, *Corneal penetration and ocular bioavailability of drugs.* Journal Of Ocular Pharmacology, 1985. **1**(3): p. 309-26.

46. Kaur, I.P., et al., *Vesicular systems in ocular drug delivery: an overview.* International Journal of Pharmaceutics, 2004. **269**(1): p. 1-14.

47. Urtti, A., *Challenges and obstacles of ocular pharmacokinetics and drug delivery.* Advanced Drug Delivery Reviews, 2006. **58**(11): p. 1131-5.

48. Cone, R.A., *Barrier properties of mucus.* Adv Drug Deliv Rev, 2009. **61**(2): p. 75-85.

49. Jarvinen, K., T. Jarvinen, and A. Urtti, *OCULAR ABSORPTION FOLLOWING TOPICAL DELIVERY.* Advanced Drug Delivery Reviews, 1995. **16**(1): p. 3-19.

50. Koevary, S.B., *Pharmacokinetics of topical ocular drug delivery: potential uses for the treatment of diseases of the posterior segment and beyond.* Curr Drug Metab, 2003. **4**(3): p. 213-22.

51. Raghava, S., M. Hammond, and U.B. Kompella, *Periocular routes for retinal drug delivery.* Expert Opin Drug Deliv, 2004. **1**(1): p. 99-114.

52. Ohm, J., *Über die Behandlung der Netzhautablösung durch operative Entleerung der subretinalen Flüssigkeit und Einspritzung von Luft in den Glaskörper.* Albrecht von Graefes Archiv für Ophthalmologie, 1911. **79**(3): p. 442-450.

53. Peyman, G.A., P. Nelsen, and T.O. Bennett, *Intravitreal injection of kanamycin in experimentally induced endophthalmitis.* Can J Ophthalmol, 1974. **9**(3): p. 322-7.

54. Forster, R.K., et al., *Further observations on the diagnosis cause, and treatment of endophthalmitis.* Am J Ophthalmol, 1976. **81**(1): p. 52-6.

55. Administration, U.S.F.a.D., *Vitravene (Fomivirsen Sodium Intravitreal Injectable) Injection*, 1998, Isis Pharmaceuticals, Inc.

56. Chang, T.S., et al., *longitudinal changes in self-reported visual functioningin AMD patients In a randomized controlled Phase I/II trial of lucentisTM (ranizumab; rHuFAB v2).* Invest. Ophthalmol. Vis. Sci., 2004. **45**(5): p. 3098-.

57. *Preclinical and phase 1A clinical evaluation of an anti-VEGF pegylated aptamer (EYE001) for the treatment of exudative age-related macular degeneration.* Retina, 2002. **22**(2): p. 143-52.

58. Jager, R.D., et al., *Risks of intravitreous injection: a comprehensive review.* Retina, 2004. **24**(5): p. 676-98.

59. Lee, S.S., et al., *Biodegradable implants for sustained drug release in the eye.* Pharm Res, 2010. **27**(10): p. 2043-53.

60. Kane, F.E., et al., *Iluvien: a new sustained delivery technology for posterior eye disease.* Expert Opin Drug Deliv, 2008. **5**(9): p. 1039-46.

61. Krohn, J. and T. Bertelsen, *Corrosion casts of the suprachoroidal space and uveoscleral drainage routes in the human eye.* Acta Ophthalmol Scand, 1997. **75**(1): p. 32-5.

62. Einmahl, S., et al., *Evaluation of a novel biomaterial in the suprachoroidal space of the rabbit eye.* Invest Ophthalmol Vis Sci, 2002. **43**(5): p. 1533-9.

63. Olsen, T.W., et al., *Cannulation of the suprachoroidal space: a novel drug delivery methodology to the posterior segment.* Am J Ophthalmol, 2006. **142**(5): p. 777-87.

64. Hou, J., et al., *In vivo and in vitro study of suprachoroidal fibrin glue.* Jpn J Ophthalmol, 2009. **53**(6): p. 640-7.

65. Olsen, T.W., et al., *Pharmacokinetics of pars plana intravitreal injections versus microcannula suprachoroidal injections of bevacizumab in a porcine model.* Invest Ophthalmol Vis Sci, 2011. **52**(7): p. 4749-56.

66. Patel, S.R., et al., *Targeted administration into the suprachoroidal space using a microneedle for drug delivery to the posterior segment of the eye.* Invest Ophthalmol Vis Sci, 2012. **53**(8): p. 4433-41.

67. Patel, S.R., et al., *Suprachoroidal drug delivery to the back of the eye using hollow microneedles.* Pharm Res, 2011. **28**(1): p. 166-76.

68. Patel, A.K., et al., *Suprachoroidal silicone oil: recognition and possible mechanisms.* Eye (Lond), 2006. **20**(7): p. 854-6.

69. Patel, S.R., H.F. Edelhauser, and M.R. Prausnitz, *Targeted Drug Delivery to the Eye Enabled by Microneedles*, in *Drug Product Development for the Back of the Eye*, U.B. Kompella and H.F. Edelhauser, Editors. 2011, Springer: New York. p. 331-360.

70. Edwards, D.A., et al., *Large porous particles for pulmonary drug delivery.* Science, 1997. **276**(5320): p. 1868-71.

71. Edwards, D.A., A. Ben-Jebria, and R. Langer, *Recent advances in pulmonary drug delivery using large, porous inhaled particles.* J Appl Physiol, 1998. **85**(2): p. 379-85.

72. Arora, S., et al., *Floating drug delivery systems: a review.* AAPS PharmSciTech, 2005. **6**(3): p. E372-90.

73. Patton, J.S., *Mechanisms of macromolecule absorption by the lungs.* Advanced Drug Delivery Reviews, 1996. **19**(1): p. 3-36.

74. Clarke, S.W. and D. Pavia, *Aerosols and the Lung: Clinical and Experimental Aspects*. 1984, London: Butterworth-Heinemann Limited.

75. Edwards, D.A., et al., *Large porous particles for pulmonary drug delivery.* Science, 1997. **276**(5320): p. 1868-1871.

76. *The Hydrodynamically Balanced System (Hbs™): A Novel Drug Delivery System for Oral Use.* Drug Development and Industrial Pharmacy, 1984. **10**(2): p. 313-339.

77. Herman, J. and J.P. Remon, *Modified starches as hydrophilic matrices for controlled oral delivery. II. In vitro drug release evaluation of thermally modified starches.* International Journal of Pharmaceutics, 1989. **56**(1): p. 65-70.

78. Ueda, S., et al., *Development of a novel drug delivery system, time-controlled explosion system (TES). IV. In vivo drug release behavior.* J Drug Target, 1994. **2**(2): p. 133-40.

79. Kawashima, Y., et al., *Preparation of controlled-release microspheres of ibuprofen with acrylic polymers by a novel quasi-emulsion solvent diffusion method.* J Pharm Sci, 1989. **78**(1): p. 68-72.

80. Jiménez-Castellanos, M.R., H. Zia, and C.T. Rhodes, *Design and testing in vitro of a bioadhesive and floating drug delivery system for oral application.* International Journal of Pharmaceutics, 1994. **105**(1): p. 65-70.

81. Atyabi, F., et al., *In vivo evaluation of a novel gastric retentive formulation based on ion exchange resins.* Journal of Controlled Release, 1996. **42**(2): p. 105-113.

82. Pickering, S.U., *CXCVI.-Emulsions.* Journal of the Chemical Society, Transactions, 1907. **91**(0): p. 2001-2021.

83. Tambe, D.E. and M.M. Sharma, *The effect of colloidal particles on fluid-fluid interfacial properties and emulsion stability.* Advances in Colloid and Interface Science, 1994. **52**: p. 1-63.

84. Binks, B.P., *Particles as surfactants - similarities and differences.* Current Opinion in Colloid & Interface Science, 2002. **7**(1-2): p. 21-41.

85. Hunter, T.N., et al., *The role of particles in stabilising foams and emulsions.* Adv Colloid Interface Sci, 2008. **137**(2): p. 57-81.

86. Miguel, A.S. and S.H. Behrens, *Permeability control in stimulus-responsive colloidosomes.* Soft Matter, 2011. **7**(5): p. 1948-1956.

87. Binks, B.P. and S.O. Lumsdon, *Pickering Emulsions Stabilized by Monodisperse Latex Particles: Effects of Particle Size.* Langmuir, 2001. **17**(15): p. 4540-4547.

88. Frelichowska, J., M.-A. Bolzinger, and Y. Chevalier, *Pickering emulsions with bare silica.* Colloids and Surfaces A: Physicochemical and Engineering Aspects, 2009. **343**(1–3): p. 70-74.

89. Ashby, N.P. and B.P. Binks, *Pickering emulsions stabilised by Laponite clay particles.* Physical Chemistry Chemical Physics, 2000. **2**(24): p. 5640-5646.

90. Stiller, S., et al., *Investigation of the stability in emulsions stabilized with different surface modified titanium dioxides.* Colloids and Surfaces A: Physicochemical and Engineering Aspects, 2004. **232**(2–3): p. 261-267.

91. Place, G.M.a.V., *Drug Delivery Device*, A. Corporation, Editor 1971: USA. p. 13.

92. Henry, S., et al., *Microfabricated microneedles: A novel approach to transdermal drug delivery.* Journal of Pharmaceutical Sciences, 1998. **87**(8): p. 922-925.

93. Prausnitz, M.R., *Microneedles for transdermal drug delivery.* Adv Drug Deliv Rev, 2004. **56**(5): p. 581-7.

94. Jiang, J., et al., *Coated microneedles for drug delivery to the eye.* Invest Ophthalmol Vis Sci, 2007. **48**(9): p. 4038-43.

95. Jiang, J., et al., *Intrascleral Drug Delivery to the Eye Using Hollow Microneedles.* Pharmaceutical Research, 2009. **26**(2): p. 395-403.

96. Park, J.H., M.G. Allen, and M.R. Prausnitz, *Biodegradable polymer microneedles: fabrication, mechanics and transdermal drug delivery.* Conf Proc IEEE Eng Med Biol Soc, 2004. **4**: p. 2654-7.

97. Hashmi, S., et al., *Genetic transformation of nematodes using arrays of micromechanical piercing structures.* Biotechniques, 1995. **19**(5): p. 766-70.

98. Henry, S., et al., *Microfabricated microneedles: a novel approach to transdermal drug delivery.* J Pharm Sci, 1998. **87**(8): p. 922-5.

99. McAllister, D.V., et al., *Microfabricated needles for transdermal delivery of macromolecules and nanoparticles: Fabrication methods and transport studies.* Proceedings of the National Academy of Sciences, 2003. **100**(24): p. 13755-13760.

100. Park, J.H., M.G. Allen, and M.R. Prausnitz, *Polymer microneedles for controlled-release drug delivery.* Pharm Res, 2006. **23**(5): p. 1008-19.

101. Lee, J.W., J.H. Park, and M.R. Prausnitz, *Dissolving microneedles for transdermal drug delivery.* Biomaterials, 2008. **29**(13): p. 2113-24.

102. Chu, L.Y. and M.R. Prausnitz, *Separable arrowhead microneedles.* J Control Release, 2011. **149**(3): p. 242-9.

103. Lee, J.W., et al., *Dissolving microneedle patch for transdermal delivery of human growth hormone.* Small, 2011. **7**(4): p. 531-9.

104. Kim, Y.C., J.H. Park, and M.R. Prausnitz, *Microneedles for drug and vaccine delivery.* Adv Drug Deliv Rev, 2012. **64**(14): p. 1547-68.

105. Gardeniers, H.J.G.E., et al., *Silicon micromachined hollow microneedles for transdermal liquid transport.* Microelectromechanical Systems, Journal of, 2003. **12**(6): p. 855-862.

106. McAllister, D.V., et al., *Microfabricated needles for transdermal delivery of macromolecules and nanoparticles: fabrication methods and transport studies.* Proc Natl Acad Sci U S A, 2003. **100**(24): p. 13755-60.

107. Martanto, W., et al., *Transdermal Delivery of Insulin Using Microneedles in Vivo.* Pharmaceutical Research, 2004. **21**(6): p. 947-952.

108. Gupta, J., E.I. Felner, and M.R. Prausnitz, *Rapid pharmacokinetics of intradermal insulin administered using microneedles in type 1 diabetes subjects.* Diabetes Technol Ther, 2011. **13**(4): p. 451-6.

109. Morales-Canton V, L.S., Vera RR, Widmann M, Patel SR, Yerxa B. . *Suprachoroidal Microinjection of Bevacizumab is Well Tolerated in Human Patients*. in *Association for Research in Vision and Ophthalmology*. 2013. Seattle, WA.

110. Csukas, S., et al., *Prostaglandin E2 binding site distribution and subtype classification in the rabbit iris-ciliary body.* Prostaglandins, 1992. **44**(3): p. 199-208.

111. Toris, C.B., B.T. Gabelt, and P.L. Kaufman, *Update on the mechanism of action of topical prostaglandins for intraocular pressure reduction.* Surv Ophthalmol, 2008. **53 Suppl1**: p. S107-20.

112. Qazi, Y., S. Maddula, and B.K. Ambati, *Mediators of ocular angiogenesis.* J Genet, 2009. **88**(4): p. 495-515.

113. Maddula, S., et al., *Horizons in therapy for corneal angiogenesis.* Ophthalmology, 2011. **118**(3): p. 591-9.

114. Aydin, E., et al., *Inhibition of experimental angiogenesis of cornea by various doses of doxycycline and combination of triamcinolone acetonide with low-molecular-weight heparin and doxycycline.* Cornea, 2008. **27**(4): p. 446-53.

115. Gupta, D. and C. Illingworth, *Treatments for corneal neovascularization: a review.* Cornea, 2011. **30**(8): p. 927-38.

116. Acar, B.T., E. Halili, and S. Acar, *The effect of different doses of subconjunctival bevacizumab injection on corneal neovascularization.* Int Ophthalmol, 2013. **33**(5): p. 507-13.

117. Bock, F., et al., *Bevacizumab (Avastin) eye drops inhibit corneal neovascularization.* Graefes Arch Clin Exp Ophthalmol, 2008. **246**(2): p. 281-4.

118. Yoeruek, E., et al., *Safety, penetration and efficacy of topically applied bevacizumab: evaluation of eyedrops in corneal neovascularization after chemical burn.* Acta Ophthalmol, 2008. **86**(3): p. 322-8.

119. Prausnitz, M.R. and J.S. Noonan, *Permeability of cornea, sclera, and conjunctiva: a literature analysis for drug delivery to the eye.* J Pharm Sci, 1998. **87**(12): p. 1479-88.

120. Hurwitz, H. and S. Saini, *Bevacizumab in the treatment of metastatic colorectal cancer: safety profile and management of adverse events.* Semin Oncol, 2006. **33**(5 Suppl 10): p. S26-34.

121. Kamba, T. and D.M. McDonald, *Mechanisms of adverse effects of anti-VEGF therapy for cancer.* Br J Cancer, 2007. **96**(12): p. 1788-95.

122. Kim, S.W., et al., *The effect of topical bevacizumab on corneal neovascularization.* Ophthalmology, 2008. **115**(6): p. e33-8.

123. Koenig, Y., et al., *Short- and long-term safety profile and efficacy of topical bevacizumab (Avastin) eye drops against corneal neovascularization.* Graefes Arch Clin Exp Ophthalmol, 2009. **247**(10): p. 1375-82.

124. Hashemian, M.N., et al., *Deep intrastromal bevacizumab injection for management of corneal stromal vascularization after deep anterior lamellar keratoplasty, a novel technique.* Cornea, 2011. **30**(2): p. 215-8.

125. Donnelly, R.F., T.R. Raj Singh, and A.D. Woolfson, *Microneedle-based drug delivery systems: microfabrication, drug delivery, and safety.* Drug Deliv, 2010. **17**(4): p. 187-207.

126. van der Maaden, K., W. Jiskoot, and J. Bouwstra, *Microneedle technologies for (trans)dermal drug and vaccine delivery.* J Control Release, 2012. **161**(2): p. 645-55.

127. Gill, H.S. and M.R. Prausnitz, *Coated microneedles for transdermal delivery.* J Control Release, 2007. **117**(2): p. 227-37.

128. Matriano, J.A., et al., *Macroflux microprojection array patch technology: a new and efficient approach for intracutaneous immunization.* Pharm Res, 2002. **19**(1): p. 63-70.

129. Mikolajewska, P., et al., *Microneedle pre-treatment of human skin improves 5-aminolevulininc acid (ALA)- and 5-aminolevulinic acid methyl ester (MAL)-induced PpIX production for topical photodynamic therapy without increase in pain or erythema.* Pharm Res, 2010. **27**(10): p. 2213-20.

130. Sullivan, S.P., et al., *Dissolving polymer microneedle patches for influenza vaccination.* Nat Med, 2010. **16**(8): p. 915-20.

131. Corbett, H.J., et al., *Skin vaccination against cervical cancer associated human papillomavirus with a novel micro-projection array in a mouse model.* PLoS One, 2010. **5**(10): p. e13460.

132. Daddona, P.E., et al., *Parathyroid hormone (1-34)-coated microneedle patch system: clinical pharmacokinetics and pharmacodynamics for treatment of osteoporosis.* Pharm Res, 2011. **28**(1): p. 159-65.

133. Palakurthi, N.K., et al., *Toxicity of a biodegradable microneedle implant loaded with methotrexate as a sustained release device in normal rabbit eye: a pilot study.* J Ocul Pharmacol Ther, 2011. **27**(2): p. 151-6.

134. Gilger, B.C., et al., *Treatment of acute posterior uveitis in a porcine model by injection of triamcinolone acetonide into the suprachoroidal space using microneedles.* Invest Ophthalmol Vis Sci, 2013. **54**(4): p. 2483-92.

135. Gill, H.S. and M.R. Prausnitz, *Coating formulations for microneedles.* Pharm Res, 2007. **24**(7): p. 1369-80.

136. Seta, F., et al., *Inhibition of VEGF expression and corneal neovascularization by siRNA targeting cytochrome P450 4B1.* Prostaglandins Other Lipid Mediat, 2007. **84**(3-4): p. 116-27.

137. Holzer, M.P., et al., *Photodynamic therapy with verteporfin in a rabbit model of corneal neovascularization.* Invest Ophthalmol Vis Sci, 2003. **44**(7): p. 2954-8.

138. Chan T, P.S., Holden BA., *Corneal thickness profiles in rabbits using an ultrasonic pachometer.* Invest Ophthalmol Vis Sci. , 1983. **24**(10): p. 1408-1410.

139. Dastjerdi, M.H., et al., *Effects of topical and subconjunctival bevacizumab in high-risk corneal transplant survival.* Invest Ophthalmol Vis Sci, 2010. **51**(5): p. 2411-7.

140. Chen, W.L., et al., *Subconjunctival injection of bevacizumab (avastin) on corneal neovascularization in different rabbit models of corneal angiogenesis.* Invest Ophthalmol Vis Sci, 2009. **50**(4): p. 1659-65.

141. Erdurmus, M. and Y. Totan, *Subconjunctival bevacizumab for corneal neovascularization.* Graefe's Archive for Clinical and Experimental Ophthalmology, 2007. **245**(10): p. 1577-9.

142. Kim, T.-i., et al., *Inhibition of Experimental Corneal Neovascularization by Using Subconjunctival Injection of Bevacizumab (Avastin).* Cornea, 2008. **27**(3): p. 349-352 10.1097/ICO.0b013e31815cf67d.

143. Papathanassiou, M., et al., *Inhibition of corneal neovascularization by subconjunctival bevacizumab in an animal model.* American Journal of Ophthalmology, 2008. **145**(3): p. 424-431.

144. Agency, E.M., *Avastin EPAR- Scientific Discussion*, 2013, European Medicine Agency.

145. Solomon, K.D., et al., *LASIK world literature review: quality of life and patient satisfaction.* Ophthalmology, 2009. **116**(4): p. 691-701.

146. Thielen, T.L., S.S. Castle, and J.E. Terry, *Anterior ocular infections: an overview of pathophysiology and treatment.* The Annals of Pharmacotherapy, 2000. **34**(2): p. 235-46.

147. Bressler, S.B., *Introduction: Understanding the role of angiogenesis and antiangiogenic agents in age-related macular degeneration.* Ophthalmology, 2009. **116**(10 Suppl): p. S1-7.

148. Janoria, K.G., et al., *Novel approaches to retinal drug delivery.* Expert Opin Drug Deliv, 2007. **4**(4): p. 371-88.

149. Merck & Co., I., *TIMOPTIC ® 0.25% AND 0.5% (TIMOLOL MALEATE OPHTHALMIC SOLUTION) [Packing Insert]*, 2005 Sept Merck & Co., InC: Whitehouse Station, NJ 08889, USA.

150. Bhatt, R., et al., *Prospective survey of adverse reactions to topical antiglaucoma medications in a hospital population.* Eye (Lond), 2005. **19**(4): p. 392-5.

151. Ozkiris, A. and K. Erkilic, *Complications of intravitreal injection of triamcinolone acetonide.* Can J Ophthalmol, 2005. **40**(1): p. 63-8.

152. Kim, S.H., et al., *Assessment of subconjunctival and intrascleral drug delivery to the posterior segment using dynamic contrast-enhanced magnetic resonance imaging.* Invest Ophthalmol Vis Sci, 2007. **48**(2): p. 808-14.

153. Gilger, B.C., et al., *A novel bioerodible deep scleral lamellar cyclosporine implant for uveitis.* Invest Ophthalmol Vis Sci, 2006. **47**(6): p. 2596-605.

154. Reitsamer, H.A. and J.W. Kiel, *A rabbit model to study orbital venous pressure, intraocular pressure, and ocular hemodynamics simultaneously.* Investigative ophthalmology & visual science, 2002. **43**(12): p. 3728-34.

155. Bala, I., S. Hariharan, and M.N. Kumar, *PLGA nanoparticles in drug delivery: the state of the art.* Crit Rev Ther Drug Carrier Syst, 2004. **21**(5): p. 387-422.

156. Rowe, R.C., et al., *Handbook of pharmaceutical excipients / edited by Raymond C. Rowe, BPharm, PhD, DSC, FRPharmS, FRSC, CPhys, MInstP, chief scientist, Paul J. Sheskey, BSc, RPh, principal research scientist, the Dow Chemical Company, Midland, MI, USA, Walter G. Cook, BSc, PhD, research fellow,*

Materials Science group of Pharmaceutical R&D, Pfizer, Sandwich, Kent, UK, Marian E. Fenton, BSc, MSc, development editor, Royal Pharmaceutical Society of Great Britain, London, UK. Seventh edition. ed. 2012, London: APhA/Pharmaceutical Press. xxviii, 1033 pages.

157. *DisCoVisc (ophthalmic viscosurgical device) pakage insert*, I. Alcon laboratories, Editor 2006, 2011, Alcon laboratories, Inc.

158. Gholam A. Peyman, S.A.M., Mandi D. Conway, *Vitreoretinal Surgical Techniques, Second Edition* ed. M.C. Gholam Peyman. 2001, United Kingdom: Martin Dunitz.

159. Gross, J.G., et al., *Useful adjuncts for vitreoretinal surgery.* Br J Ophthalmol, 1989. **73**(6): p. 435-9.

160. Burke B, P.S. *Comparison of the Total Amount of Triamcinolone Acetonide Delivered Via Suprachoroidal or Intravitreal Administration*. in *Association for Research in Vision and Ophthalmology*. 2013. Seattle, WA.

161. Edelhauser HF, M.C., Dean R,Powell K,Verhoeven RS. *Suprachoroidal Microinjection Delivers Triamcinolone Acetonide to Therapeutically-Relevant Posterior Ocular Structures and Limits Exposure in the Anterior Segment*. in *Association for Research in Vision and Ophthalmology*. 2013. Seattle, WA.

162. Verhoeven RS, V.K., Cacciamani F,Amar T, Yerxa B., *Suprachoroidal Microinjection of Triamcinolone Acetonide is Well Tolerated in the Albino Rabbit*, in *Association for Research in Vision and Ophthalmology*2013: Seattle, WA.

163. Reardon, G., S. Kotak, and G.F. Schwartz, *Objective assessment of compliance and persistence among patients treated for glaucoma and ocular hypertension: a systematic review.* Patient Preference and Adherence, 2011. **5**: p. 441-63.

164. Osterberg, L. and T. Blaschke, *Adherence to medication.* N Engl J Med, 2005. **353**(5): p. 487-97.

165. Claxton, A.J., J. Cramer, and C. Pierce, *A systematic review of the associations between dose regimens and medication compliance.* Clinical therapeutics, 2001. **23**(8): p. 1296-1310.

166. Hoyng, P.F. and L.M. van Beek, *Pharmacological therapy for glaucoma: a review.* Drugs, 2000. **59**(3): p. 411-34.

167. Camras, C.B., C.B. Toris, and R.R. Tamesis, *Efficacy and adverse effects of medications used in the treatment of glaucoma.* Drugs & aging, 1999. **15**(5): p. 377-88.

168. Rizzo, S., et al., *Suprachoroidal drug infusion for the treatment of severe subfoveal hard exudates.* Retina, 2012. **32**(4): p. 776-84.

169. Tetz, M., S. Rizzo, and A.J. Augustin, *Safety of submacular suprachoroidal drug administration via a microcatheter: retrospective analysis of European treatment results.* Ophthalmologica, 2012. **227**(4): p. 183-9.

170. Wang, M., et al., *Pharmacokinetic Comparison of Ketorolac after Intracameral, Intravitreal, and Suprachoroidal Administration in Rabbits.* Neurosurgery, 2012.

171. Waterbury, L.D. and R.M. Eglen, *Ocular hypotensive activity of sulprostone, a potent and selective prostanoid EP1/EP3 receptor agonist.* Clinical Pharmacology & Therapeutics, 1990. **47**(2): p. 150-150.

172. Liu, J.H. and J.E. Jumblatt, *Neuromodulatory effect of sulprostone on the circadian elevation of intraocular pressure in rabbits.* Curr Eye Res, 1993. **12**(11): p. 975-80.

173. Liu, J.H.K., B.E. Shieh, and J.E. Jumblatt, *Sulprostone decreases intraocular-pressure in rabbits by prejunctional inhibition of norepinephrine release.* Investigative Ophthalmology & Visual Science, 1993. **34**(4): p. 921-921.

174. Waterbury, L.D., et al., *EP3, but not EP2, FP, or TP prostanoid-receptor stimulation may reduce intraocular pressure.* Investigative ophthalmology & visual science, 1990. **31**(12): p. 2560-2567.

175. Bernstein, P., *A comparison of latanoprost, bimatoprost, and travoprost in patients with elevated intraocular pressure: a 12-week, randomized, masked-evaluator, multicenter study.* Am J Ophthalmol, 2004. **137**(2): p. 387-8; author reply 388-9.

176. Koz, O.G., et al., *Comparison of the effects of travoprost, latanoprost and bimatoprost on ocular circulation: a 6-month clinical trial.* Acta Ophthalmol Scand, 2007. **85**(8): p. 838-43.

177. Orihashi, M., et al., *Potent reduction of intraocular pressure by nipradilol plus latanoprost in ocular hypertensive rabbits.* Biol Pharm Bull, 2005. **28**(1): p. 65-8.

178. Morales, M., et al., *Hypotensive effect of profilin on rabbit intraocular pressure.* European Journal of Pharmacology, 2007. **567**(1-2): p. 145-8.

179. Impagnatiello, F., et al., *A dual acting compound with latanoprost amide and nitric oxide releasing properties, shows ocular hypotensive effects in rabbits and dogs.* Experimental Eye Research, 2011. **93**(3): p. 243-9.

180. Ohashi, M., et al., *Local effect of topical FP-receptor agonists on retinal vessels of the ipsilateral posterior retina in normal rabbit eyes.* Clinical & experimental ophthalmology, 2008. **36**(8): p. 767-74.

181. Akaishi, T., et al., *Effects of repeated administrations of tafluprost, latanoprost, and travoprost on optic nerve head blood flow in conscious normal rabbits.* Journal of Ocular Pharmacology and Therapeutics, 2010. **26**(2): p. 181-6.

182. Orihashi, M., et al., *Potent reduction of intraocular pressure by nipradilol plus latanoprost in ocular hypertensive rabbits.* Biological & Pharmaceutical Bulletin, 2005. **28**(1): p. 65-8.

183. Kurashima, H., et al., *Effects of prostaglandin F(2alpha) analogues on endothelin-1-induced impairment of rabbit ocular blood flow: comparison among tafluprost, travoprost, and latanoprost.* Experimental Eye Research, 2010. **91**(6): p. 853-9.

184. Atkinson, K.E., *An introduction to numerical analysis*. 2nd ed. 1989, New York: Wiley. xvi, 693 p.

185. Burke, J., et al., *Adrenergic and imidazoline receptor-mediated responses to UK-14,304-18 (brimonidine) in rabbits and monkeys. A species difference.* Ann N Y Acad Sci, 1995. **763**: p. 78-95.

186. Huang, Y., et al., *Localization of alpha 2-adrenergic receptor subtypes in the anterior segment of the human eye with selective antibodies.* Investigative Ophthalmology & Visual Science, 1995. **36**(13): p. 2729-39.

187. Toris, C.B., et al., *Effects of brimonidine on aqueous humor dynamics in human eyes.* Archives of ophthalmology, 1995. **113**(12): p. 1514-7.

188. Toris, C.B., C.B. Camras, and M.E. Yablonski, *Acute versus chronic effects of brimonidine on aqueous humor dynamics in ocular hypertensive patients.* American journal of ophthalmology, 1999. **128**(1): p. 8-14.

189. Burke, J.A. and D.E. Potter, *Ocular effects of a relatively selective alpha 2 agonist (UK-14, 304-18) in cats, rabbits and monkeys.* Curr Eye Res, 1986. **5**(9): p. 665-76.

190. Angelov, O.V., et al., *Preclinical safety profile of brimonidine.* Eur J Ophthalmol, 1996. **6**(1): p. 21-5.

191. Tsonis, P.A., *Animal models in eye research*. 2008, Amsterdam ; London: Academic Press.

192. Burke, J. and M. Schwartz, *Preclinical evaluation of brimonidine.* Surv Ophthalmol, 1996. **41 Suppl 1**: p. S9-18.

193. El Chehab, H., et al., *Effect of topical pressure-lowering medication on prevention of intraocular pressure spikes after intravitreal injection.* Eur J Ophthalmol, 2013. **23**(3): p. 277-83.

194. Van der Reis, M.I., et al., *A systematic review of the adverse events of intravitreal anti-vascular endothelial growth factor injections.* Retina, 2011. **31**(8): p. 1449-69.

195. Acheampong, A.A., et al., *Distribution of brimonidine into anterior and posterior tissues of monkey, rabbit, and rat eyes.* Drug metabolism and disposition: the biological fate of chemicals, 2002. **30**(4): p. 421-9.

196. Acheampong, A.A., M. Shackleton, and D.D. Tang-Liu, *Comparative ocular pharmacokinetics of brimonidine after a single dose application to the eyes of*

albino and pigmented rabbits. Drug metabolism and disposition: the biological fate of chemicals, 1995. **23**(7): p. 708-12.

197. Alm, A., I. Grierson, and M.B. Shields, *Side effects associated with prostaglandin analog therapy.* Survey of Ophthalmology, 2008. **53 Suppl1**: p. S93-105.

198. Beckers, H.J., et al., *Side effects of commonly used glaucoma medications: comparison of tolerability, chance of discontinuation, and patient satisfaction.* Graefes Arch Clin Exp Ophthalmol, 2008. **246**(10): p. 1485-90.

199. Chiba, T., et al., *Iridial pigmentation induced by latanoprost ophthalmic solution in Japanese glaucoma patients.* Journal of glaucoma, 2001. **10**(5): p. 406-10.

200. Alm, A., J. Schoenfelder, and J. McDermott, *A 5-year, multicenter, open-label, safety study of adjunctive latanoprost therapy for glaucoma.* Archives of ophthalmology, 2004. **122**(7): p. 957-65.

201. Schuman, J.S., *Clinical experience with brimonidine 0.2% and timolol 0.5% in glaucoma and ocular hypertension.* Survey of ophthalmology, 1996. **41 Suppl 1**: p. S27-37.

202. Kleinberg, T.T., et al., *Vitreous substitutes: a comprehensive review.* Survey of ophthalmology, 2011. **56**(4): p. 300-23.

203. Aveyard, R., B.P. Binks, and J.H. Clint, *Emulsions stabilised solely by colloidal particles.* Advances in Colloid and Interface Science, 2003. **100–102**(0): p. 503-546.

204. Herzig, E.M., et al., *Bicontinuous emulsions stabilized solely by colloidal particles.* Nature materials, 2007. **6**(12): p. 966-71.

205. Frelichowska, J., M.A. Bolzinger, and Y. Chevalier, *Effects of solid particle content on properties of o/w Pickering emulsions.* J Colloid Interface Sci, 2010. **351**(2): p. 348-56.

206. Benz, M.S., et al., *Short-term course of intraocular pressure after intravitreal injection of triamcinolone acetonide.* Ophthalmology, 2006. **113**(7): p. 1174-1178.

207. Liu, Y., H. Miyoshi, and M. Nakamura, *Encapsulated ultrasound microbubbles: therapeutic application in drug/gene delivery.* Journal of controlled release : official journal of the Controlled Release Society, 2006. **114**(1): p. 89-99.

208. Weinberger, D., et al., *Long-term follow-up of perfluorocarbon liquid in the anterior chamber.* Retina (Philadelphia, Pa), 1998. **18**(3): p. 233-7.

209. Haidt, S., L. Clark, and J. Ginsberg, *Liquid perfluorocarbon replacement in the eye (abstr).* Invest Ophthalmol Vis Sci, 1982. **22**: p. 233.

210. Allansmith, M., A. de Ramus, and D. Maurice, *The dynamics of IgG in the cornea.* Invest Ophthalmol Vis Sci, 1979. **18**(9): p. 947-55.

211. Crank, J., *The mathematics of diffusion*. 2d ed. 1975, Oxford,: Clarendon Press. viii, 414 p.

212. Allansmith, M., A. de Ramus, and D. Maurice, *The dynamics of IgG in the cornea.* Investigative ophthalmology & visual science, 1979. **18**(9): p. 947-55.